SANDIA REPORT
SAND2003-3819
Unlimited Release
Printed November 2003

Suppression of Electron Emission from Metal Electrodes
LDRD 28771 Final Report

David J. Johnson, William E. Fowler, Harry C. Ives, Mark E. Savage, and William A. Stygar

Prepared by
Sandia National Laboratories
Albuquerque, New Mexico 87185 and Livermore, California 94550

Sandia is a multiprogram laboratory operated by Sandia Corporation, a Lockheed Martin Company, for the United States Department of Energy's National Nuclear Security Administration under Contract DE-AC04-94AL85000.

Issued by Sandia National Laboratories, operated for the United States Department of Energy by Sandia Corporation.

Available to DOE and DOE contractors from
U.S. Department of Energy
Office of Scientific and Technical Information
P.O. Box 62
Oak Ridge, TN 37831

Telephone: (865)576-8401
Facsimile: (865)576-5728
E-Mail: reports@adonis.osti.gov
Online ordering: http://www.doe.gov/bridge

Available to the public from
U.S. Department of Commerce
National Technical Information Service
5285 Port Royal Rd
Springfield, VA 22161

Telephone: (800)553-6847
Facsimile: (703)605-6900
E-Mail: orders@ntis.fedworld.gov
Online order: http://www.ntis.gov/help/ordermethods.asp?loc=7-4-0#online

SAND2003-3819
Unlimited Release
Printed November 2003

Suppression of Electron Emission from Metal Electrodes LDRD 28771 Final Report

David J. Johnson, William E. Fowler, Harry C. Ives, Mark E. Savage, and William A. Stygar
Beam Applications and Initiatives
Sandia National Laboratories
P.O. Box 5800
Albuquerque, NM 87185-1182

Abstract

This research consisted of testing surface treatment processes for stainless steel and aluminum for the purpose of suppressing electron emission over large surface areas to improve the pulsed high voltage hold-off capabilities of these metals. Improvements to hold-off would be beneficial to the operation of the vacuum-insulator grading rings and final self-magnetically insulated transmission line on the ZR-upgrade machine and other pulsed power applications such as flash radiograph and pulsed-microwave machines. The treatments tested for stainless steel include the Z-protocol (chemical polish, HVFF, and gold coating), pulsed E-beam surface treatments by IHCE, Russia, and chromium oxide coatings. Treatments for aluminum were anodized and polymer coatings. Breakdown thresholds also were measured for a range of surface finishes and gap distances. The study found that: 1.) Electrical conditioning and solvent cleaning in a filtered air environment each improve HV hold-off 30%. 2.) Anodized coatings on aluminum give a factor of two improvement in high voltage hold-off. However, anodized aluminum loses this improvement when the damage is severe. Chromium oxide coatings on stainless steel give a 40% and 20% improvement in hold-off before and after damage from many arcs. 3.) Bare aluminum gives similar hold-off for surface roughness, R_a, ranging from 0.08 to 3.2 μm. 4.) The various EBEST surfaces tested give high voltage hold-off a factor of two better than typical machined and similar to R_a = 0.05 μm polished stainless steel surfaces. 5.) For gaps > 2 mm the hold-off voltage increases as the square root of the gap for bare metal surfaces. This is inconsistent with the accepted model for metals that involves E-field induced electron emission from dielectric inclusions. Micro-particles accelerated across the gap during the voltage pulse give the observed voltage dependence. However the similarity in observed breakdown times for large and small gaps places a requirement that the particles be of molecular size. This makes accelerated micro-particle induced breakdown seem improbable also.

Acknowledgments

The principle author wishes to thank William A. Stygar who initiated the original proposal that was accepted. The important study of the Russian EBEST treatment process was suggested and strongly advocated by Dillon McDaniel and Rick Spielman. David Wenger designed the electrode support apparatus. Gerard Torres assisted in the taking of the data and was very helpful in the design and fabrication of the experimental hardware. He also designed and fabricated the filtered air system. Gregory A. Mann designed the LIVA and was extremely valuable in maintaining and upgrading the pulser systems to 100% reliability. The assistance of Charles Harjes was also very helpful in the design and evaluation of the LIVA circuit. John McKenney and Steve Toledo ordered the electrodes from Gull Group. Jeff Gluth and Dennis Lobley prepared the Z-protocol electrodes. Tim Wagner measured the roughness of the machined surfaces of the aluminum electrodes. Isidro Molina gave valuable advice on pulsed power problems and supplied us with many spare parts that kept our experiments on track. Steve Cordova supplied the EVO 191 solution.

Table of Contents

List of Figures

I. Introduction

The potential to improve the high-voltage hold-off of metal electrodes is relevant to the improved operation of existing or planned pulsed power machines. This would be relevant to Z-pinch, flash radiography, and pulsed microwave generators. An example of particular relevance is the vacuum transmission line near the final power flow section on the Z accelerator. Improvements to hold-off would allow smaller transmission line spacing and lower inductance in the final convolute region. This reduction in inductance results in higher currents to the z-pinch load and more efficient x-ray production. This report includes the results of studies of the hold-off of Z-protocol treatment used for the Z accelerator convolute parts, pulsed electron beam surface melted, polished, and chromium oxide coated stainless steel which could be applied to the convolute parts.

We were interested in whether the vacuum insulator stack on the Z accelerator could be improved to allow an upgrade to the power transmitted across the vacuum interface. The present Z accelerator uses anodized aluminum grading rings in the insulator stack and must operate for thousands of shots with damage to the anodized coatings from emission arcs. There is also the presence of air-born laboratory particles that settle on the rings. Better knowledge of how the grading rings hold off voltage under these conditions is very important for future accelerator developments such as the ZR, Z-Refurbishment, project of up-grading the pulse power section of the Z accelerator to 40% more power. Minimizing changes to the existing system could save over a million dollars.

History of Field Emission and High Voltage Breakdown Research

Extensive research has been performed over the last century in attempts to gain an understanding of the breakdown mechanisms that culminate in arcing between electrodes exposed to high voltages. The paper by Alpert and colleagues [1] has an excellent synopsis of the early research viewed from a mid 1960's perspective. Field emission from cathode micro-protrusions and accelerated loosely bound macro-particles explained much of the existing data obtained with small and large gaps, respectively. The breakdown voltage for small gap is proportional to the inverse of the gap (E-Field) and for large gap the square root of the gap. Mesyats and Proskurosky [2] gives a more detailed treatment of the same concepts and briefly discusses the concept of field emission from dielectric inclusions that was developed by Latham [3]. Finally the book edited and partially written by Latham [4] has the best synopsizes of this work and the present understanding of the processes leading to electrical breakdown.

The initial studies of pre-emission current phenomenon were carried out by Millikan and co-workers [5] who studied reversible pre-breakdown currents from localized emission sites on the cathode. It was assumed then that the emission currents were from the hypothetical metal micro-protrusions. They established [6] that these currents followed a well-defined empirical relationship such that a graph of log I versus 1/E gave a straight line. It was then recognized that the Fowler and Nordheim [7] quantum mechanical tunneling theory of field emission from metal surfaces gave a physical basis for the empirical relationship. This allowed a determination of the emission area and enhancement factor, β, for a single emission site if a work function was assumed. A work function value of ~ 4.5 eV applies to most electrode materials and gives typical

enhancement factors of 100 or more over the theoretical value [1] of the E-field of ~ 6.5 x 10^9 V/m (6.5 x 10^4 kV/cm) for emission in a "perfect" vacuum gap. This model appeared to explain the field emission phenomenon until the presence of visible light and no obvious metallic protrusions were observed at the emission sites.

Latham studied emission from metallic protrusons [8] as early as 1968 and shortly thereafter breakdown from accelerated micro-particles [9]. Latham and coworkers [10] then studied the emission sites with an electron microscope and concluded that the emission could originate from sites that were not metallic protrusions. Cox [11,12] next used a SEM to study the emission sites and noted that emission was occurring at low-enhancement regions like cracks or grain boundaries on the metallic surfaces. This work was followed by a collaborative effort by Allen, Cox, and Latham [13] that presented a solid state physics picture of the emission. This mechanism has become known as the metal-insulator-vacuum (MIV) model. Dielectric inclusions were assumed that allowed the external E-field to penetrate through them to the metal cathode surface. Then above a certain field strength, electrons can tunnel through the barrier at the metal-dielectric boundary into the conduction band of the dielectric. These electrons cause formation of avalanches. The holes produced in this way move toward the metal surface, aiding the consequent tunneling of electrons from the metal. The tunneling electrons, while passing through the dielectric at the bottom of the conduction band, rapidly thermalize. They then enter the region with a strong field near the vacuum-dielectric interface, where they gain energies up to several eV before passing through the potential barrier.

This mechanism has been studied extensively via use of scanning anode probe diagnostics to measure the quantity and spectral nature of the < 1 μA current emitted from the pre breakdown emission sites. Further studies by Hurley [14] have examined the electroluminesent nature of the sites. The results of these studies have firmly established the Latham MIV model [3] as the mechanism for much of the emission phenomenon observed in small HV voltage vacuum gaps. The model can explain in great deal the spectral and spatial distribution of electrons emitted from the sites. Latham [4] even shows (see Section 4.3.3 his book) that the MIV model gives pre-emission currents that agree with the Fowler and Nordheim equation. At sufficiently high E-field the emission current becomes large enough to desorbe gas which then forms plasma on the cathode surface.

A variation of the MIV model assumes the 5 to 100 nm oxide layers present on most metal surfaces together with a metal flake lying on the oxide layer is the source of electron emission. This electron emission mechanism is called the metal-insulator-metal, (MIM) model [15]. Although the majority of emission sites can be explained by the MIV or MIM model rough metal surfaces can probably also give pre-emission currents via the traditional metallic microprotrusion (MM) model. With this model sufficiently high current density at the microscopy tip will cause the tip to become vaporized and initiate plasma followed by electrical breakdown.

A third mechanism was shown by Cranberg [16] in 1952 to apply to gaps > 2 mm that are exposed to DC or long pulses. In this model loosely bound particles acquire surface charge and in-turn are accelerated across the gap. At sufficiently high voltages the particles release a cloud of gas from the cathode or anode that turns into plasma from

stray electrons in the high E-field or if accelerated to ~ 10 km/s forms plasma directly. This mechanism gives a breakdown voltage that scales roughly as the square root of the gap. The mechanism is called the "total voltage effect". A qualitative reason for this dependence is as follows. Assume that the breakdown occurs when the energy per unit area delivered to the target electrode exceeds a constant C, which is characteristic of the electrode. The energy delivered is a product of the voltage and charge density of the particle. Since charge density is proportional to the E-field at the origin electrode, $VE > C$. Substituting for E gives $V > (Cd)^{0.5}$.

This mechanism was further refined by Slivkov [17] who developed the scaling relationship: $V_b = C_s d^{0.625}$ and more recently by Chatterton [18]. Eastham and Chatterton [19] developed a twin beam laser system to detect ~ 1-μm-diameter micro-particles accelerated across a HV gap and concluded that 95% of the particles originate from the anode. Tests were performed with a 6 mm gap using a 200 kV, 1-ms-FWHM, voltage pulse. Breakdowns occurred 10 to 70 μs after application of the 3-μs-rise-time pulse. Gray [20,21] studied the effects of EHD generated micro-particles from localized molten metal anode surface regions in vacuum diodes driven by a 400 kV, 40 ns power pulse. He infers velocities of 10^4-10^6 m/s from damage craters. A 10^5 m/s velocity would allow a micro-size particles to cross a 5 mm gap in 50 ns.

Latham has continued to be interested in the total voltage effect and co-authored a study of the effect with Xu [22] in 1989 that concluded with copper electrodes there was no change in the field emission enhancement factor, β, for gaps from 0.45 to 0.75 mm. He also devotes a chapter in his book [4] to micro-particle phenomenon. Some of the best review papers of the physics of electron breakdown were given at the "5th Workshop on Electrode Phenomena", that took place in East Berlin in May 1982. These papers were later published in the IEEE Trans. on Elect. Insulation E1-18 (3) June 1983. Latham [23] lists 15 experimental observations related to HV electron induced emission phenomenon that had been explained by various models. He points out that the "total voltage effect" remains obscure. The field has languished somewhat since the 1982 workshop with the work now concentrated on aspects of the problem that relate to applications where improvements in hold-off would have a monetary benefit.

Attempts to Improve Hold-off

An experiment relevant to this work was performed by Jedynak in 1964 [24]. He studied the breakdown in the 5 mm gap between 15-cm-diameter Rogowski curve electrodes. The films were several μm thick silicon monoxide, Mylar, Formvar, titanium dioxide, cerium oxide, iron oxide and tin oxide. The first four coatings gave improvements in hold-off up to 70% and the others gave inferior performance. Frazier [25] studied emission from anodized aluminum. Tests were performed with a 75-ns-FWHM, 530 kV pulse, from a 5.3 Ω pulsed power machine. The hold-off for 23-cm-diameter electrodes increased by 30%. Voss [26] performed similar experiments on anodized aluminum, chromium oxide (green) and Glyptol coated stainless steel, nickel and chrome plated stainless steel. He obtained comparison data for bare machined aluminum , stainless steel carbon, copper, and molybdenum. His tests for anodized aluminum and green stainless showed an 80 and 40% improvement in hold-off compared to the bare surfaces.

The influence of surface oxide on copper cathodes was studied by Latham and colleagues [27]. They saw a reduction in the site emission current and a decrease in the cathode Fermi level as witnessed by a 2 to 3 eV reduced energy of the emitted electrons compared to the gap voltage. Mayberry, et.al. [28] sputter deposited 500-nm-thick oxide and metal coatings on a stainless steel screen cathode and saw an improvement in hold-off from 300 to > 500 kV/cm for 10 μs to 100 ms pulses. These tests were made with a 1-mm-wide gap.

Batrakov [29] reported hold-offs of ~ 5 MV/cm for stainless steel (Ni = 5.5, Ti=3.4, Cu=2 MV/cm) treated with a pulsed low energy high current electron beam, LEHCEB. The beam acted to melt the surface and remove dielectric inclusions. The high voltage tests were done with 0.1 mm gap and ~ 1 mm^2 area using a 45 kV, 1.2 ms pulse. Batrakov [30] later obtained hold-offs of ~ 2.5 MV/cm LEHCEB treated 304 stainless steel using a ~ 1-mm-gap, 1-cm-area and square 80 ns, 240 kV pulse. The maximum hold-off was attained with 30, 100, and 1000 electrical conditioning shots when the surface was exposed to RF discharge cleaning plus LEHCEB, LEHCEB only, and electrochemically polished, respectively.

Recent Trends of Research in the Field

The most intense effort in recent years has been the continued study of emission from high conductivity materials such as copper and super-conducting niobium used in RF accelerators. Ph. Niedermann and colleagues [31] performed 2-D measurements of the pre-emission sites of niobium samples with an anode-scanning probe. They showed that the sites were essentially eliminated when the test samples were heated to > 1400° C for 15 minutes. Mahner, Pupeter, and colleagues [32, 33] have performed similar studies on copper and niobium. Jimenez and colleagues [34] measured emission sites from metallic, oxide, and sulfide particulate contaminants selectively placed on gold and niobium surfaces. They also used a scanning anode probe and saw no emission from aluminum and silicon oxide particles but strong emission from metallic particles.

There has also been a concerted effort to find methods of cleaning or preparing metal surfaces for reduces emission and higher hold-off voltages. Much of this work has been done in relation to vacuum breaker switches that are used for AC power transmission control. Cuneo [35] reviewed the work on electrode contamination, cleaning, and conditioning as related to pulsed-power applications.

Motivation for this LDRD research

There has not been an extensive research performed on the physics of E-field breakdown of stainless steel and aluminum that are used for pulsed power applications. We felt that if the MIV model was applicable to stainless steel we could improve hold-off by eliminating the dielectric inclusions. We chose to confirm if this is possible by measuring breakdown for different grades of stainless steel with varying amounts of inclusions and stainless steel that had been subjected to pulsed electron beam surface treatment, EBEST, that greatly reduced the number of surface inclusions.

We also measured breakdown for Z-protocol treated stainless steel electrodes that are gold-coated. These electrodes would not have the oxide layer that is necessary for emission in the MIM model. Finally we studied breakdown for electrodes with thick dielectric layers such as anodized aluminum and chromium oxide coated stainless steel. It was hoped that by measuring the differences between different surface layers we could gain insight into the important mechanisms that initiate breakdown from the materials commonly used in pulsed power generators. This empirical data would at least give guidance when selecting the best materials and coatings for pulsed power applications.

We also wanted to measure breakdown versus gap for 100 ns duration pulses, because the empirical scaling relations with gap have been observed for longer pulse breakdown. Okawa and colleagues [36] reported that with a 2.3 ms voltage pulse, the hold-off for stainless steel and copper electrodes decreases as the inverse fourth root of the area for areas < 30 cm^2. They also showed that the hold-off decreased with increasing gap roughly as gap to the negative 0.4 power. These tests were done with ring-plane, cylindrical, and spherical tip geometries. Schumann and Kurrat [37] used a 50 μs 120 kV pulses, to measure breakdowns for 0.5, 1, and 1.5 cm gaps as a function of R_a = 0.08 to 0.6 μm and A = 8 to 80 cm^2. They showed the hold-off E-field dropping with area as $A^{-0.19}$. We desired to determine if this scaling relation applied to the hold-off of the large planar surface area metal electrodes used in pulsed power generators. We were also motivated to confirm the excellent hold-off of 2.5 MV/cm reported by Batrakov [30], for pulsed electron beam treated stainless steel surfaces

II. Experimental Setup

A view of the electrode test assembly is shown in Fig. 1. The electrodes were fabricated by Gull Group [38] with Chang curve profiles to give uniform E-fields with a 5-mm-wide anode-cathode gap. The shape of the curves was specified by the Chang formula,

$$z = \frac{g}{2} \cdot \left(1 + 0.001 \cdot \cosh\left(\frac{\pi \cdot r}{g} \right) \Big/ \cosh\left(\frac{\pi \cdot Ro}{g} \right) \right)$$

where g is the AK gap. The E-field deviates from uniform by 0.001 at the radius, R_o = 7 cm for 17-cm-diameter electrodes. For gaps less than 5 mm the E-field drops off slightly towards the edges. For 7.5 mm gaps the E-field is enhanced by 5% near the edges. The machined surface roughness, R_a, was typically 0.4 μm (16-μinch rms).

The electrode mounting plates are supported on three 16.5-cm-tall Rexolite cross-linked polystyrene dielectric rods. The alignment of the plates was accurate to ± 25 μm. The gap was adjustable with spacer rings at the cathode mounting fixture. The assembly was mounted in a 74.2-cm-diameter, 40.6-cm-tall vacuum chamber. A turbo-molecular pumping system produced a 4e-7 Torr pressure during overnight pump down but data were typically obtained after 3 hr pump down and < 3e-6 Torr. The chamber was surrounded by a clean air tent supplied with 0.25 m^3/s of air flowing through a HEPA filter. This gave a background air purity of 100 particles/m^3 for cleaning and installation of electrodes (Fig.52). Electrodes were cleaned with acetone using Kimwipe wipers and compressed CO_2 blown across the surfaces prior to installation into the vacuum chamber.

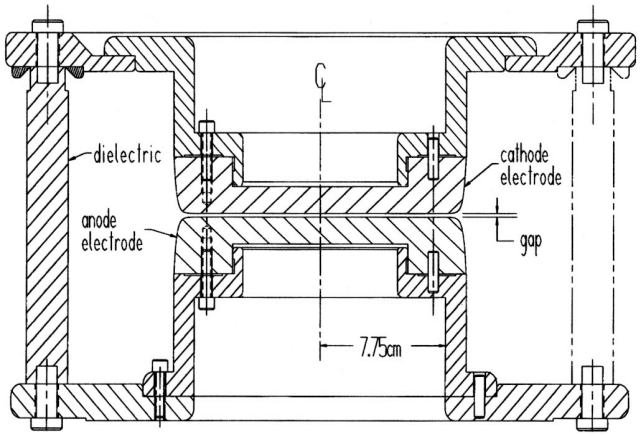

Figure 1. A cross-sectional view of the electrode support apparatus showing the 17-cm-diameter stainless steel electrodes.

Tests were also performed with 8, 12, and 15 cm-diameter electrodes. A second view of the support assembly is shown in Fig. 2 that indicates the adapter flanges used to mount these electrodes. This drawing also shows the assembly in relation to the vacuum chamber wall and includes the three knob shaped field shapers that gave a more uniform field distribution along the Rexolite support rods. The support rods were redesigned several times to achieve reliable operation. Different materials such as Lucite and Epoxy were tried but Rexolite gave the best results. However these rods still flashed over in ~ 120 ns when a 500 kV pulse was applied. There was no visible damage to the rods from these flashovers. A photo of the gap with 15 cm electrodes is also shown in Fig. 2.

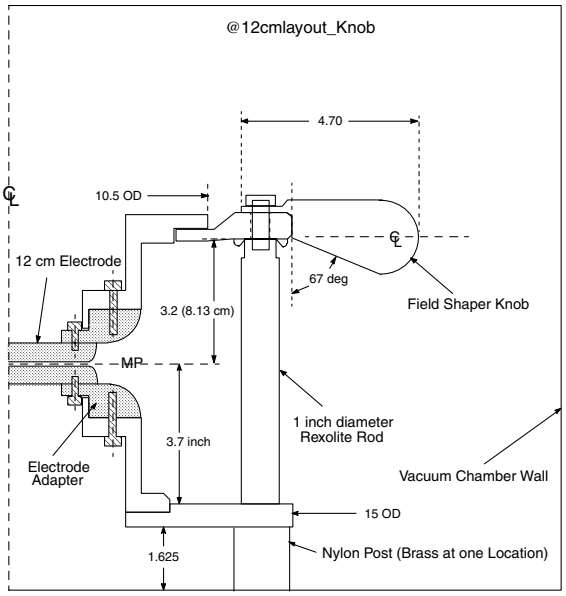

Figure 2. A layout of the high voltage test support assembly with adapters for 8, 12, and 15-cm-diameter electrodes as located in the vacuum chamber. The dimensions are indicated in inches.

The surface R_a of the electrodes varied from 0.05 to 3 μm and was measured with a Qualitest, TR100, surface-roughness tester. Diamond polishing gave R_a ~ 0.05 μm, and 2000 grit silicon carbide sandpaper R_a ~ 0.08 μm. The E-fields calculated with the Electro [39] computer code for 5 to 6.4 mm gaps with 12-cm-diameter electrodes are shown in Fig. 3. The calculations show the E-field enhancement at ~ 5.3 cm radius that occurs when the gaps are opened beyond 5 mm. The E-field is reduced in similar manner in this region when the gap is closed below 5 mm.

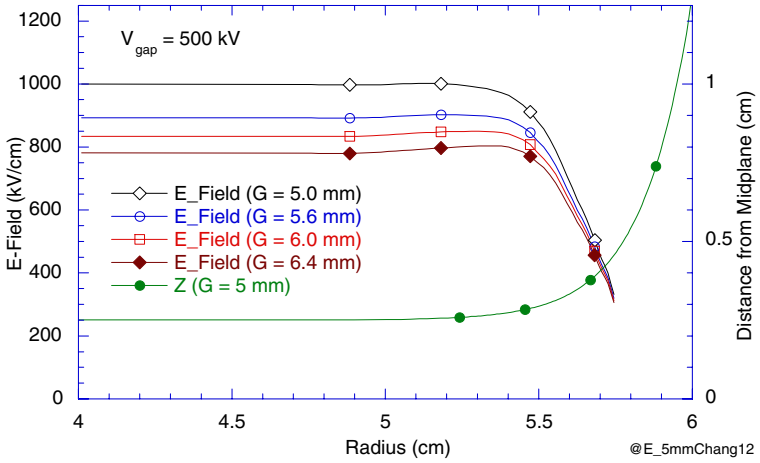

Figure 3. Numerically calculated E-Fields for 5-mm-gap Chang curves assuming an applied voltage of 500 kV, The Chang curve shape is shown by the green curve.

A schematic of the electrical circuit of the cable pulser system is shown in Fig. 4. The voltage was supplied by a Pulsar Company, TG-125 pulser, with max. voltage of 88 kV, discharged through four 104-ns-duration 50 Ω cables. The voltage is doubled by a linear induction voltage adder, LIVA, that utilized a 4-inch-thick,13-inch-diameter, 0.3 V-s metglass core. The LIVA core was reset with 12 A DC current supplied though a 100 μH isolation inductor. The circuit generates a 250-ns-FWHM square pulse with maximum voltage of 300 kV at the vacuum chamber interface. A 35 μH ring-up coil in the chamber increases the voltage to 500 kV with ~ 175-ns-FWHM 1-cos(ωt) shape. The voltage on the 0.1 μF, TG125 capacitor, decays with τ = 1.3 μs, set by the 13 Ω NaCl load resistor.

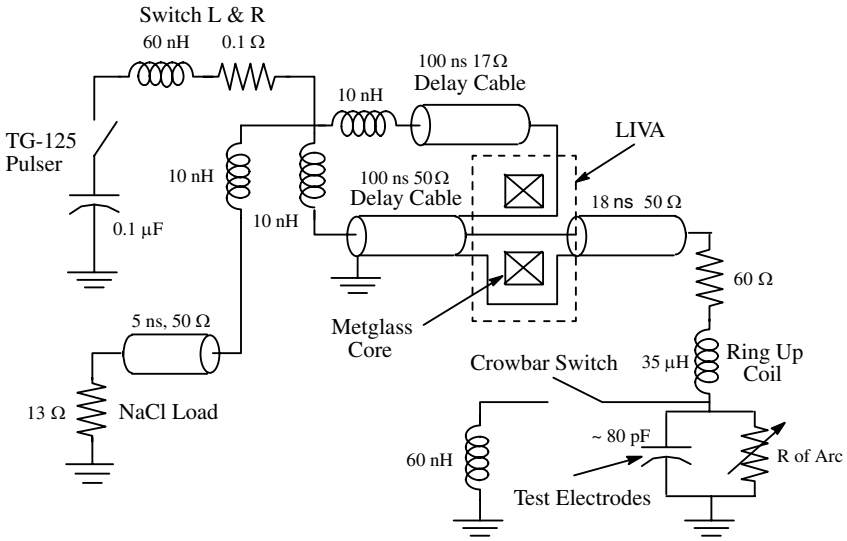

Figure 4. A schematic of the cable pulser circuit.

The multiple reflected pulses were terminated with a self-break gas crowbar switch. The shorted crowbar switch terminated the oscillating pulse in the cable via the 60 Ω series resistor. The pulser circuit evolved over the course of the experiment. During the first year we did not have the LIVA or ring-up coil. Therefore some of the initial experimental testing the Z-protocol electrodes was made with a square 210-ns-FWHM 165 kV maximum voltage pulse. The clean air tent was added the second year during our tests of the 12-cm-diameter EBEST electrodes. The LIVA was added the last year of the LDRD for the 12 cm EBEST stainless steel, 15 cm aluminum, and 17 cm stainless steel electrode tests.

The electrical diagnostics are illustrated in Fig. 5. The current measured at the post was the combination of currents in the AK-gap and the dielectric support rods. The post Rogowski's and dB/dt loop had 1.5 to 7 ns L/R times that were numerically corrected. The monitor signals were integrated with 1 ns response time passive RC integrators with τ = 1 μs that was numerically droop corrected. The diode dV/dt monitor was recorded directly and used to determine the displacement current in the diode. The gauge of the voltage monitor was corrected for changes in distance to the cathode flange which changed with AK-gap. This current was of similar amplitude to the measured current because of the ~ 80 pF AK-gap capacitance. The discharge current was determined from the difference between the AK-gap Rogowski current and the displacement current. The diode voltage measurements were determined accurate to ± 2% by calibrations against a resistive voltage monitor. The voltage on the TG-125 pulser was set to a precision 0.1 kV with a digital meter and determined accurate to ± 0.5% by comparisons to electrostatic voltmeters. The current monitors were calibrated to an accuracy of ± 5% on short circuit shots against the Ion Physic current monitor. Photographs of the vacuum chamber, electrode-support assembly with ring-up coil, clean air tent, and blower fan and HEPA filter are shown in Fig. 5.

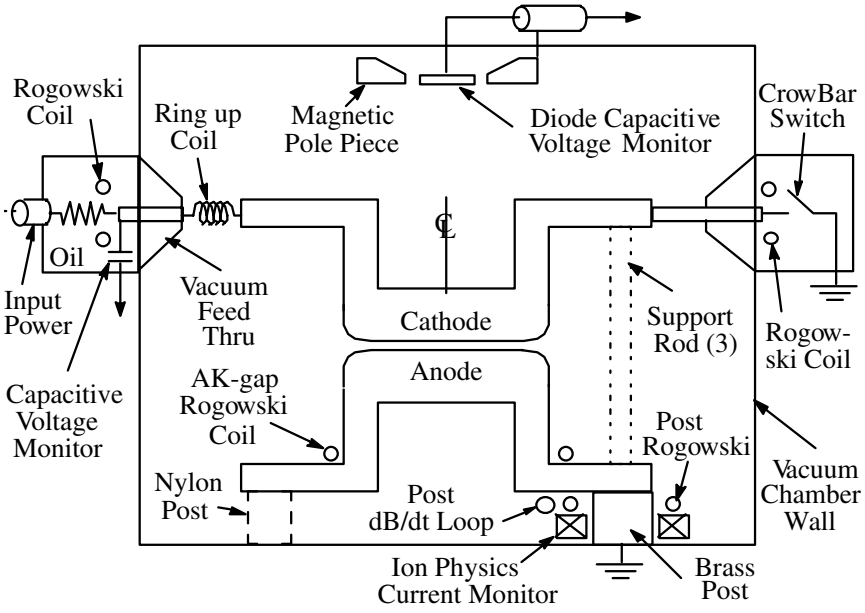

Figure 5. A schematic of the electrical diagnostics.

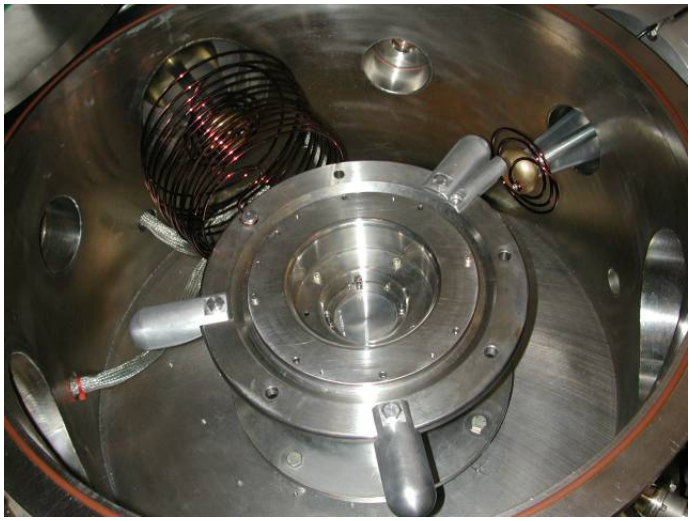

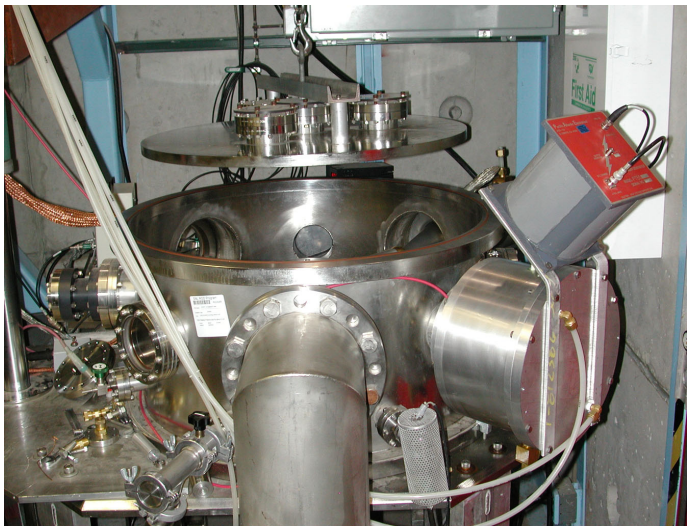

Figure 6. Photographs of the high voltage test stand and filtered air systems. (top) The interior of the test stand vacuum chamber showing the electrode support hardware, ring up coil, and vacuum feed thru's. (center) The vacuum chamber, (lower left) Top view of filtered air tent showing the HEPA filter and blower fan. (lower right) Side view of the filtered air tent showing the point of entry.

III. Russian EBEST Contract

A contract was established with Dr. Dmitry Proskurovsky's group at the Institute of High Current Electronics (IHCE), Tomsk, Russian Federation to treat stainless steel electrodes that we could test to verify their reported factor of two increase [40] in HV hold-off using EBEST. It was felt that EBEST could be an alternative to the Z-protocol process used on the final convolute hardware for the Z-generator that must be replaced every shot. The SNL contract 18754 for this purpose was paid for by SNL Research Foundations and International Programs funds.

The IHCE 2 μs-duration e-beam is transported to the treatment sample in a Penning discharge plasma. The e-beam voltage and energy density is sufficient to melt the surface to a depth of ~ 5 μm. The contract required IHCE to install an turbo-molecular pumping system on their facility to make their vacuum system oil free and comparable with SNL testing systems. SNL supplied a Pfeiffer Vacuum Components 6-inch-inlet, 250 l/s, turbo-molecular pumping system to IHCE. The system, which included valves and a roughing pump, was purchased from Applied Vacuum Industries, GmbH, Sargans, Switzerland. Import to Russia was handled by GeoLogistics. Alexandria, Virginia. The IHCE EBEST facility with the Pfeiffer pumping system is shown in Fig. 7.

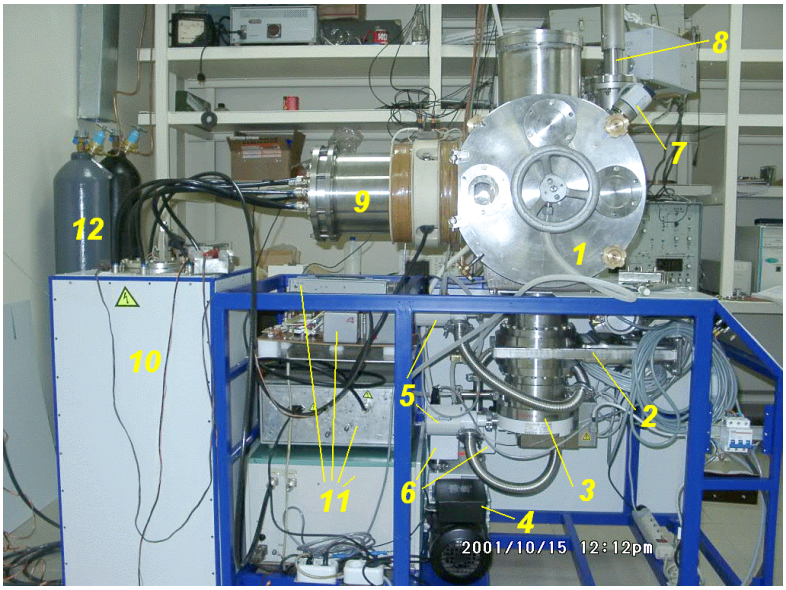

Figure 7. View of the Russian IHCE electron beam treatment installation. *1* – vacuum chamber; *2* – HV gate valve; *3* – turbo drag pump, *4* – rotary pump; *5* – vacuum valves; *6* – oil mist filter and condensate separator; *7* – compact full range vacuum auge; *8* – mass-spectrometer for residual gas analysis; *9* - e-gun; *10* – high voltage pulse generator; *11* – power supplies and control units of e-gun, *12* – pure argon bottle.

We desired to test the hold-off for EBEST treated stainless steel with a range of dielectric inclusion present near the surface. Therefore we specified that IHCE treat 4 types of stainless steel electrodes: 1.) 304L rod stock, 2.) 304L plate stock, 3.) hydrogen vacuum furnace fired, (HVFF) 304L plate stock, and 4.) 316L SCQ rod stock electrodes. Rod stock electrodes sectioned perpendicular to the rod axis possess the greatest number of near surface carbon and sulfur inclusions. The inclusions are more abundant with rod stock material because more grain boundaries, which harbor the inclusions, intersect the surface. The high density of grain boundaries occurs when the rod is drawn and the grain boundaries are stretched along the axis. With rolled plate the grain boundaries are stretched parallel to the surface, thereby reducing the number of boundaries that intersect

the surface. This reduces the number of exposed inclusions near the surface by 10. The HVFF process reduces the number of inclusions by another factor of 10. Finally 316L SCQ stainless steel has an order of magnitude less inclusions than 304L.

The contract was amended to include titanium ion implantation plus EBEST to 304L plate stock electrodes after discussions with Dr. Proskurovsky in Tomsk during a Nov. 2001 visit. The titanium beam was known to increase the conductivity of inclusions by several orders of magnitude and expected to further reduce. Initially five 2-cm-diameter, 3-mm-thick samples of each type were sent to IHCE for EBEST and SEM and AES analysis. Because their electron beam was ~ 8 cm diameter they designed and installed the manipulating stage shown Fig. 8 to allow them to treat 12-cm-diameter electrodes.

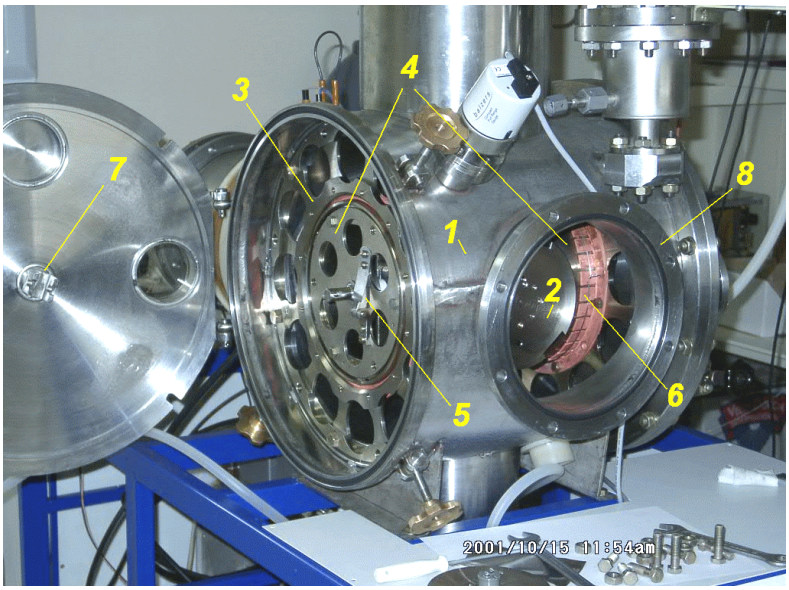

Figure 8. Russian mechanism of positioning electrodes under the treatment. *1* – vacuum chamber, *2* – specimen holder, *3* – stator, *4* – rotor, *5* – ratchet mechanism, *6* – current tap, *7* – drive shaft, *8* – specimen loading port.

The electrodes sent to IHCE were manufactured by Gull Group [38]. These included sixty 8-cm-diameter (12 of each category) electrodes for preliminary EBEST and evaluation with their 220 kV, 60-ns-FWHM pulser. The remaining sixty electrodes were12 cm in diameter, which was the largest they could treat in their EBEST chamber. These electrodes were returned to SNL and evaluated for HV breakdown with fresh EBEST surfaces. All the electrodes were shipped to IHCE in Lucite shipping containers filled with argon gas. The results of these hardware developments, tests, and treatments were reported to SNL in five IHCE Task Reports.

During FY2003 we established a new contract with IHCE to optimize the design of their e-beam source and treatment procedure to achieve improved EBEST. The contract calls for study of the emission sites that are responsible for low hold-off of vacuum gaps. In fulfillment of the contract they designed and built a needle-anode-scanning probe to analyze the properties of separate emission sites over a stainless steel surface. The contract also specifies that the group install filtered air environments around their treatment and HV test stands. They plan to correlate the observed pre-emission sites with actual breakdowns that occur with their HV pulser.

IV. Z-protocol Electrode Data

Our preliminary experiments in FY 2001 were with the Z-protocol electrode treatment processes and did not use the LIVA or filtered clean air. The results were documented in the 20th IEEE ISDEIV [42]. The Z-protocol processes are the individual and combined treatment processes for 304L rod stock stainless steel that are used for the final convolute section hardware of the Z-accelerator. The electrode preparation processes were combinations of the following: 1.) Solvent clean with 200 proof ethyl alcohol using paper delicate laboratory wipers. The electrodes were buffed with the wipers to remove the few minor streaks from the alcohol cleaning. 2.) Electro polish at 200 A-min/ft^2 for one minute. This removes 5 μm of stainless steel. 3.) Hydrogen fire at 1000 °C for 30 minutes with Argon purges of vacuum furnace before and after at 800 °C. 4.) Gold coating - deposit 15 nm of chromium followed by 3 μm gold by sputter physical vapor deposition. The Z-protocol used to treat parts for the final MITL convolute section of the SNL Z-accelerator is a combination of preparation steps 1, 2, 3, and 4. The electrodes tested were 18 cm diameter and 3 cm thick. Because of the Chang curve the effective diameter was ~ 17 cm. The surface R_a was specified to be 0.4 μm.

Typical waveforms for shots without crowbar or AK-gap discharge are shown in Fig. 9 and illustrate how the circuit operated with and without the ring-up coil. The diode voltage measurements were determined accurate to ± 1% by calibrations against a resistive voltage divider and comparisons to SNL SCREAMER [43] code circuit analysis calculations shown as dotted curves in Fig. 9. The crowbar was set to trigger at about 180 ns on the time scale of Fig. 9. The crowbar impedance was sufficiently high on the second pulse to allow measurement of short circuit AK-gap arcing on many shots that did not show initial arcs. This was an indication of the HV conditioning process.

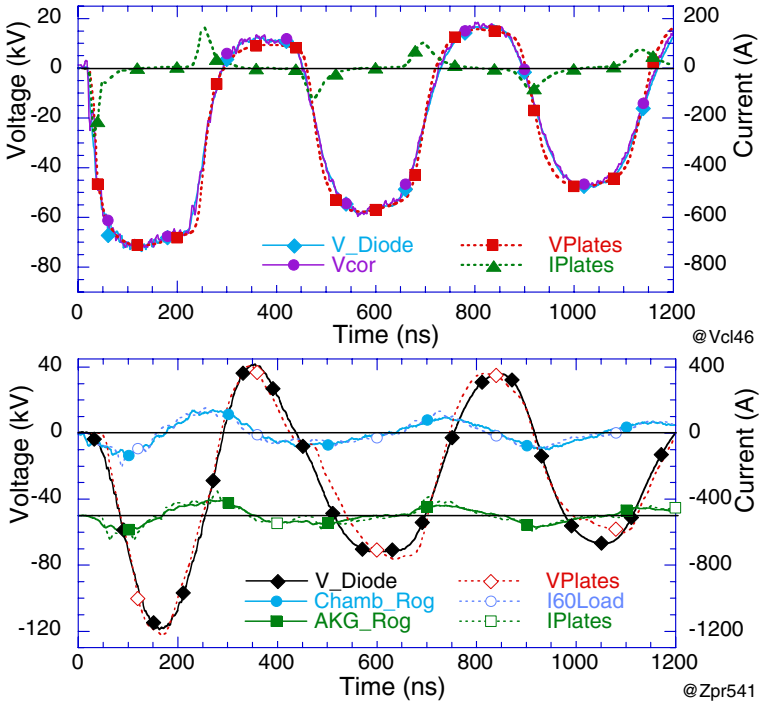

Figure 9. The diode voltage and current from the pulser circuit without (upper) and with (lower) ring-up coil. Data were acquired with 40 kV charge on the pulser and 3.8 mm AK-gap without crowbar circuit. Dotted curves were calculated with the SCREAMER circuit analysis program.

Results

Typical data for a breakdown shot with precleaned 304L electrodes are shown in Fig. 10. This shot was fired with the flat voltage pulse achieved without ring-up coil. The breakdown current is fit to space-charge-limited current (Child-Langmuir), ICL, in a model with a linearly closing gap and increasing emission area from one cathode spot. One cathode spot was assumed because anode photographs taken before and after shots only showed one damage spot. This model serves to assess differences between electrode preparations and gives an indication of the evolution of cathode plasma. We ignore the fact that the anode reaches T = 500 C in ~ 20 ns after the onset of a typical discharge. Liberated gas would then form an anode plasma and transition the emission to bipolar flow. With the flat pulse the breakdown current increased to 1.2 kA if the breakdown began early in the pulse. The advantage of beginning tests at low voltage and slowly increasing the E-field in subsequent tests is that minor cathode whisker explosions occur harmlessly and condition the electrodes for increased fields. Often these conditioning shots showed no observable AKG current during the primary pulse but short circuit AKG current on the reflected pulse even when the crowbar circuit fires. This was an indication of conditioning and occurred because the crowbar switch impedance increased to > 1 Ω between pulses.

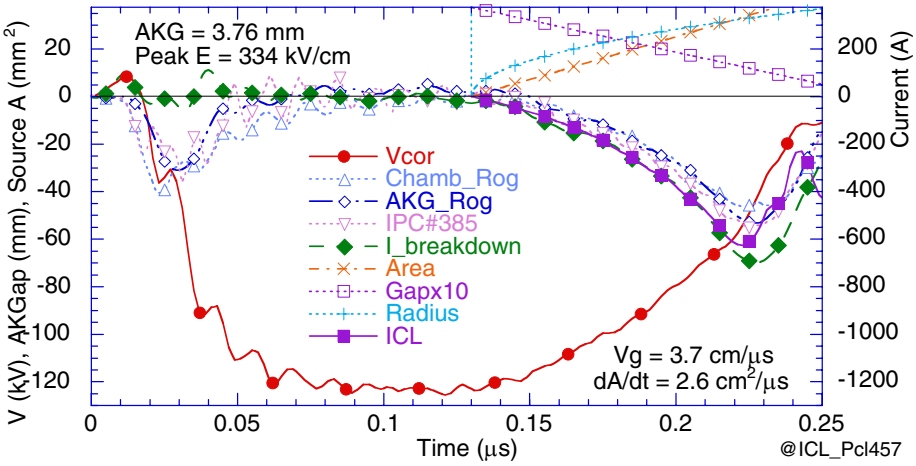

Figure 10. Electrical data for flat pulse shot Pcl457 with solvent cleaned 304L electrodes. The size of the gap and area for the ICL fit are plotted with square and × symbols. The crowbar circuit did not fire, as was often the case with breakdowns at early or middle times.

Data for a series of shots for the pre-cleaned only and Z-protocol are shown in Fig. 11. The data show a peak E-field of ~ 500 kV/cm for both preparations and that an occasional breakdown occurred as the fields were increased. When a major arc occurred near maximum voltage it was necessary to clean the electrodes to get similar results on later shots. It is speculated that severe arcs deposited chunks of debris that could be wiped off the cathode. It was rare for two arcs to occur in the same area because apparently the high temperature of the arc melts debris near the arc. Eventually a large arc would occur that permanently damaged the cathode and negated the effects of cleaning, however.

The data for a shot with the 1-cos pulse is shown in Fig. 12. The displacement current measured during the rise of the voltage pulse is ~ 150 A and the breakdown current ~ 240 A. The cathode plasma expansion rates are similar to the flat pulse shots indicating that the plasma expansion rate is set at the time of cathode whisker explosion. The data for a series of shots acquired with pre-cleaned and Z-protocol using the 1-cos pulse are shown in Fig. 13. Note that the peak hold-off E-fields are ~ 700 kV/cm with these tests. The fields are higher because the peak voltage duration is shorter. The data illustrate the non-reproducible nature of the breakdowns. There is a tendency for the Vgap to be slightly higher at higher breakdown E-fields. We do not understand why the Z-protocol tests with the 1-cos pulse show more breakdowns than the flat pulse. However it was noted that cleaning the gold surfaces with alcohol often improved reproducibility and hold-off significantly. This was the case even when the normal procedure of blowing all visible dust from the surfaces was followed during installation into the test apparatus.

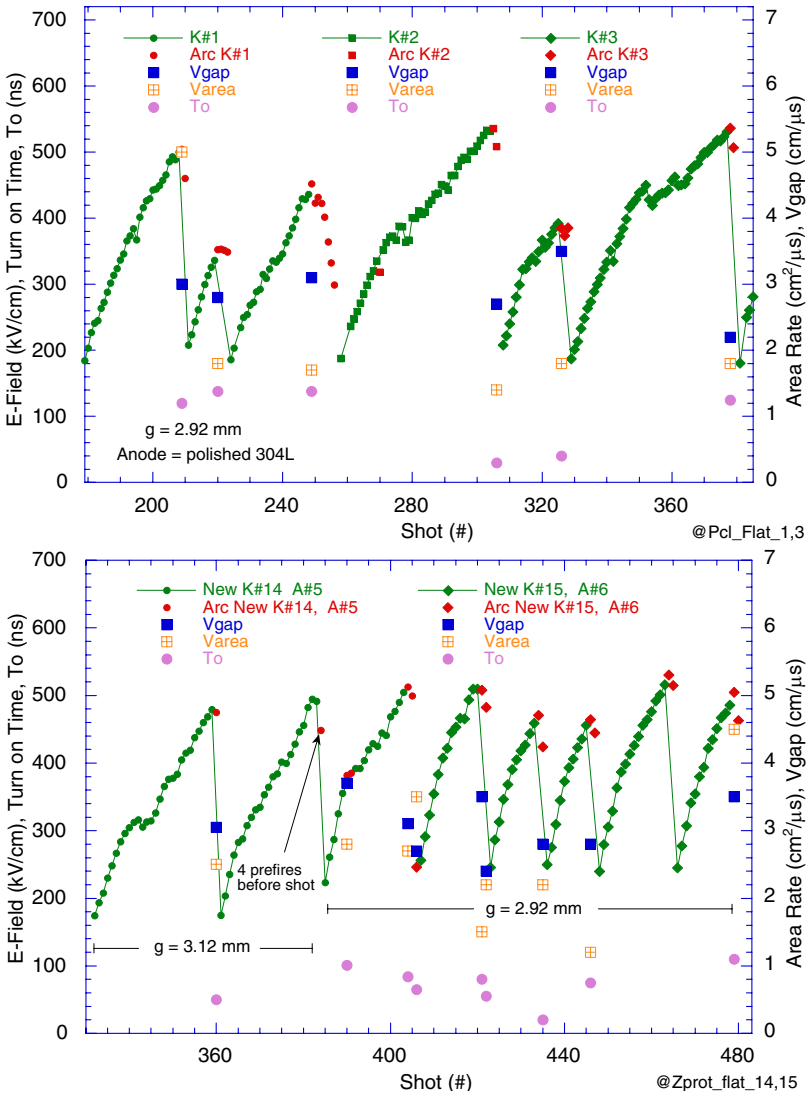

Figure 11. Breakdown data (closed symbols no arc, open arc) together with plasma area, Varea, closure rates, Vgap, and turn on time, To, for shots with solvent precleaned (upper) and Z-protocol (lower) treated electrodes using the square-wave voltage pulse.

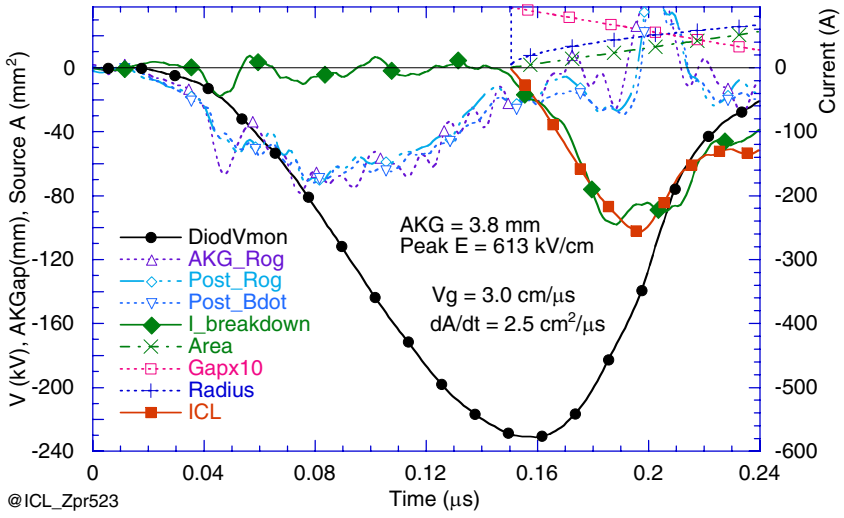

Figure 12. The electrical and ICL fit data for a shot with Z-protocol 304L electrodes. The test pulse was a 1-cos(ωt) shape.

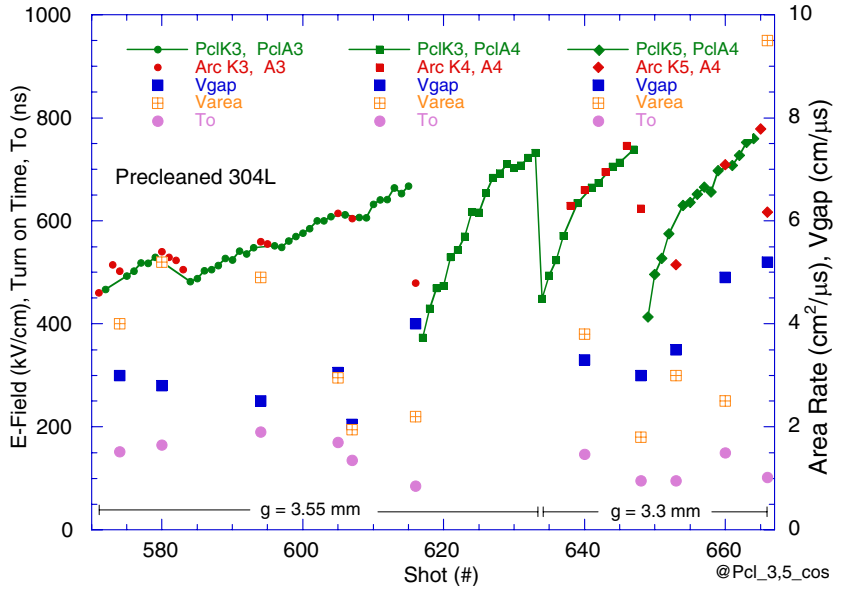

Figure 13. Breakdown E-field thresholds together with plasma area expansion and closure rates for shots with solvent precleaned (upper) and Z-protocol (lower) treated electrodes using the 1-cos(ωt) voltage pulse. See Fig. 10 for details.

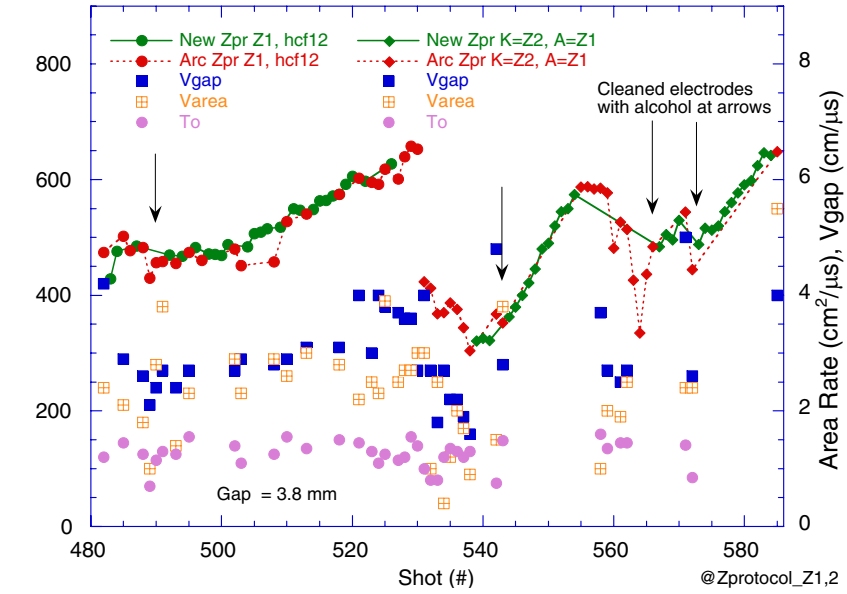

The results of tests with different preparations are shown in Fig. 14. The mean 1st breakdown E-field and highest E-field without breakdown together with the mean FWHM for the highest E-fields are shown above the ICL fit data graph. The results show that R_a = 0.4 μm finish 304L electrodes showed no significant improvement in E-field hold-off or reduction in the nominal 3 cm/μs gap closure rate when subjected to the treatments tested. More data will be necessary to determine this conclusively because of the small differences, however. We observed that careful surface cleaning, just before installing the electrodes in the test chamber, was an important method of increasing hold-off. Perhaps wiping with the delicate paper pads removed small amounts of dust or minor imperfections on the 1-μm-roughness surfaces.

A limited number of shots were fired with the ring-up coil and peak voltages ~ 200 kV to assess the first shot hold-off of solvent cleaned, hydrogen fired, and Z-protocol 304L stainless steel electrodes. Breakdowns typically occurred at 350 to 400 kV/cm for these preparations. These tests resulted in electrode damage that prevented further useful tests.

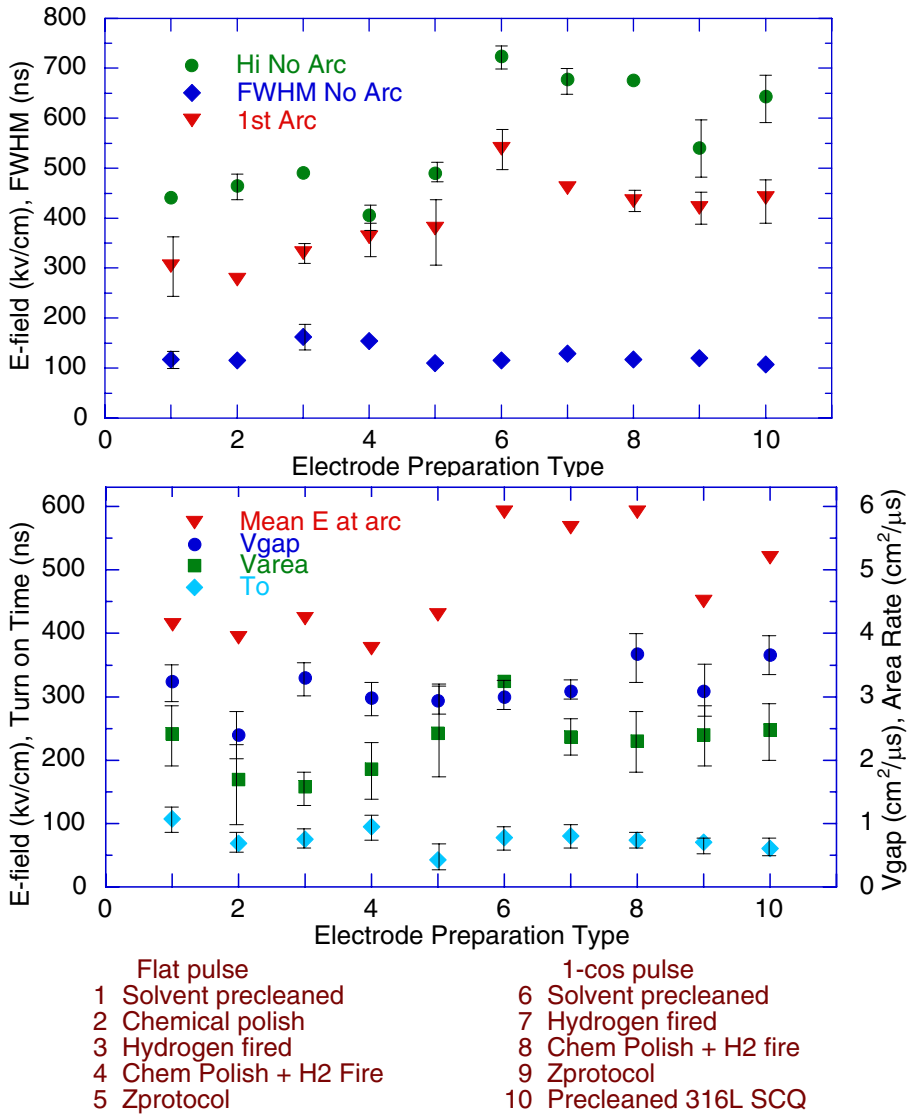

Figure 14. Summary of the data from various surface preparations on 304L, except for #10 on 316L stainless steel. See text for details. (upper) Average E-fields for 1st breakdowns and without breakdowns. The error bars are ± the standard deviation divided by #shots$^{1/2}$ for 3 or 4 shots. Errors smaller that 10% are not shown. (lower) The average ICP fit data. The error bars are ± the standard deviation for 7 to 49 shots. The To begins at 20 and 80 ns for the flat and 1-cos pulses, respectively.

V. 8 cm EBEST Stainless Steel Electrode Tests

We high voltage retested many of the 8-cm-diameter stainless steel electrodes that were given EBEST at the IHCE, Tomsk, RF. The principle investigator for the treatment and high voltage testing at IHCE was Dr. Alexander Batrakov. We repeated his tests to determine how sensitive the electrical breakdown was to previous arc mark damage and to make a comparison of results with our 165 ns FWHM 1-cos(ωt) pulse to the IHCE 60 ns square pulse. The method of treatment and result of these tests were reported by Proskurovsky [44]. The SNL and IHCE measurement were made using laboratory air during cleaning and installation into the vacuum chambers. The breakdown data and photos of the electrodes and surface features presented in this section illustrate how arc marks are the result of electron beam melting similar to EBEST and do not degrade performance if the precaution is taken to remove loose debris after a severe arc.

The E-beam parameters for the treatment were 25 kV, 20 kA, 2 μs, and ~10 J/cm^2. The number of pulses on the front and edge surfaces of each electrode was 60. The electrodes were rotated at 1.132 rpm and shots fired every 10 seconds. Six electrode pairs of 304L rod, 316L-SCQ rod, 304L plate, and HVFF (Hydrogen Vacuum Furnace Fired) 304L plate were E-beam treated. In addition six pairs of 304L plate electrodes were E-beam and ion implantation treated [44]. The ion implantation was performed with a 50 kV, 0.1 A, 200 μs titanium beam operated at 50 Hz. The titanium beam area was 500 cm^2 so the entire electrode surface area was treated at the same time. All electrode pairs were HV-tested with a 220 kV, 60-ns-FWHM square pulse. The E-field was varied by changing the anode-cathode gap. The Chang curves for these electrodes were for a 3 mm gap.

Electrodes for the EBEST were ordered and shipped to IHCE in two sets. The first set of 44 electrodes were labeled 1/# and the second #. The following chart denotes the labeling for the different electrode types tested. The HVFF and four 304L plate electrodes used for ion implantation were shipped in a Lucite container filled with 1 atmosphere argon. We retained nine 304L and 316L rod electrodes from the first order and two 304L plate electrodes from each order for comparison testing.

First shipment	Electrode #	Second shipment	Electrode #
Ion Imp 304L plate	1/1 to 1/8	HVFF 304L plate	1 to 12
304L plate	1/9 to 1/20	Ion Imp 304L plate	13 to 16
304L rod	1/21 to 1/32		
316L rod	1/33 to 1/44		

The average surface roughness, R_a, is important parameter of HV hold-off. The following chart gives the experimental R_a before and after E-beam treatment measured at SNL with a Qualitest TR100 surface roughness tester. The results are the average of seven scans of 6-mm-long regions along a diameter. The 304L rod stock electrodes varied from 0.02 to 0.22 μm roughness because some were machined and others polished after machining. Although the 304L plate electrodes were purchased in two orders they were made from the same material lot. The second order is labeled S2 in Table 1.

Stainless Steel Material	Machined R_a (μm)	EBEST R_a (μm)	Crater Density (mm^{-2})
304L Rod	0.120 ± 0.07	1.46±0.26	10
304L Plate (S1)	0.188 ± 0.02	0.37±0.07	1
HVFF 304L Plate (S2)	0.193 ± 0.02	0.3± 0.2	0.1
Ion Imp 304L Plate (S1,2)	0.193 ± 0.02	0.25, 0.45	0.5
316L Rod	0.366± 0.07	0.57±0.08	5

Table 1. Roughness and crater density of EBEST stainless steel electrodes.

The roughness data for individual EBEST electrodes are shown in Fig. 15. The data show an increase as expected for EBEST. The increase is about a factor of 10 for the 304L rod and only 50% for the 316L rod stock electrodes. There are some inconsistencies that are hard to explain. The most important is that the second shipment EBEST surfaces appear to have a factor of two higher roughness even though we measured the initial surface to be the same.

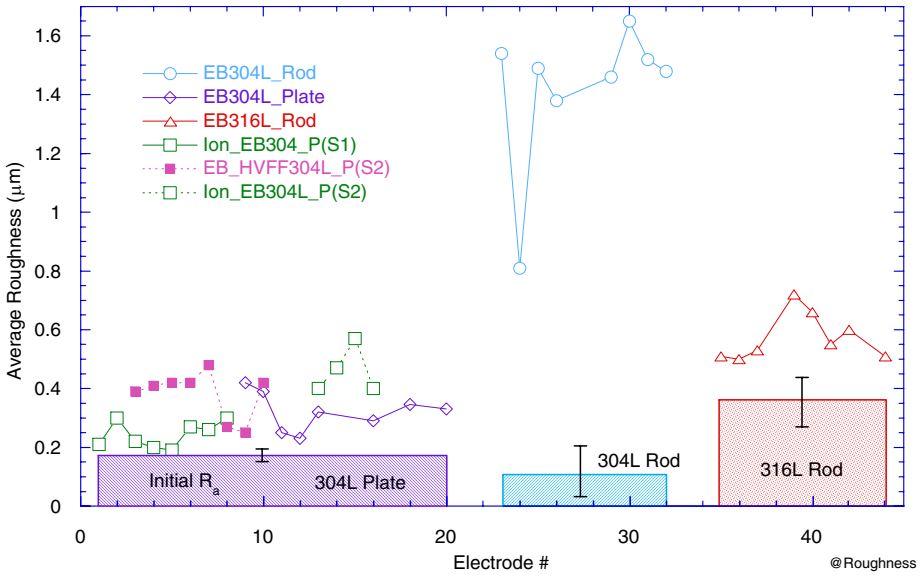

Figure 15. The average surface roughness, R_a, of the 8 cm electrodes returned from IHCE tested at SNL. The 304L plate electrode from the second order are labeled with dotted curves. The mean R_a's for untreated electrodes are indicated as boxes with cross hatches. The error bars on the boxes indicate the range of the measured R_a.

The results of IHCE and SNL HV-tests are summarized in Fig 16. Data were obtained with electrodes that showed several arc marks from the IHCE testing but < 5% of the SNL tests showed breakdown initiating from previous arc marks. Therefore the SNL HV tests should be fairly reliable. The only significant disagreement between the SNL and IHCE results is for the ion implantation. We did not see a difference with the 0.75, 1.5, and 3 hour ion beam implantation treatment. Also we did not observe that the ion implantation improved the results for EBEST only on 304L plate. We observed that it was very important to clean the electrodes with solvent very carefully before testing. A vigorous 2-minute cleaning with acetone and Kimwipes often gave a 20% improvement.

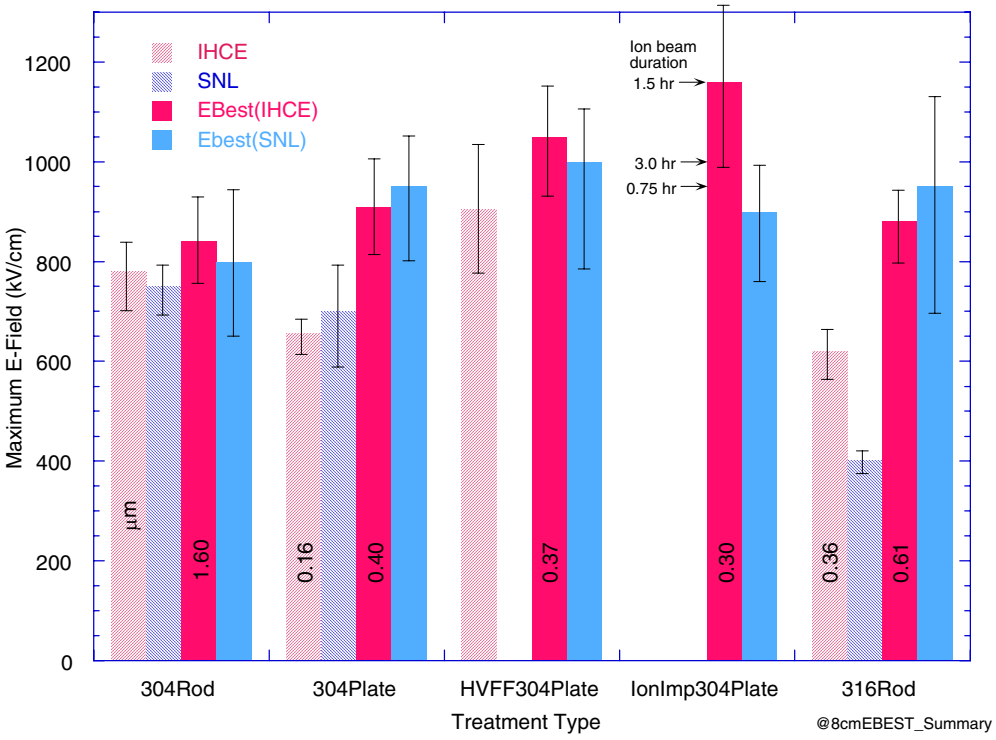

Figure 16. A summary of the test results before and after E-beam treatment of stainless steel electrodes. The SNL ion implantation results are the average of 0.75, 1.5 and 3 hr ion treatments with no consistent better results at 1.5 hr.

Data were acquired with a140-ns-FWHM 1-cos(ωt) voltage pulse generated with 20 µH ring-up coil and no LIVA. The peak voltage could be varied from 60 to 260 kV with 1% accuracy. The gap was ~ 2.25 mm and planar to ± 0.02 mm for most shots. Most shots had the crowbar trigger near the end of the principal pulse or at beginning of the first reflected pulse. The highest E-field achieved by IHCE and SNL for the cathodes tested are plotted in a Fig. 17.

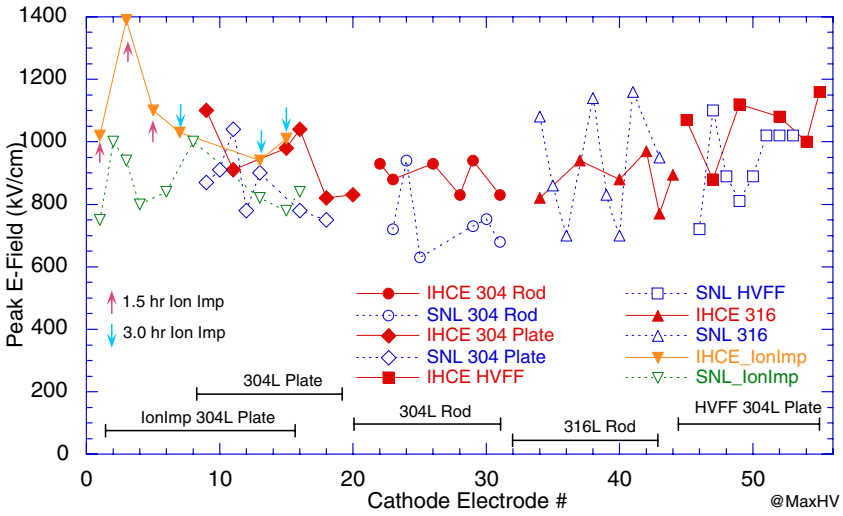

Figure 17. The highest E-field reached by IHCE and SNL versus cathode number.

The results for untreated electrodes are shown in Fig. 18. Note that the 304L rod and plate stock electrodes held 700 to 800 kV/cm after the voltage was progressively increased during conditioning. The 316L electrodes (blue) held only ~ 400 kV/cm, presumably because of the rougher surface which was machined in a saw-tooth pattern.

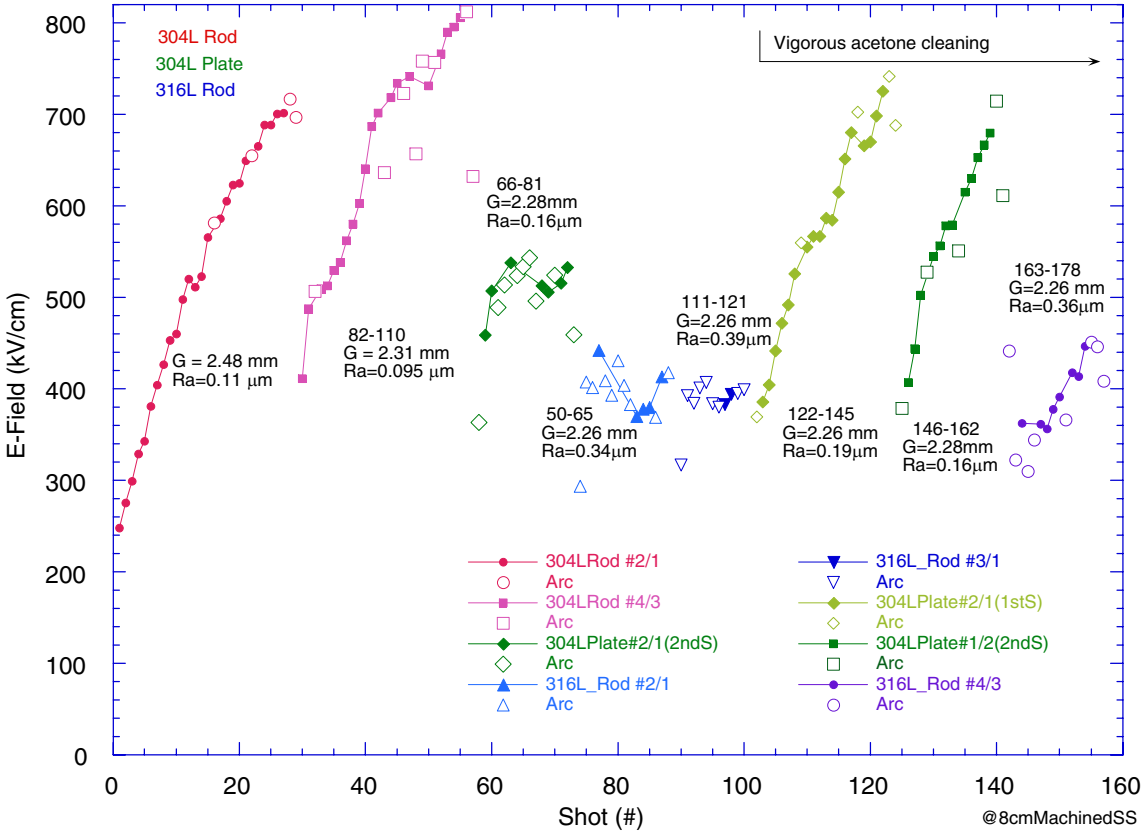

Figure 18. The HV-test results for various machined stainless steel electrodes. The shots that held the voltage pulse without arcs are indicated as closed symbols. Many of the arcs with very little voltage drop below the mean value were minor conditioning arcs that caused no visible damage to the electrodes. The numbers near the data are the shot numbers, AKG spacing, and average roughness, Ra. The electrode numbers are indicated after the electrode description in the legend, with the number of the cathode/anode.

Data for EBEST electrodes are shown in the figures below followed by photos of the electrode surface before and after EBEST. The data for 304L rod stock is shown in Fig. 19. The results were similar for the treated and untreated surfaces. Here the large roughness increase from the numerous craters produced by the EBEST on 304L rod stock electrodes may have prevented an increase in HV hold-off. Note that the initial surface roughness was extremely good for these electrodes because they were polished by the manufacturer, Gull Group [38], in California. Apparently the good hold-off characteristics of the EBEST treated surfaces avoided a decrease in hold-off even though the EBEST caused the roughness to increase by a factor ~15. Vigorous cleaning with acetone began on shot 729 (shot 122 for untreated electrodes) and only improved the hold-off of cathode #1/24 which had only a factor of 8 increase in roughness.

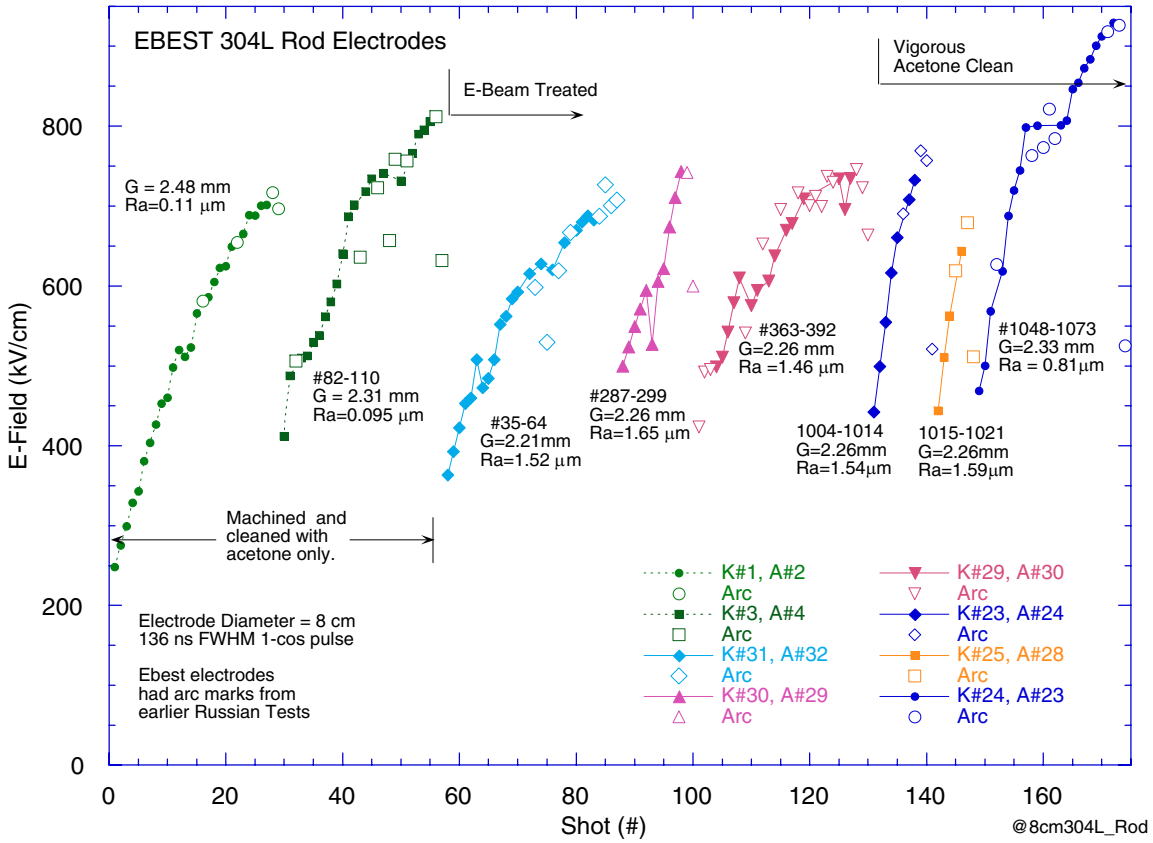

Figure 19. The HV-test results for machined (dotted) and EBEST (continuous) 304L rod stock stainless steel electrodes. Photographs of 304L rod electrodes before (lower left) and after EBEST treatment (lower right). The EBEST photograph is from electrode 1/31. The typical crater density of this type electrode was 10/mm^2.

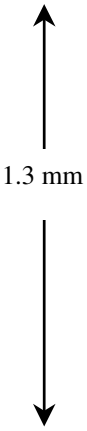

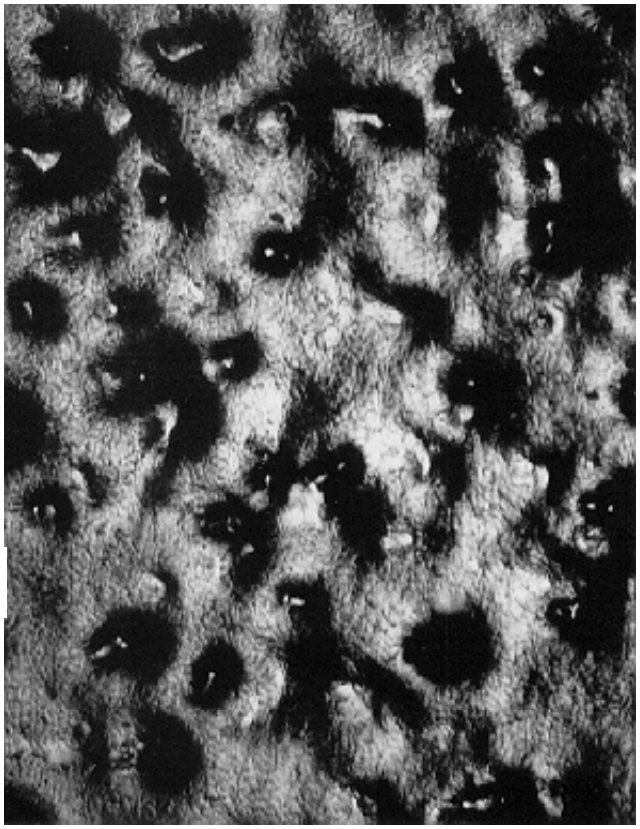

Photographs of 304L rod electrodes #1/30, 1/29, 1/24, and 1/23 are shown in Fig. 20. The photos show the speckled surfaces typical of the EBEST 304L rod electrodes. Apparently the many inclusions in 304L rod are able to more easily produce the craters via propagation of gas released from the inclusions along grain boundaries during EBEST. It is thought that the grain boundaries are preferentially stretched along the axis of the rod when the rod stock is drawn. For this reason we also chose to test 304L plate stock because the grain boundaries are elongated parallel rather that perpendicular to the surface in this case. Cathode #1/24 has a factor of two lower roughness than the other EBEST 304L rod electrodes and perhaps for this reason held 20% higher voltage even though it has a large number of arc marks from previous tests. The new arc mark attributed to shot 1073 occurred in a very smooth region of the cathode.

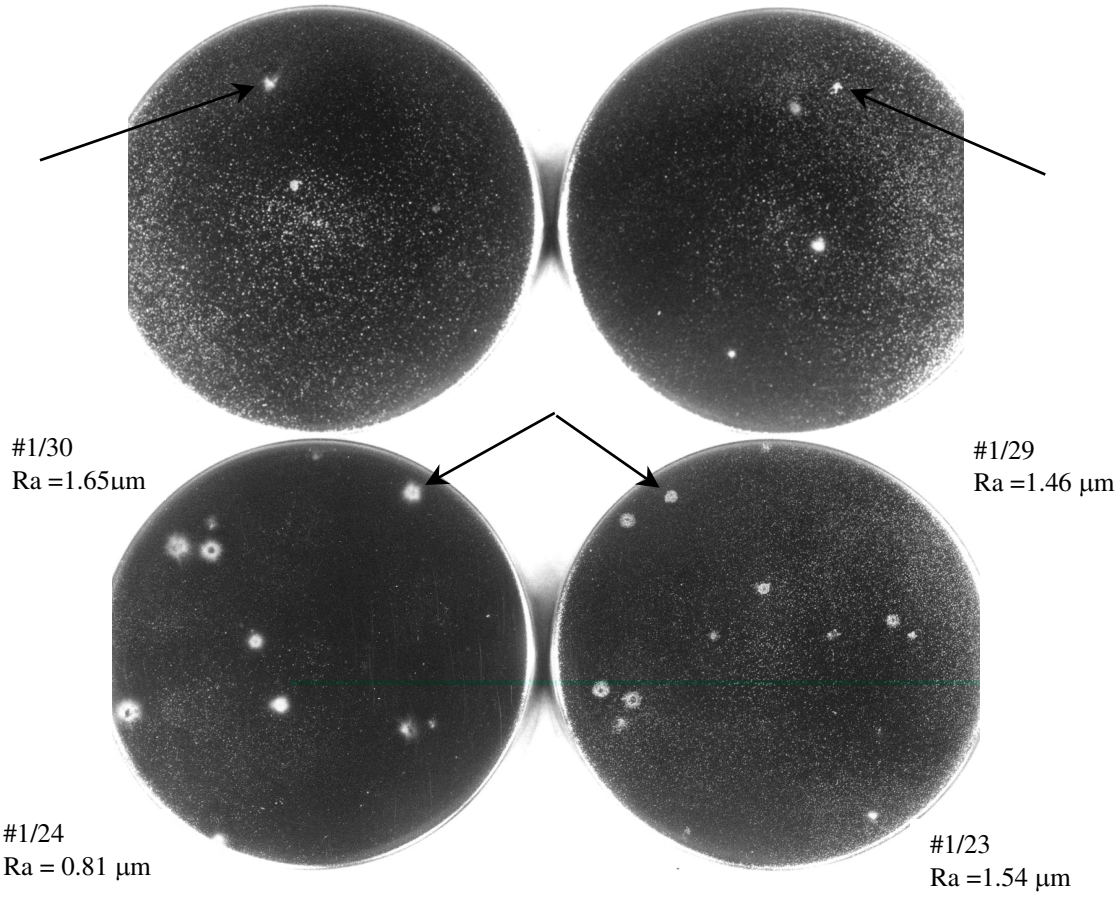

Figure 20. Photographs of EBEST 304L rod electrodes. (upper) Cathode #1/30 (left) and anode #1/29 (right) after shot 299 for magenta data series in Fig. 14. (lower) Cathode #1/24 (left) and anode # 1/23 (right) after shot 1074 from blue data series in Fig. 14. The arrows point to damage spots from the only new arc marks that were visible after the test series.

The data in Fig. 21 show the breakdown and surface microscope photographs for EBEST 304L plate electrodes. Fig. 22 upper shows microscope photos of two EBEST 304L plate electrodes. Fig. 23 shows a photograph of electrodes #1/9 and 1/10 after shot 417, the first blue test series in Fig. 21. Note that these electrodes do not show the speckled appearance of the EBEST 304L rod electrodes shown in Fig. 20.

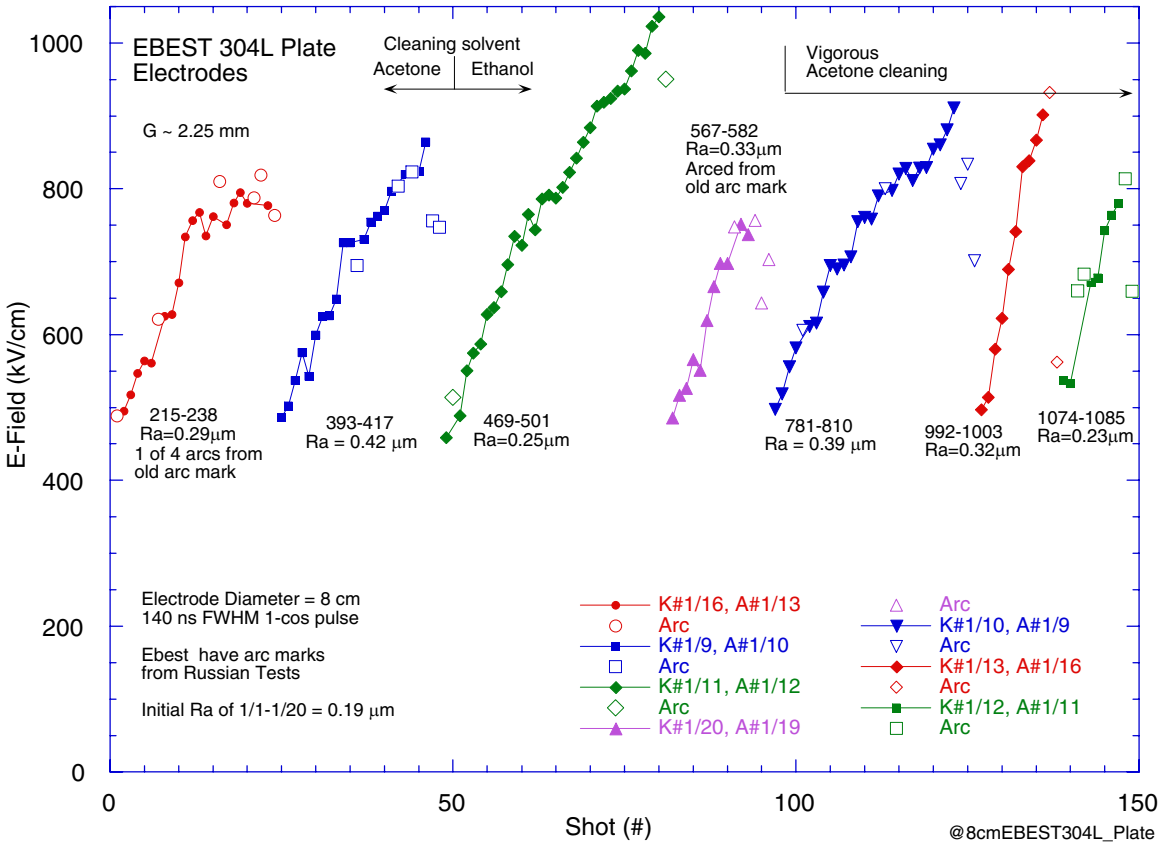

Figure 21. The HV-test results for EBEST 304L plate stock stainless steel electrodes. Microscope photographs of 304L plate electrode before (lower left) and after EBEST (right). The EBEST electrode was #1/12 with R_a = 0.23 μm. The typical crater density of this type electrode was 1/mm^2.

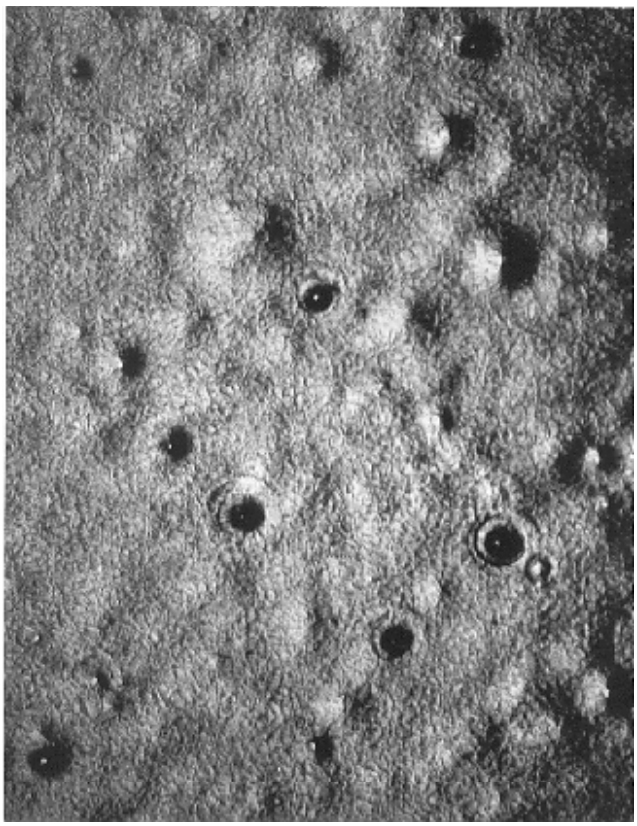

Photographs of the surface quality of two EBEST 304L plate electrodes are shown in Fig. 22 along with comparison photos for EBEST + HVFF 304L plate electrodes. The photos show typical crater densities. The electrodes illustrate the surface quality at the extreme range of roughness measured and shown in Fig. 14. Note that electrode #1/10 has a bumpy pattern not seen on electrode #1/11 and a factor of two less craters. The EBEST + HVFF electrodes have only ~ 0.1 craters/mm^2 and #10 is 40% rougher than the average EBEST + HVFF electrode.

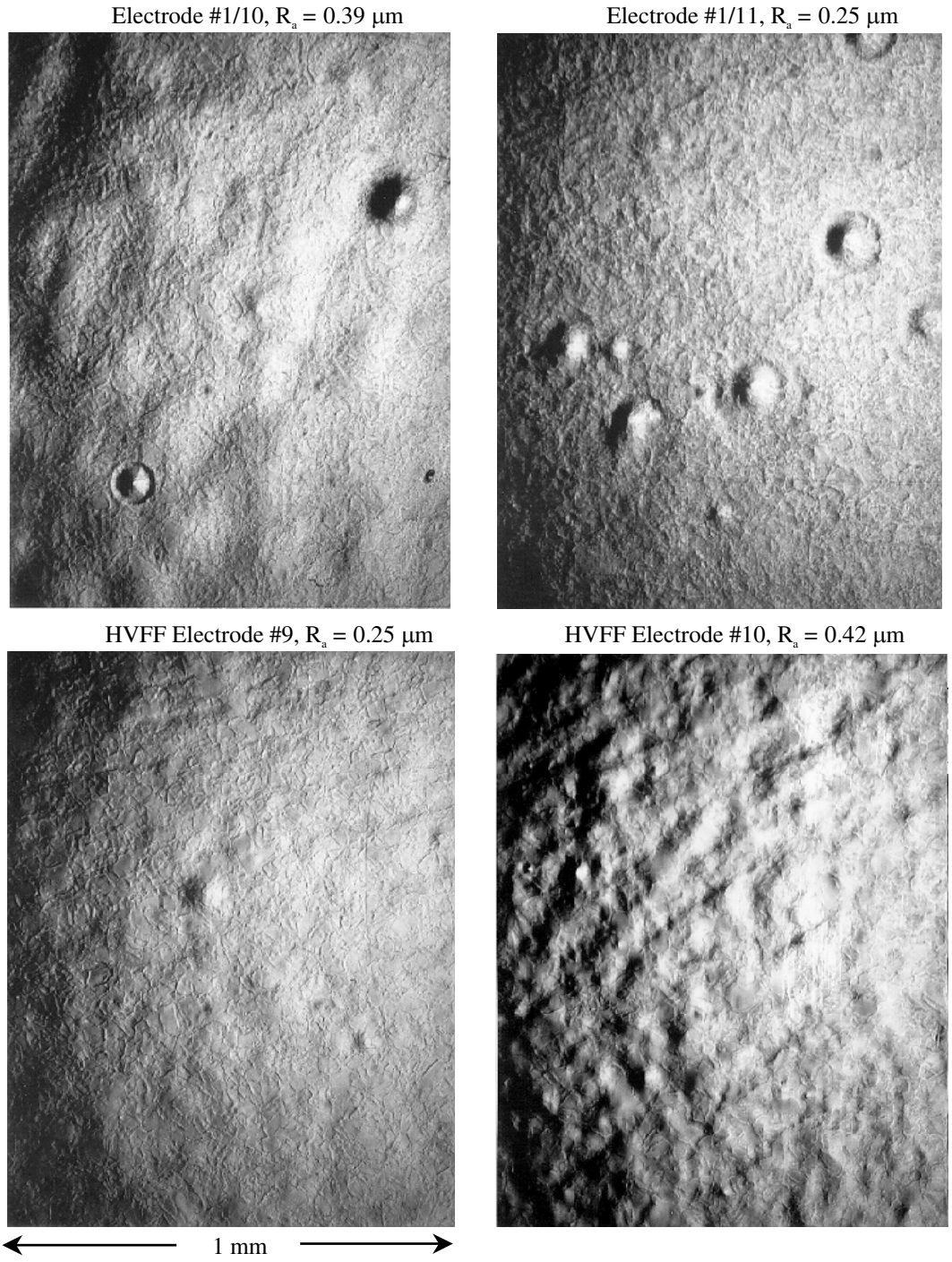

Figure 22. Surface photos of EBEST 304L plate (upper) and EBEST+HVFF 304L plate (lower) electrodes.

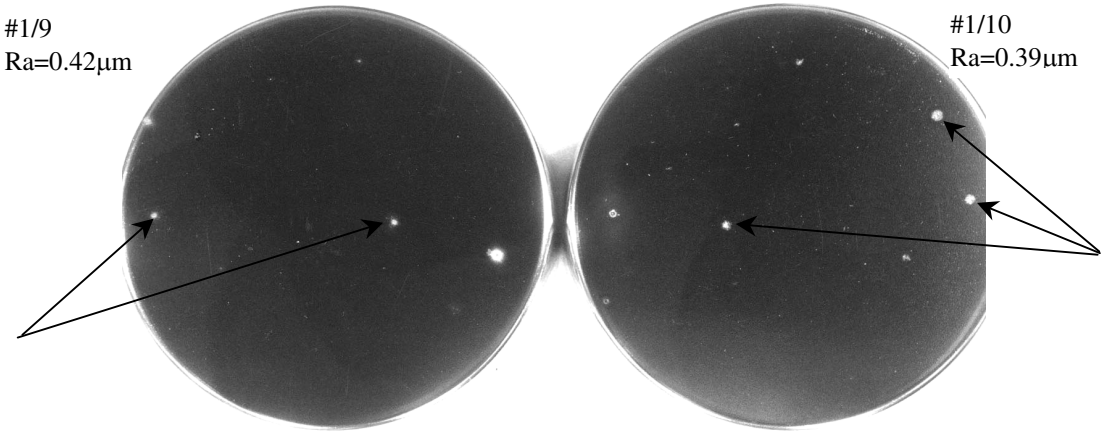

Figure 23. A photograph of EBEST 304L plate cathode #1/9 (left) and anode #1/10(right) after shot 417. This was the last shot of first blue curve data series in Fig. 19. The arrows point to damage spots from the only new arc marks that were visible.

Photographs of two interesting pairs of EBEST + HVFF 304L electrodes are shown in Fig. 24 (upper). After vigorous cleaning electrodes #4 and 3 (upper) showed only one breakdown at 1.1 MV/cm as shown in Fig. 25. It is remarkable that the scratches visible on the cathode #4 that happened during shipping from Tomsk, RF, did not initiate any arcs. Electrodes #9 and 10 (lower Fig. 24) show very severe surface dentrites that occurred during EBEST. These also did not initiate arcs.

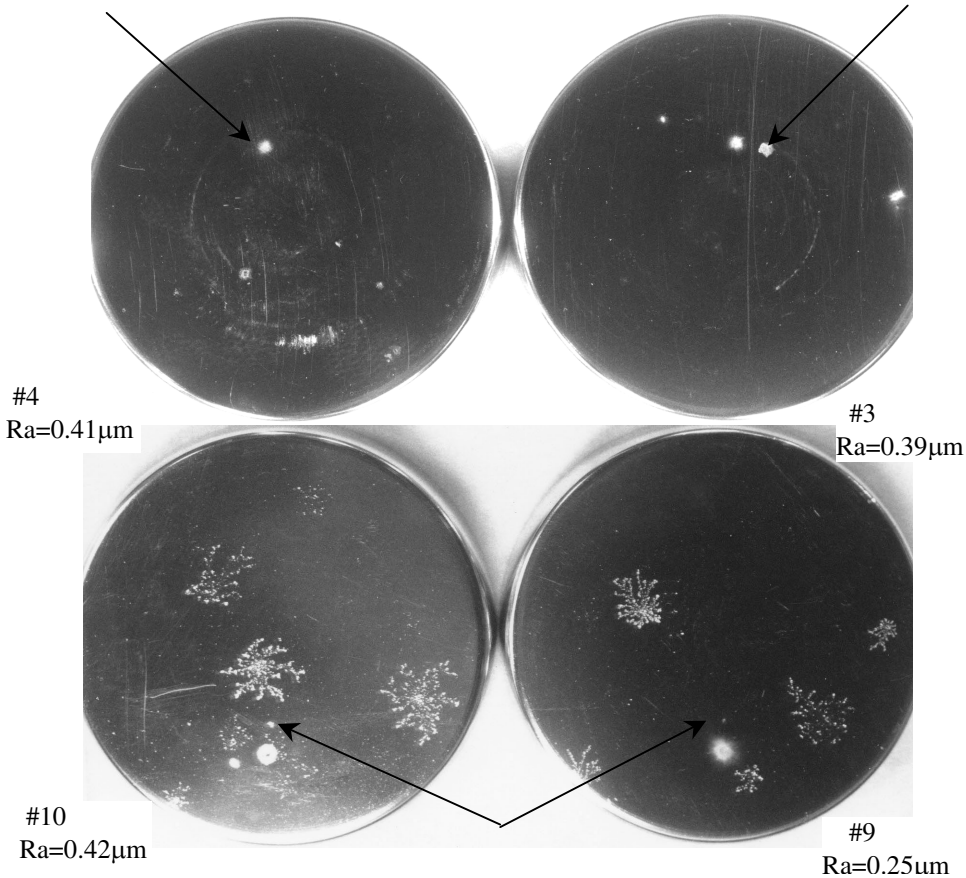

Figure 24. Photographs of EBEST HVFF 304L plate cathode #4 (left) and anode #3(right) after shot 892. Similar EBEST HVFF 304L plate electrodes #10 and #9 are shown as they appeared before shot 566 are shown below. These have surface dendrites from EBEST. Arrows point to one new arc marks on upper electrodes. The lower electrodes did not have new arc marks visible in the photo after shot 566.

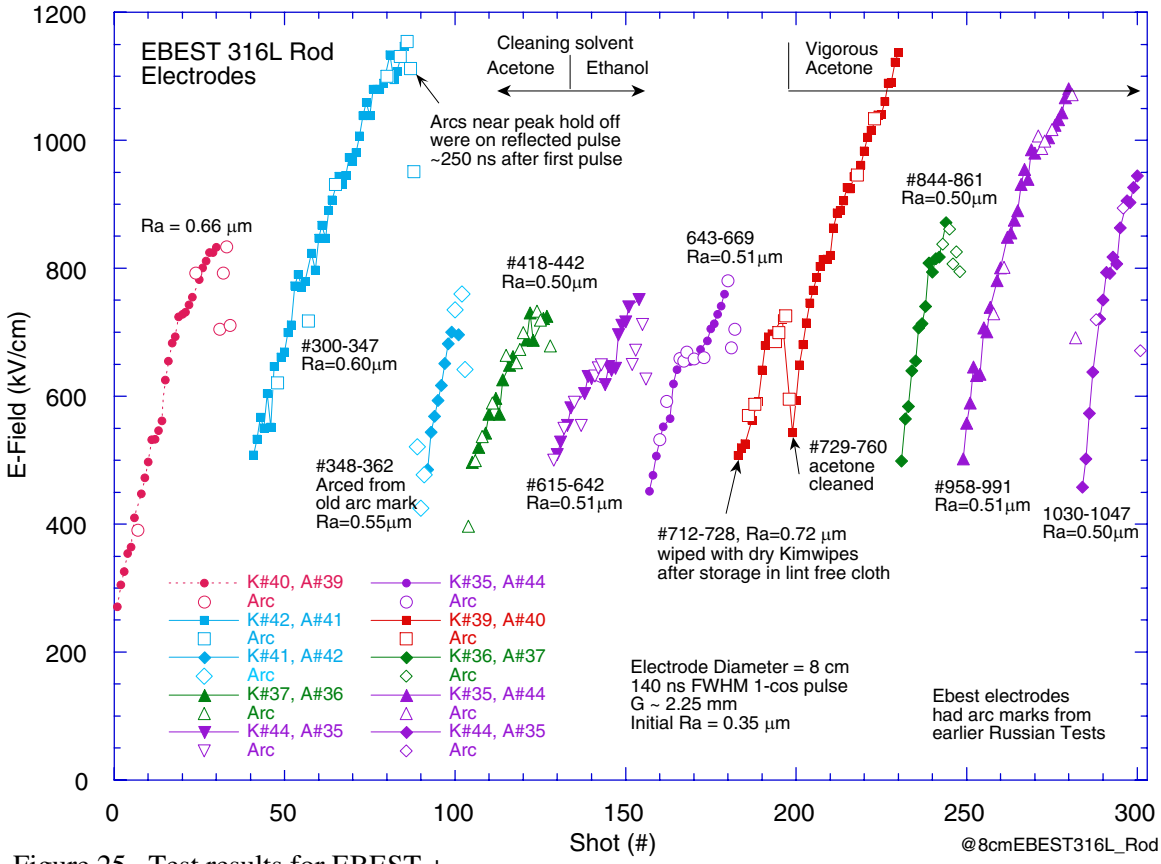

Figure 25. Test results for EBEST + HVFF 304L plate stock SS electrodes. (lower right) Photo of electrode #7 after EBEST treatment. The typical crater density was 0.1/mm^2. (lower left) Photo of a 2-cm-diameter HVFF 304L plate sample before EBEST.

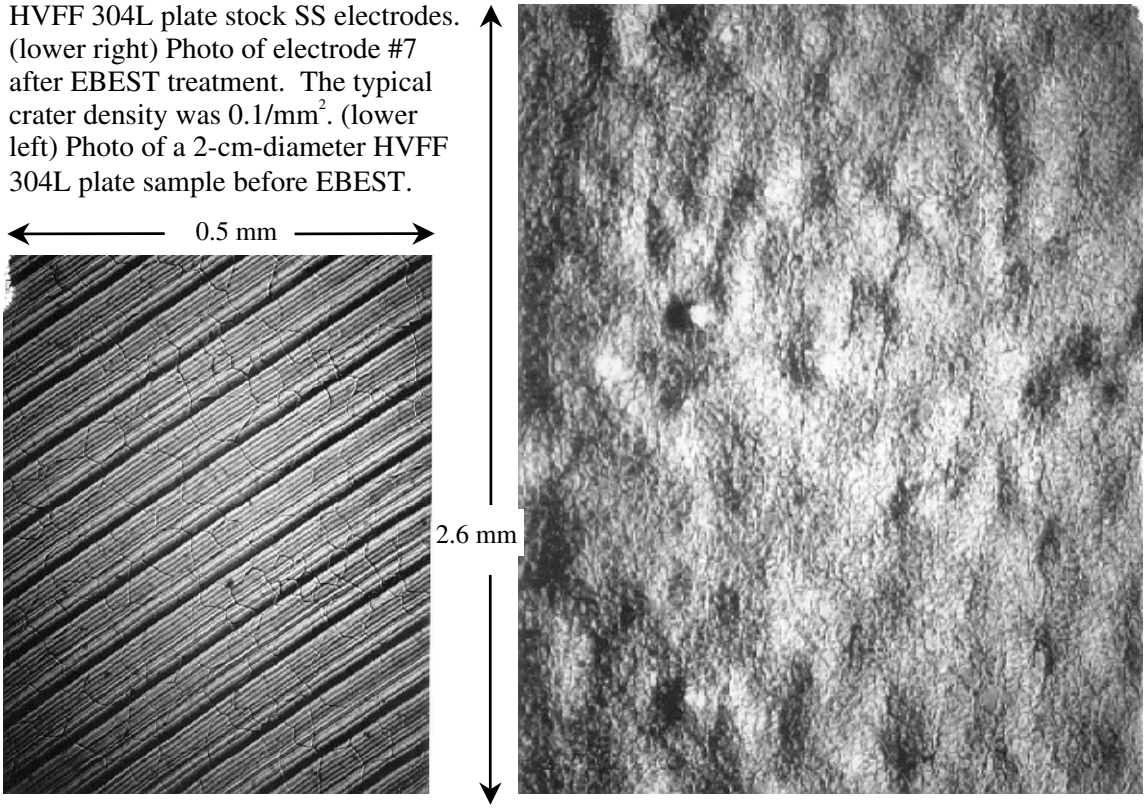

The photograph of the HVFF 304L plate sample sample in the lower left image in Fig. 25 shows the grain boundaries that are exposed during hydrogen firing. This sample was machined from the same 304L plate material lot as the EBEST electrodes. The HVFF process involves 6 steps. The steps applied to the vacuum furnace are: 1.) load the electrodes and evacuate to10^{-6} Torr, 2.) back fill with argon to 3 psi while raising the temperature to 800 °C, 3.) displace argon with hydrogen with 5 purges over 1 hr, 4) heat to 1000 °C for 30 min. (to burn off hydrocarbons), 5.) displace hydrogen with argon with 5 purges over 1.33 hr while dropping temperature to 800 °C, and 6.) evacuate to 10^{-6} Torr and cool to 40 °C over 8 hrs. The result of HVFF is to lower the carbon and raise the oxygen content near the stainless steel surface. The results of AES analysis preformed at SNL on a similar 304L plate sample are shown in Fig. 26 along with comparison data for 304L and 316L rod. We assume the initial 304L plate had a similar concentration to the 304L rod based on the experience of Diane Pebbles, Org. 1822, who acquired the data. The 304L plate data were acquired 30 minutes and 30 days after HVFF to get information on the effect of the shipment delay time to IHCE. The actual electrodes were treated ~ 60 days after HVFF but this additional time should not effect the increased penetration of the oxygen in the surface layer. The data acquired at 30 days show some increase in carbon in the front surface < 1 nm but that the concentration from1 to 10 nm is still much below the initial level. The lower carbon concentration after HVFF indicates a reduction in hydrocarbon inclusions at the grain boundaries. This reduction results in almost no craters after EBEST as shown by the EBEST surface photograph in Fig. 25.

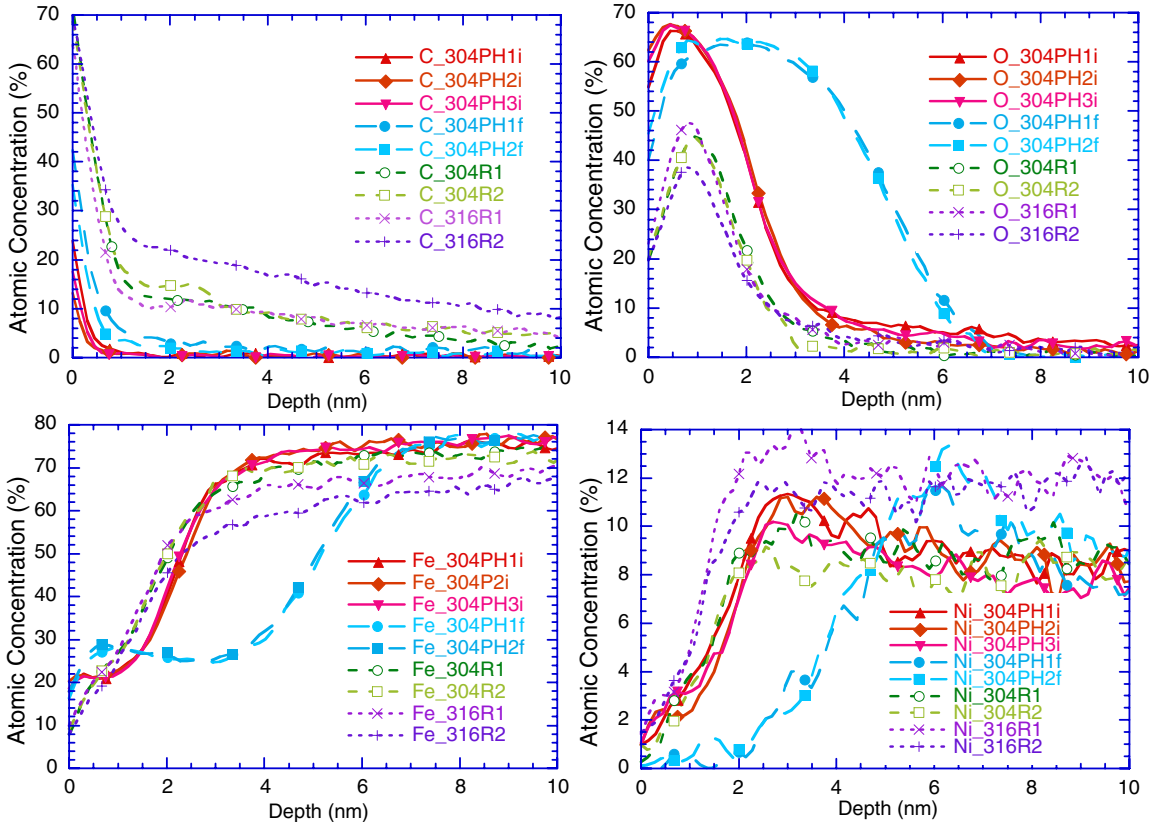

Figure 26. Auger electron spectroscopy atomic concentration results for 304L plate and rod and 316L rod stainless steel. The letters and numbers of the labels in the legends designate, element, SS type, stock (P=plate,R=rod), process (H=HVFF, blank=none), sample number, and time delay for 304L plate (i = 30 min, f = 30 days). The bulk carbon and sulfur concentration specifications for 304L and 316L stainless steel are < 0.03%.

Photographs of Ti ion implantation electrodes #16 and 13 are shown in Fig. 27. The photograph was taken after the first test series ending in shot 95 (red data in Fig. 28) There was one new set of arc marks indicated by the arrows. These electrodes were previously HV tested by IHCE after 0.75 hrs of ion implantation followed by additional implantation to give a total of 3 hrs. We chose to begin with them because they had the best physical appearance of the ion implantation electrodes we received back from IHCE. They were a part of the second shipment sent to IHCE. There is a speckled appearance to these electrodes also but it is less evident than for the EBEST 304L rod stock. We next tested #1/3 and 1/4 from the first shipment to IHCE that were implanted for 1.5 hr. They have more scratches and #1/3 has a whitish appearance that was the most pronounced of the ion implantation electrodes. These electrodes held 940 kV/cm when we repeated the test after vigorous acetone cleaning. The two arcs on the first test of these electrodes appear to originate from an arc mark on the cathode from previous IHCE testing.

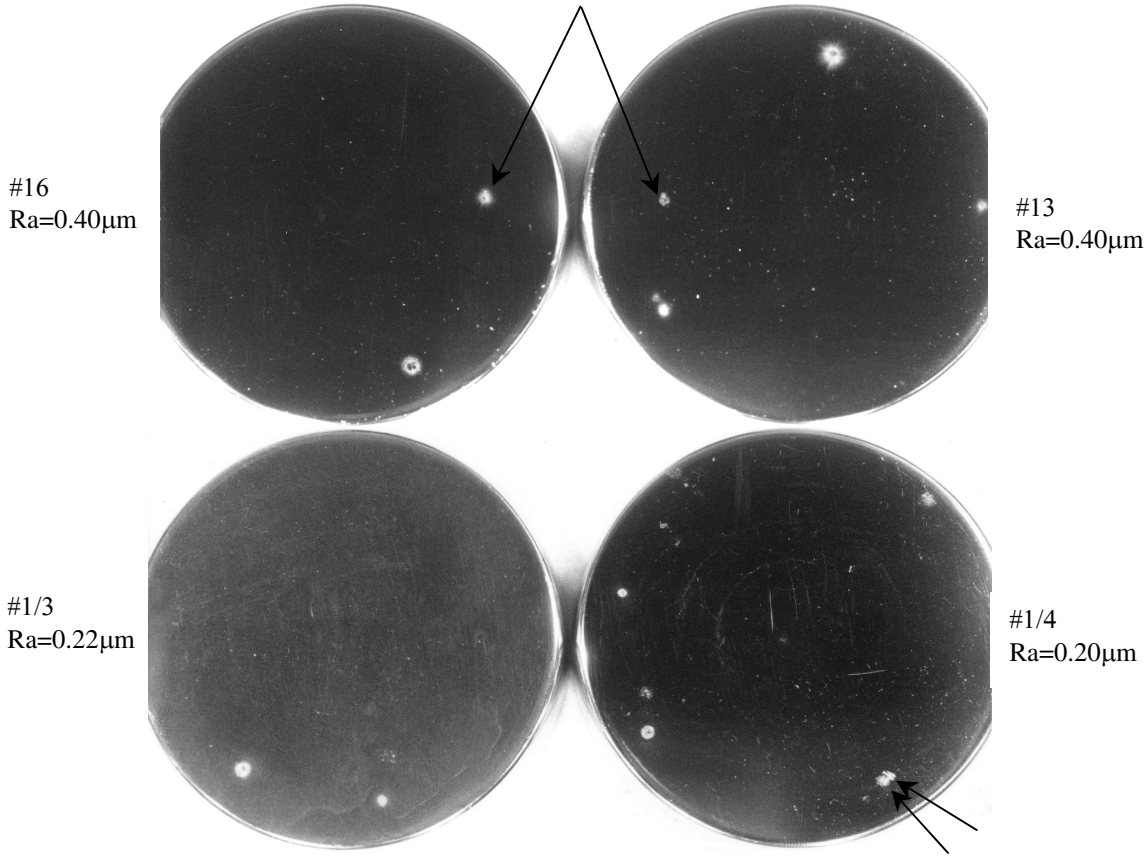

Figure 27. (top) A photograph of Ti implantation + EBEST 304L plate cathode #16 (left) and anode #13 (right) after shot 108. This was the first data series in Fig. 27 with red data points. (bottom) A photograph of Ti implantation + EBEST 304L plate cathode #1/3 (left) and anode #1/4 (right) after shot 134. This was the second data series in Fig. 27 with green data points. The arrows point to damage spots from the new arc marks.

The results of testing the Ti ion implantation electrodes are shown in Fig. 28 together with microscope photographs of the surfaces before and after treatment. Note that cathode #1/6 has a fine structure surface roughness that does not appear on the non ion implanted electrodes. Photographs of electrodes #15, 16, and 1/5 illustrate this more clearly in Fig. 29. Photographs from electrodes #1/3, 1/4, 15, and 16 are shown in Fig. 30 with higher magnification.

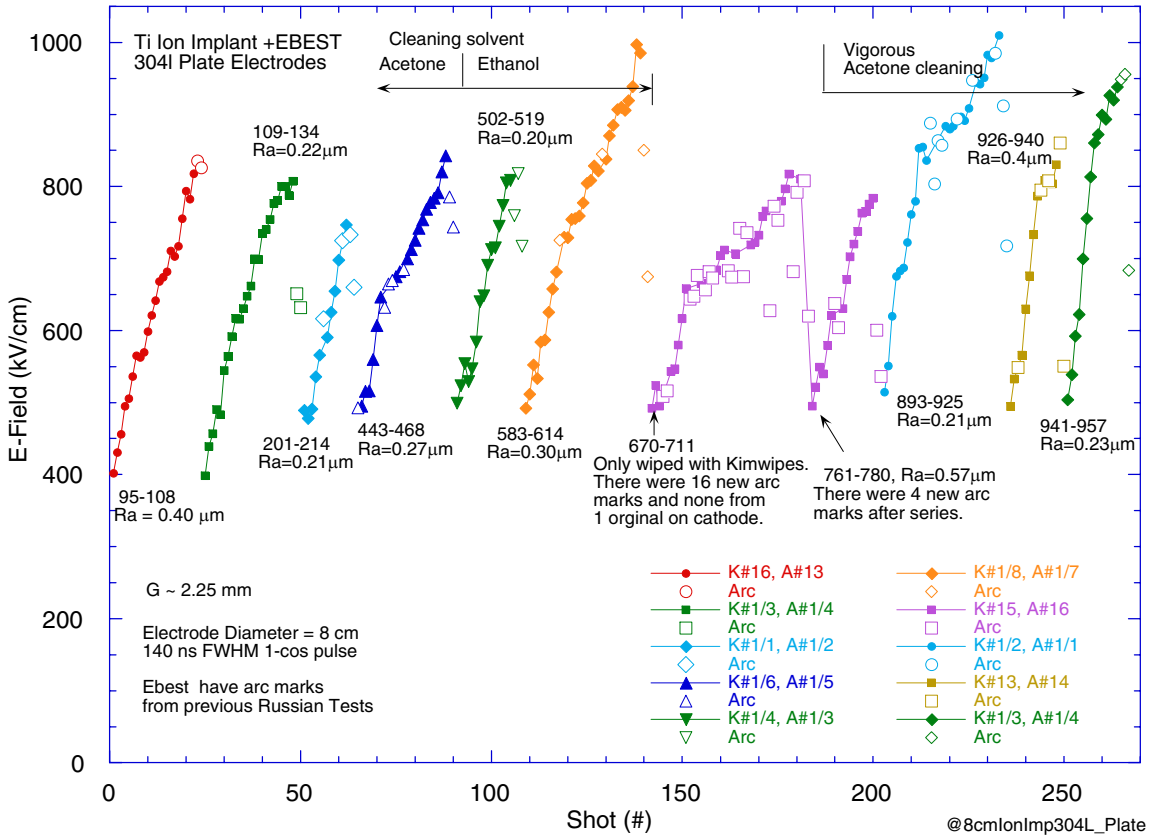

Figure 28. The HV-test results for Ti ion implantation + EBEST 304L plate stock stainless steel electrodes. Photographs of 304L plate electrodes before (lower left) and after implantation + EBEST treatment (lower rght). The photograph is from electrode #1/6. The typical crater density of this type electrode was 0.5/mm^2.

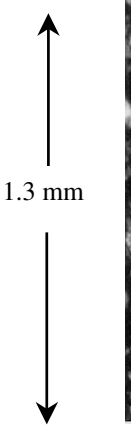

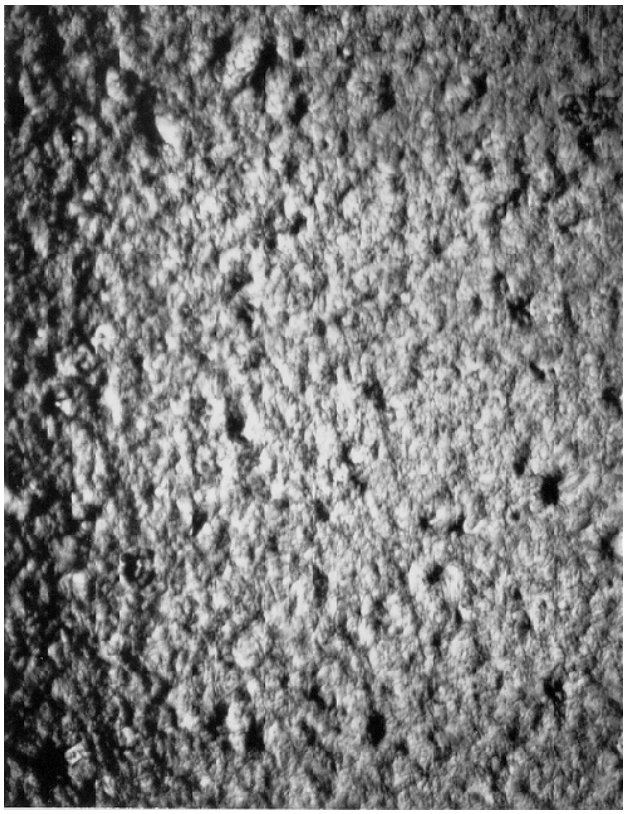

Photographs of the surfaces of three ion implantation electrodes are shown in Fig. 29 along with one photo of a medium size anode arc. The photos show the variation of surface roughness that is indicated in Fig. 15. The lower right photo is an example of an anode arc that would probably not cause a HV breakdown on later tests.

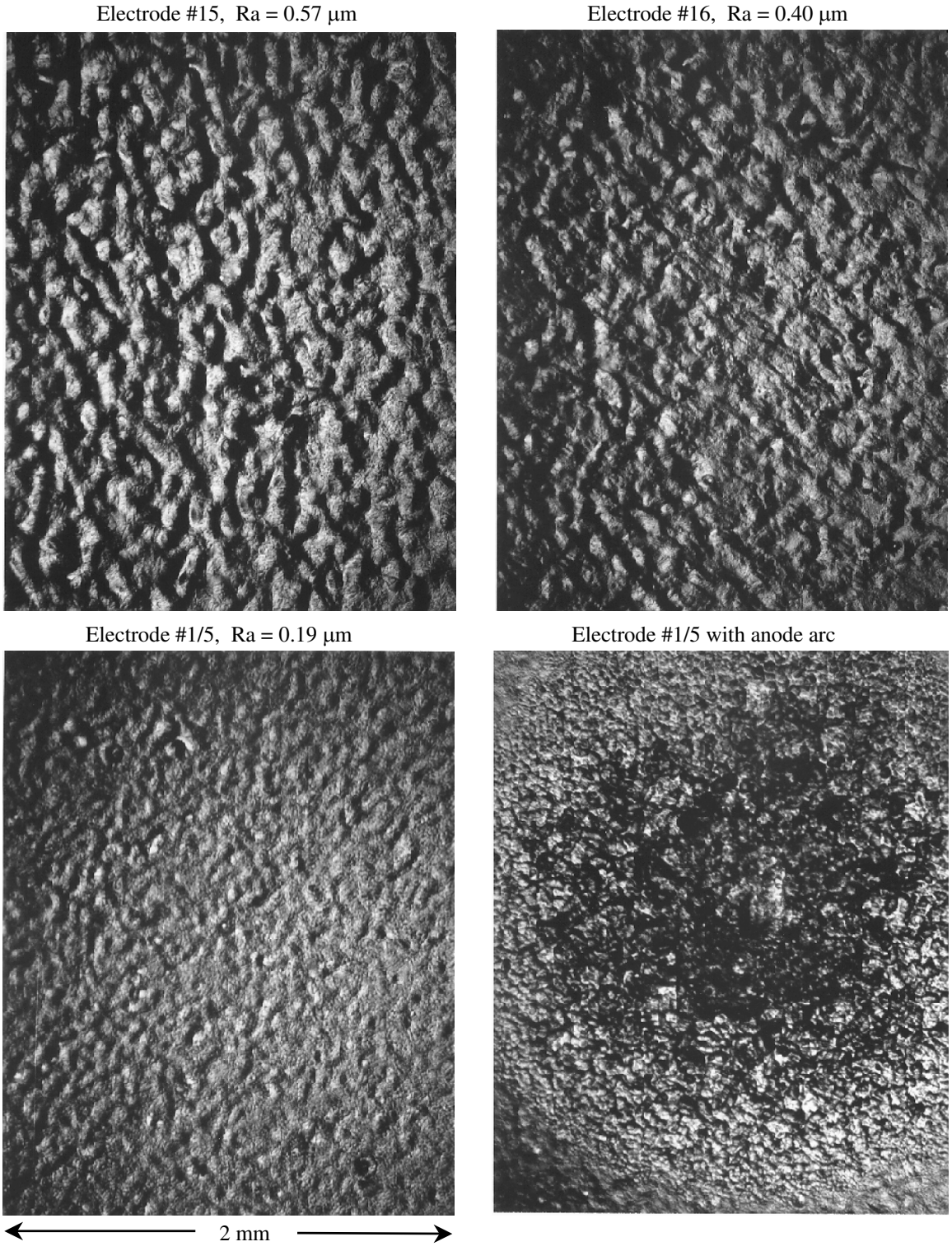

Figure 29. Microscope photos of 3 Ti implantation electrodes with the full range of R_a observed.

Photographs of the surfaces of four ion implantation electrodes are shown in Fig. 30. The upper two photographs show second shipment electrodes that have larger surface R_a, as measured with the roughness meter, than those from the first shipment shown be below.

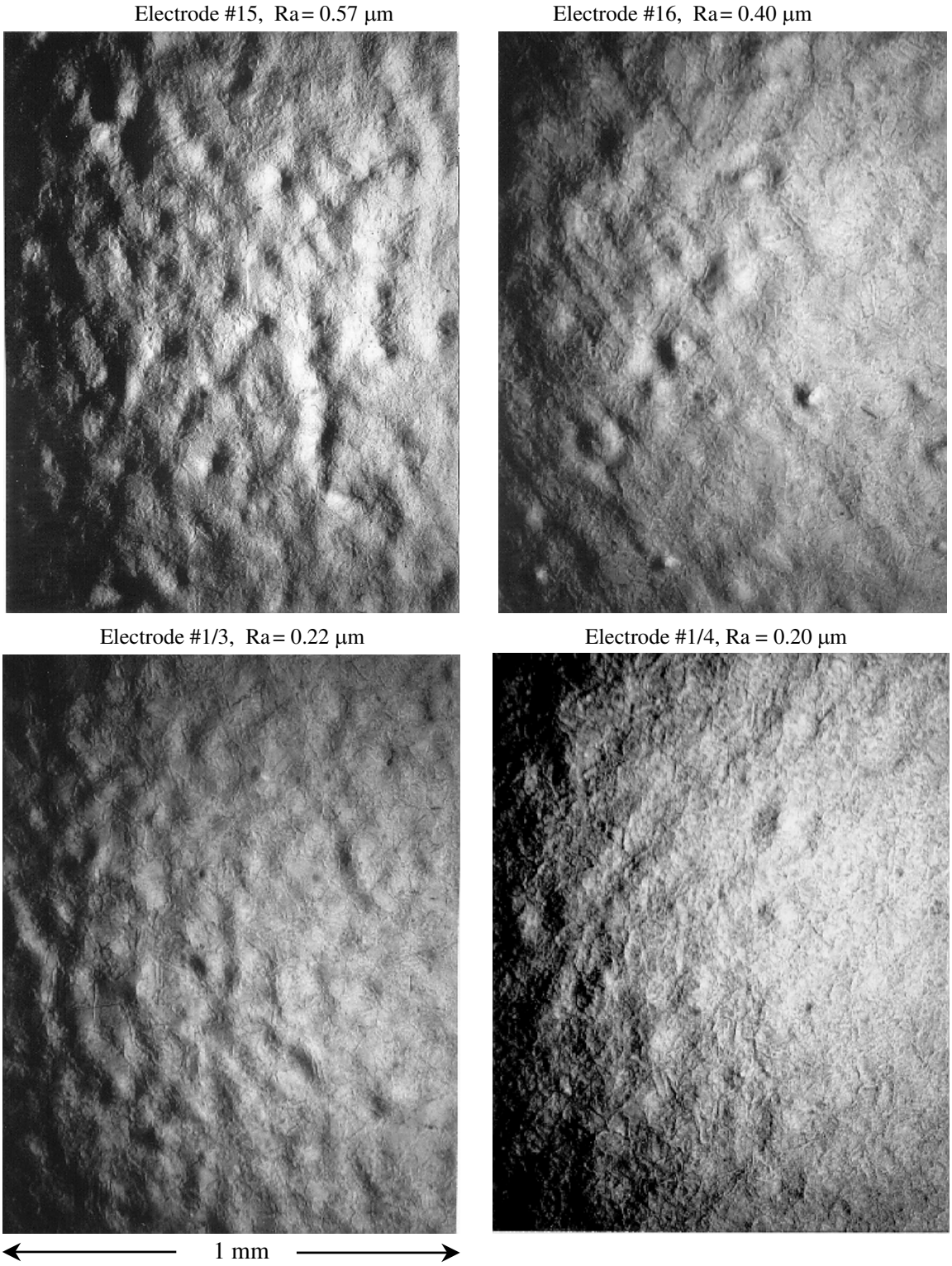

Figure 30. (upper) Photographs of second shipment ion implantation + EBEST 304L plate electrodes. (lower) Photographs of first shipment ion implantation electrodes.

The appearances of two pairs of EBEST 316L rod electrodes are shown in Fig 31 after our HV tests. The upper pair of electrodes gave the highest E-field of 1.15 MV/cm observed for any of the various types of 8 cm electrodes we tested. The HV-test results are shown as the blue squares data in Fig. 32. Even though there were previous arc marks the HV breakdowns occurred in virgin areas. This is illustrated by four new visible arc marks are shown in the figure. Lower Fig. 31 shows data from electrodes 1/36 and 1/37 with more scratches that could have caused these electrodes to give 20% lower HV hold-off that other EBEST 316L electrodes.

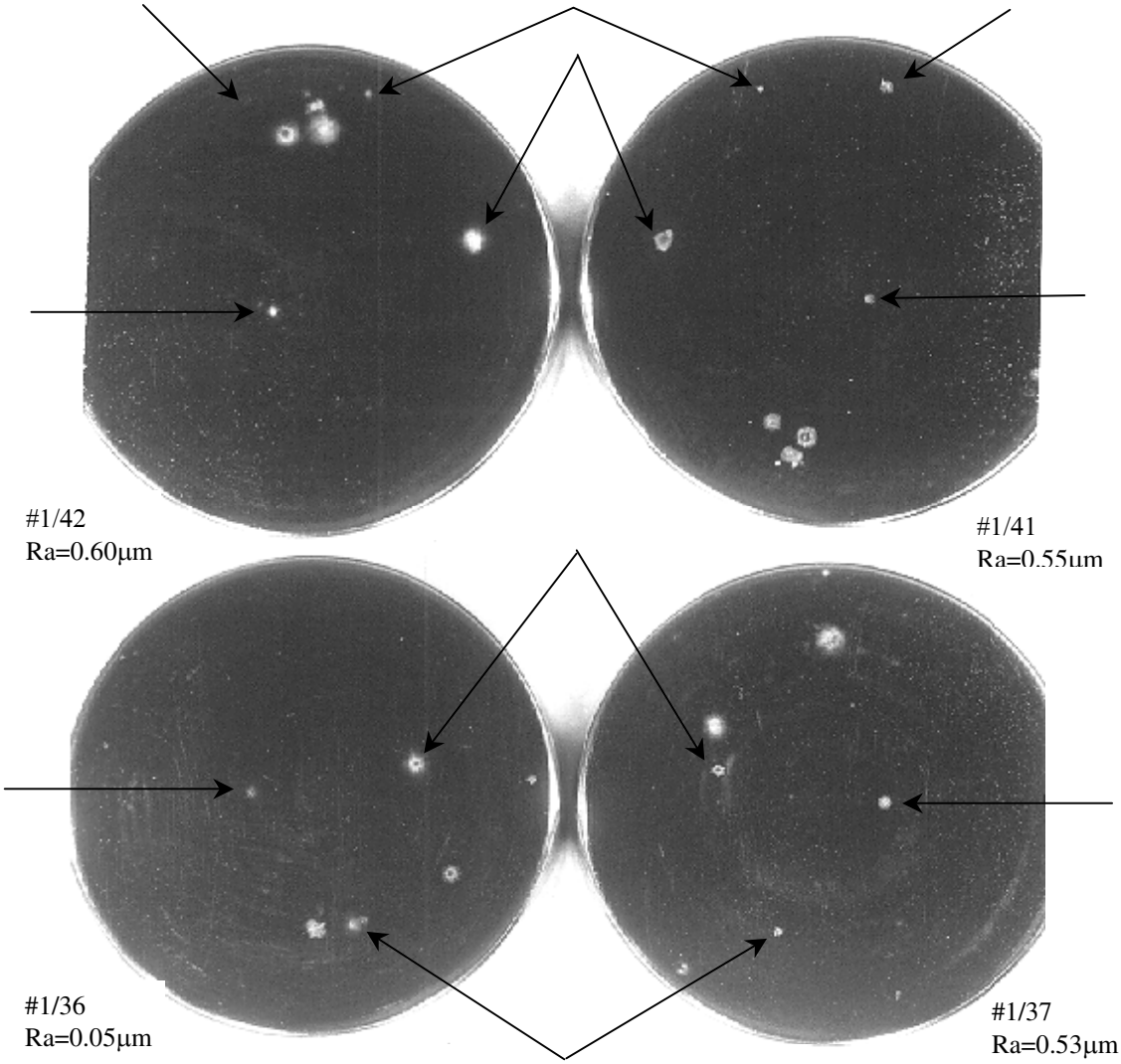

Figure 31. (top) A photo of EBEST 316L rod cathode #1/42 (left) and anode #1/41 (right) after shot 347. This was the 2nd data series in Fig. 31 with blue data points. (bottom) A photograph of EBEST 304L plate cathode #1/36 (left) and anode #1/37 (right) after shot 861. These were from the eighth data series in Fig. 31 with green data points. These electrodes have more scratches than other EBEST 316L electrodes. The arrows point to damage spots from the new arc marks.

The results from EBEST 316L rod were quite variable as shown in Fig. 32. One puzzling observation is that some of the EBEST 316L electrodes with highest R_a gave the highest HV hold-off E-field. This is illustrated in Fig. 32 by the 7th test series (red squares data) with R_a = 0.72 μm.

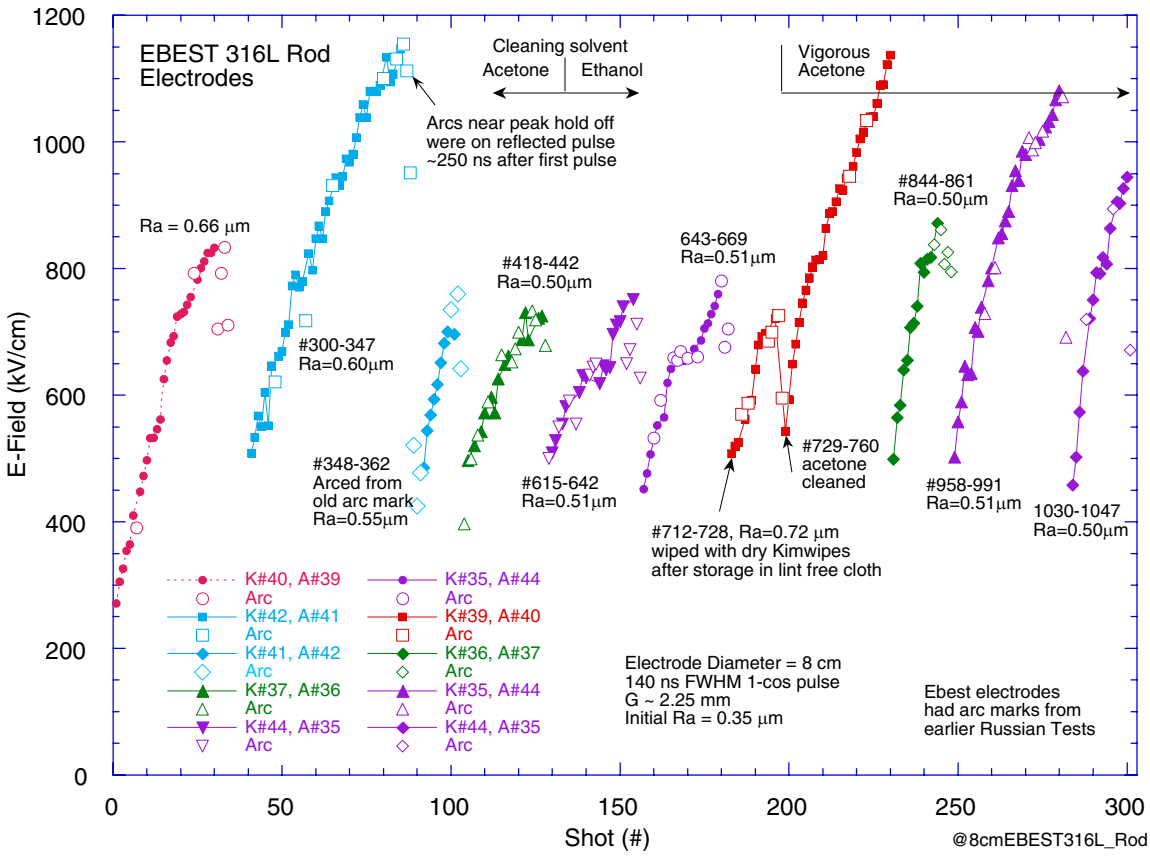

Figure 32. Test results for EBEST 316L plate stock stainless steel electrodes. Photos of 316L plate electrodes before (lower left) and after EBEST (lower right). The photo from EBEST electrode #1/39 shows a typical crater density of 5/mm^2 even thought the roughness measurement was the highest for the EBEST 316L electrodes, with R_a = 0.76 μm.

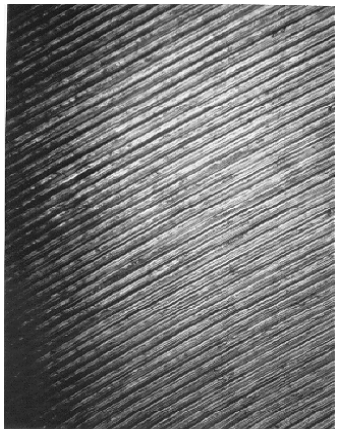

1.3 mm

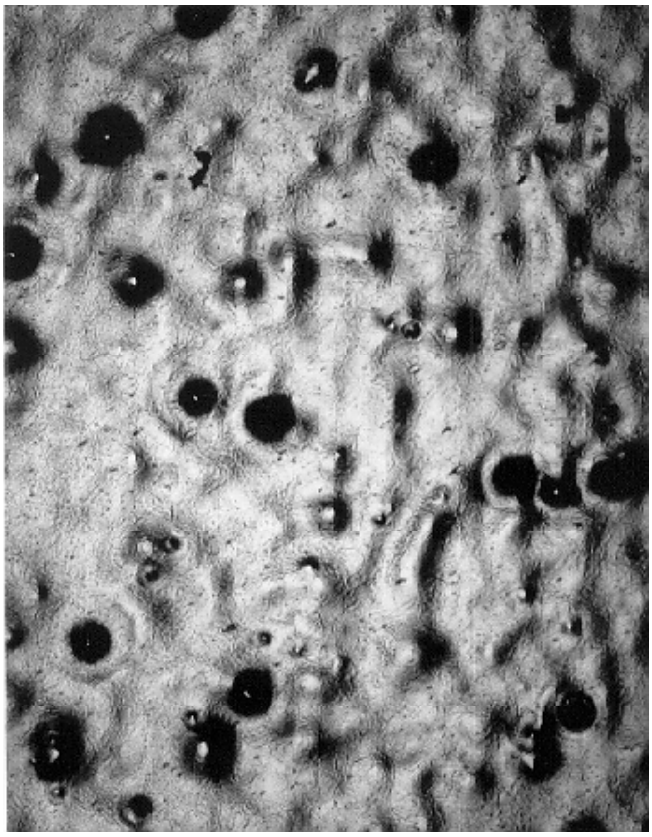

It is surprising that the EBEST 316L electrodes show so much variation in HV hold-off. There was a variation in R_a but it did not correlate with hold-off. Electrode #1/39 had the highest R_a but the highest HV hold-off. There also was no correlation of hold-off to the crater density. Most areas on all the 316L electrodes had ~ 5 craters/mm^2. The photos in Fig. 33 show the typical appearance of EBEST 316L rod at different magnifications. The photos show how the EBEST smoothed the surface, exposed grain boundaries, and produced craters. Many of the craters show only a smooth dimple in the anode surface.

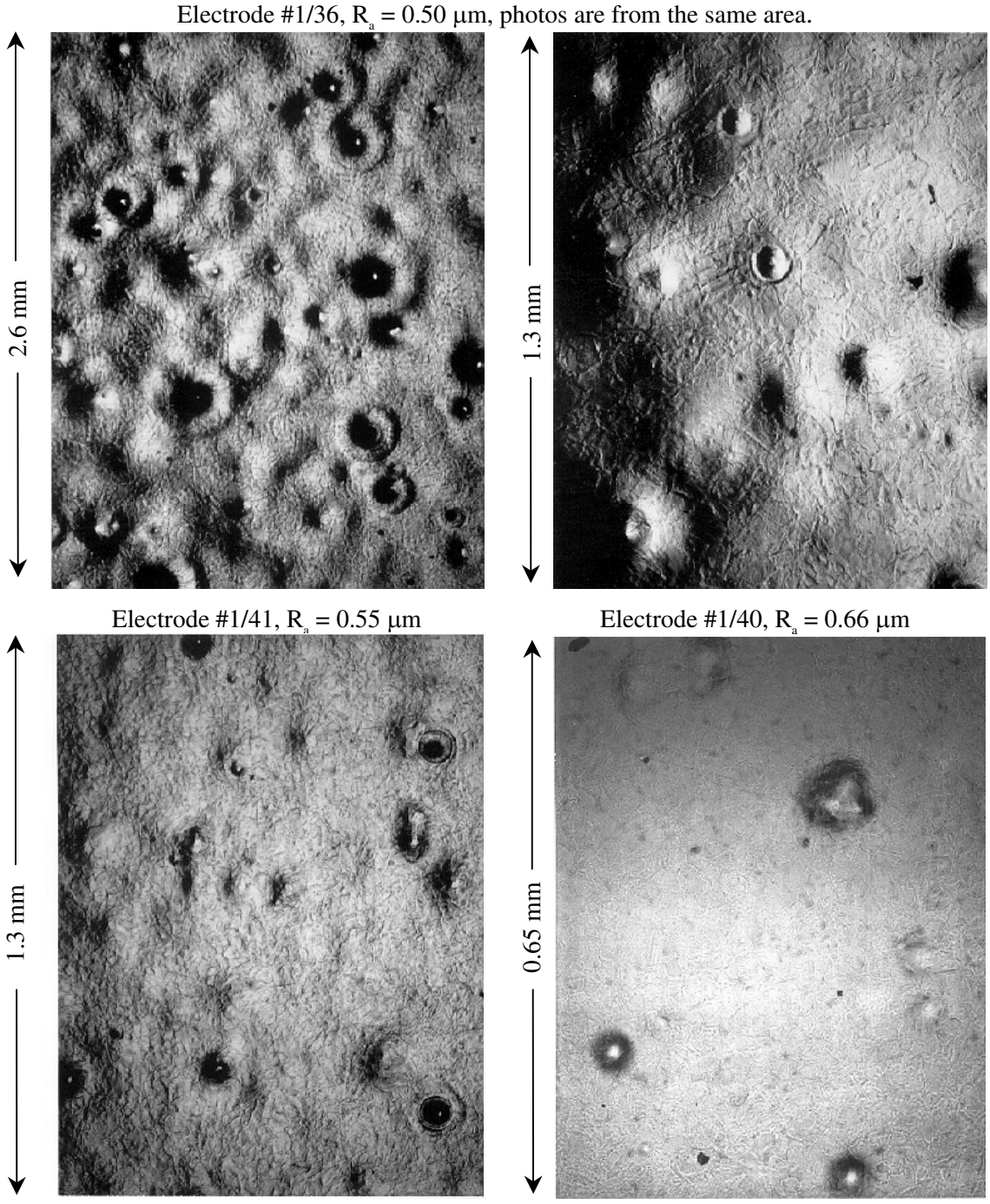

Figure 33. Photographs of EBEST 316L rod stock electrodes. The photos show the typical appearance of the surfaces at different microscope magnifications.

Our first conclusion from these measurements is that EBEST can make a big improvement HV hold-off on a poor quality machined surface. This is demonstrated by the factor two increase for 316L. However with a very smooth, essentially polished mirror surface, the improvement in HV hold-off is minimal. This was demonstrated in an separate experiment by Alexander Batrakov at IHCE and by ourselves at SNL with polished stainless steel. We see large variations in HV hold-off that are hard to explain. This is particular the case with the 316L rod electrodes. There was a significant difference in the surface uniformity and crater density for the different type of electrodes. This allowed us to show that hold-off was not strongly dependent on surface roughness. However, there is a 30% improvement for the EBEST + HVFF 304L electrodes which have only about 1% as many craters as the EBEST 304L rod electrodes. Surprisingly arc damage marks do not often initiate new arcs if the electrodes are carefully cleaned after the most sever arcs. Minor conditioning arcs do not require electrode cleaning.

VI. 12 cm EBEST Stainless Steel Electrode Tests

The procedure used by IHCE to treat the 12-cm-diameter stainless steel electrodes was the same as is described in the previous section for the 8 cm electrodes. The results of these tests were reported on by Proskurovsky [44]. The surface roughness, R_a, before and after EBEST is shown in Fig. 34. We did not retain any 304L rod stock electrodes for comparison tests so were not able to measure their initial R_a. All of the 12 cm electrodes appeared to have been diamond polished by Gull Group. The electrodes were loaded into the Lucite shipping containers after treatment by IHCE without the precaution to filter their laboratory air. Their laboratory room was remodeled for the SNL contract and is considered to have a cleaner working environment than is typical of SNL pulsed power laboratory space. An idea of their laboratory environment can be seen in Figs. 7 and 8. The technician that handled the electrodes used the good laboratory practice of wearing dust free laboratory coat, hair net, and rubber gloves. The Lucite shipping containers filled with1 ATM argon. The electrodes were shipped back to SNL in August 2002 by Unifreight, LTD, Novosibirsk, RF.

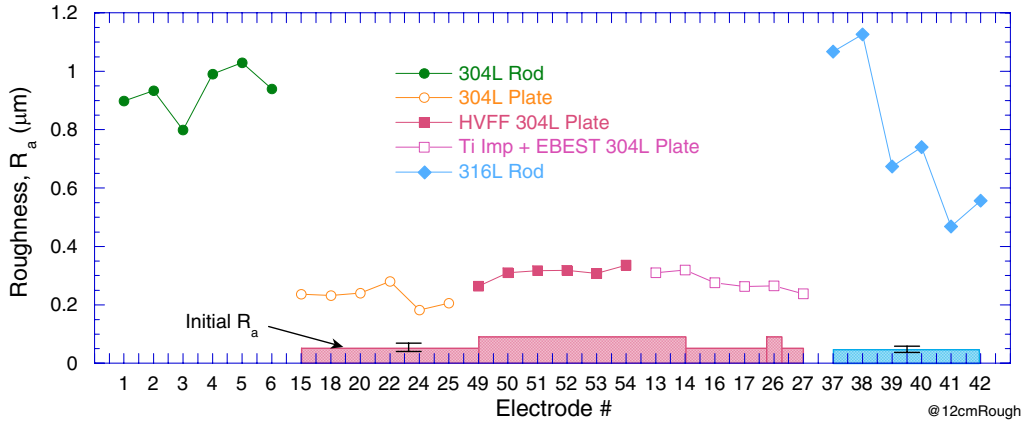

Figure 34. The average surface roughness, R_a, of the 12 cm electrodes measured before and after EBEST. The initial surface R_a of the HVFF and 3 Ti Imp electrodes came from the second order and are estimated from the higher R_a of #13 and #14 because the only electrode retained was polished before the roughness gauge was available.

Small Gaps

We began our tests 12 cm EBEST electrode tests in November 2002 without the LIVA so the maximum voltage was initially 260 kV with 165 FWHM. These tests were taken with a ~ 2.3-mm-wide gap. The electrodes were cleaned with acetone and Kimwipe laboratory wipers in the filtered clean air tent. A summary of the hold-off results for the ~ 12 tests series preformed with each electrode and treatment type is shown in Fig. 35. The range of highest hold-offs for the individual test series plotted in Figs. 39 to 43 are shown by the error bars. Two pairs of each electrode type were tested. The results show a hold-off ~ 1.05 MV/cm for all the electrode surface types. This was different from our results for 8 cm electrodes where slightly better hold-off was observed (see Fig. 16) for electrodes with fewer craters from dielectric inclusions. Also the hold-off was similar for the rod stock electrodes with four times rougher surfaces. This is not well understood but could be due to the clean air environment used for cleaning and installation on these tests. Perhaps we were able to adequately remove dust even with the rough surfaces under these conditions. There was not a drop in hold-off due to the area increasing from 43 to 95 cm^2 for 12 cm compared to the 8 cm electrodes. Others [36,37] have also observed that the "area effect" plateaus beyond 30 cm^2. The continuous and dotted lines shows the typical hold-off after a severe arc that produced metal droplets on EBEST and smooth electrode surfaces.

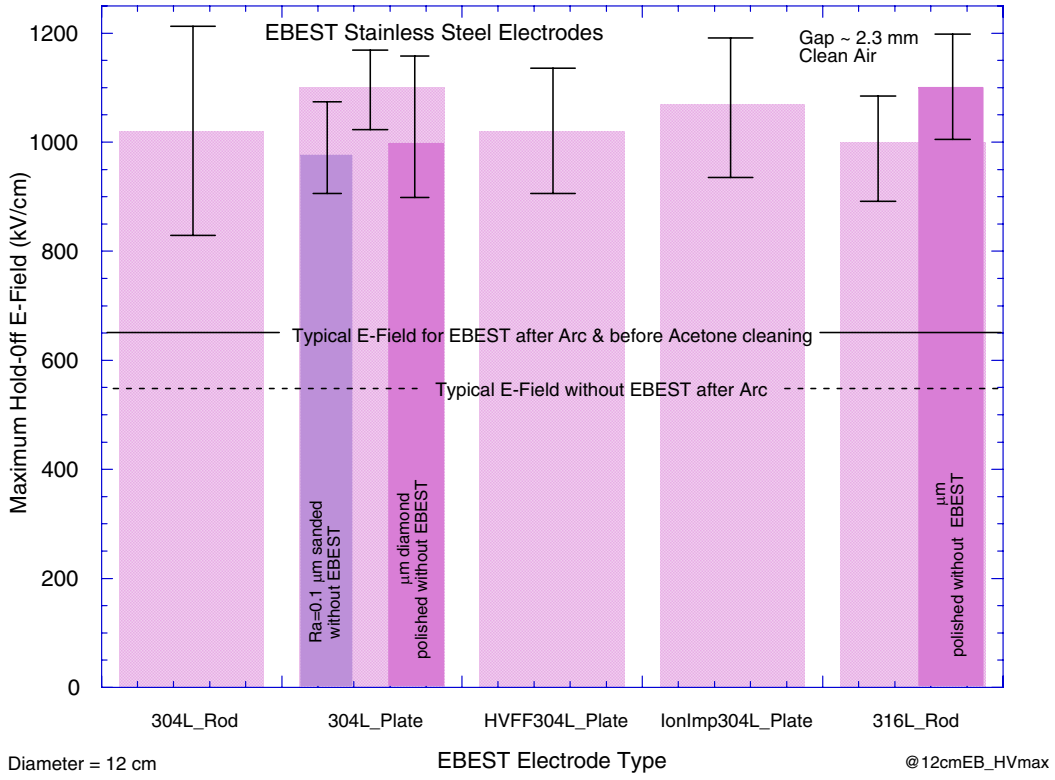

Figure 35. A summary of the HV hold-off results for tests of 12-cm EBEST electrodes. The range of the maximum hold-offs are shown by the error bars. The dark purple bar shows data for electrons wet sanded to R_a = 0.1 µm with 2000 grit carborundum paper. The dark purple bars are data for electrodes that were diamond polished to give R_a = 0.05 µm.

The breakdown data for various electrodes tested with the small gaps are shown in Figs. 39 to 43. The closed symbols were shots without breakdown. The open symbols show the breakdown arcs. The test procedure was similar to that used with the 8 cm electrodes except that the E-field was increased in 40 kV/cm rather that 20 kV/cm steps. This gave fewer electrical conditioning shots where cathode emissions sites could be eliminated by late time breakdowns with insignificant current. For this reason the high breakdown values obtained with the 12 cm EBEST electrodes are even more remarkable. The breakdown arcs were typically randomly located on fresh areas as with the 8 cm electrodes. The figures have annotations that show some significant observations during the tests. There was no noticeable difference when electrodes were stored for several weeks to allow the oxide layer to thicken. When the shot numbers differ from the abscissa numbers the shot numbers are listed below the shot sequence curves preceded by #. The electrode numbers are listed in the legends as K# and A# followed by the gap. The R_a for each electrode is listed in the lower right corner of the figures. The electrodes were new at the beginning shot series of each graph.

At the beginning of the shot series for 304L electrodes the electrodes were removed from the Lucite containers in the clear air and the surfaces were only dusted off with compressed CO_2 before installation into the test chamber. These initial tests are annotated in the top of Figs. 39-42 and gave breakdown at about 550 kV/cm. We then performed a vigorous acetone cleaning with several laboratory wipers and observed a ~ 50% improvement in hold-off on the subsequent tests. The mottled surface noted for the 304L rod electrodes is illustrated by Fig. 36 in the photo of electrodes 1 and 2 taken after shot 32 (4^{th} series upper Fig. 39). The arcs for shots 1 and 2 produced one minor mark on the anode at r = 3.5 cm, and 12:00 that is not visible in the photo. The cathode was rotated 67.5° counter clockwise for shots 18-24 and 67.5° clockwise (as shown in Fig. 36) for shots 25-32.

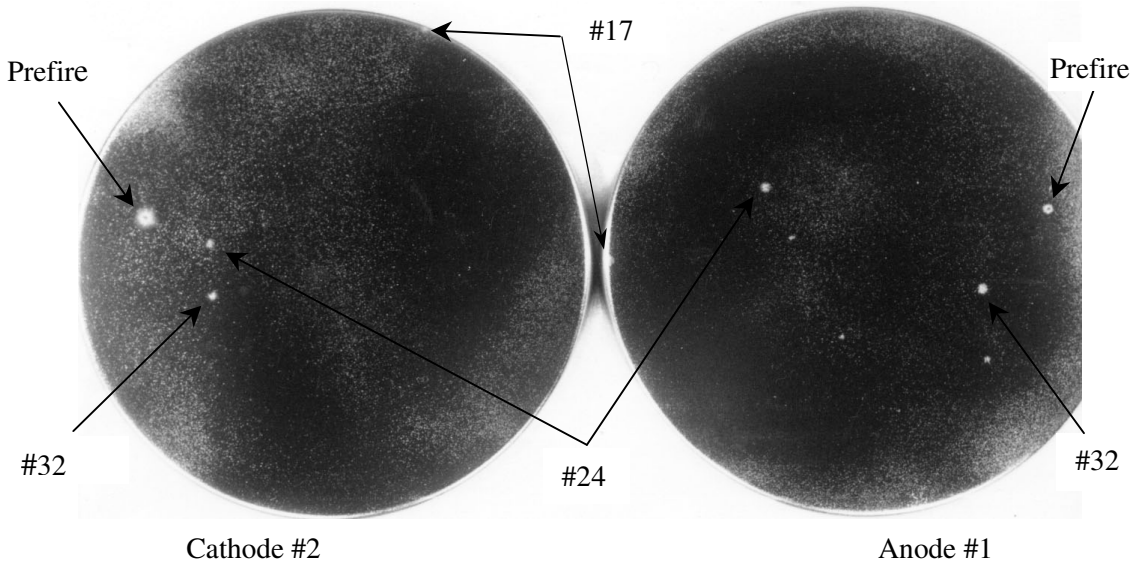

Figure 36. A photograph of EBEST 304L rod electrodes #1 and 2 taken after shot 32. Shot numbers label the identified arc marks. There are 3 unidentified arc marks on the anode that occurred on prefires associated with shot #32.

The electrical waveforms for shot 24 illustrated in Fig. 37 shows the general nature of a typical breakdown with stainless steel electrodes and a 2.5 mm gap. The current begins 108 ns after the onset of voltage in this shot but on some shots begins as late as 200 ns. The current then rises rapidly and is well fit by the Child-Langmiur current model first described in section IV. The electron beam heats the anode until the surface temperature is sufficient to form anode plasma that generates a proton beam. The total current then increases by 1.8 because of the space-charge neutralization of the electrons by the protons. The anode temperature is calculated for the electron beam in Fig. 37, via the method that is explained in more detail in our later section on machined stainless surfaces. Here we wish to illustrate the typical behavior that occurs on most shots with small gaps after the anode surface reaches ~ 500 °C. The jump in current produces a rapid collapse of the diode voltage to 20 kV that occurs in about 10 ns. The voltage then is sustained for another 500 ns as the voltage drops to nearly zero. The 20 ns period oscillations that occur during ring down of the voltage are apparently excited by the rapid collapse of diode impedance and the plate capacitance and arc inductance. After 500 ns multiple reflected TG-125 power pulses cause an oscillating current that continues for several μs. With larger gaps the CL model was often able to replicate much of the current shape during a 200 ns late time window. This is illustrated for the waveforms for shots 188 and 179 that used 5 and 7.4 mm gaps. With larger gaps the impedance did not collapse fast enough to created the ringing current. However there were often late time current pulses that exceeded the CL model current for about 20 ns. These pulses are attributed to bipolar flow and perhaps the plasma density was sufficiently low that plasma erosion from the proton beam can extinguish them.

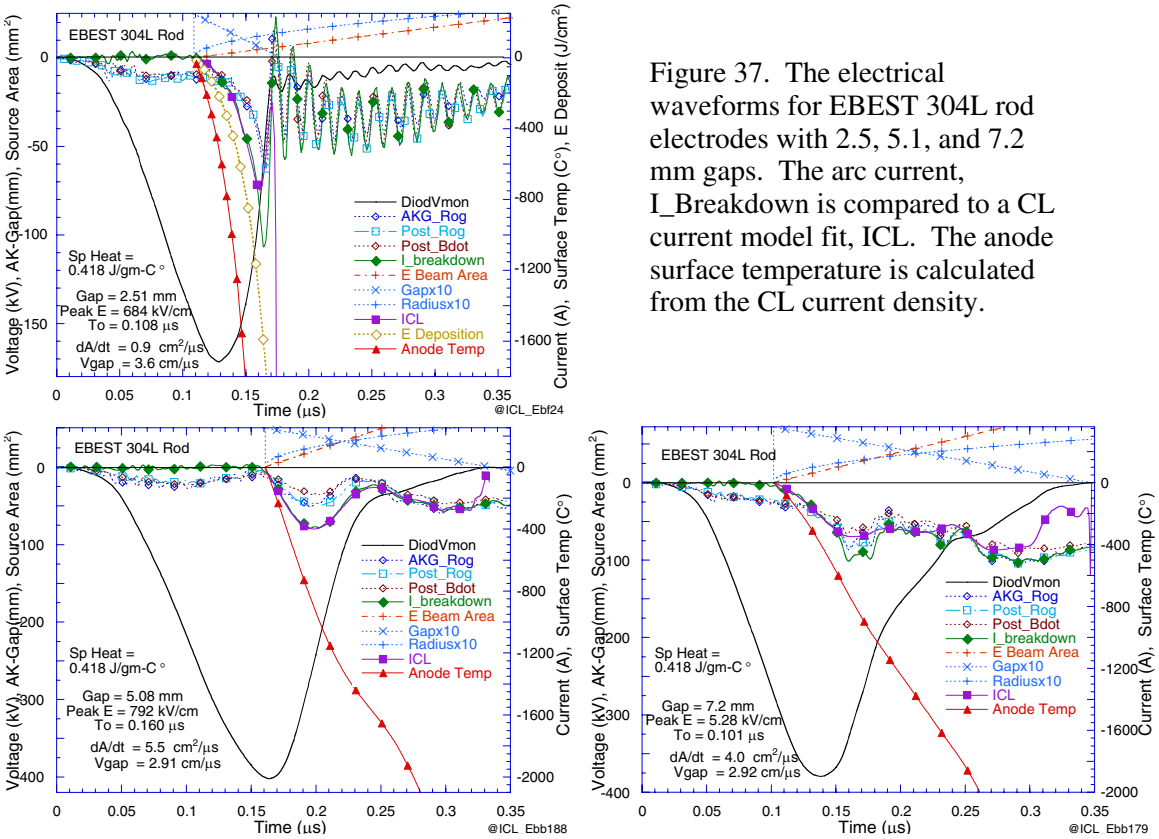

Figure 37. The electrical waveforms for EBEST 304L rod electrodes with 2.5, 5.1, and 7.2 mm gaps. The arc current, I_Breakdown is compared to a CL current model fit, ICL. The anode surface temperature is calculated from the CL current density.

A photograph of EBEST + HVFF electrodes #50 and $49 taken after shot 226 (5th series upper graph of Fig. 41) is shown in Fig. 38. It shows the much smoother surfaces observed on the 304L plate stock electrodes that have many fewer crater pits (see Fig. 25) from hydrocarbon or sulfide inclusions that were vaporized during the EBEST process. A measurement was not made of the crater density for the 12 cm EBEST electrode types. However since the material and treatment method was the same as was used for the 8 cm electrodes we believe the factor of 100 reduction for the HVFF 304L plate, compared to 304 L rod, listed in Table 1 applies for the 12 cm electrodes also. The electrodes had been rotated several times and switched once prior to shot 226 so the electrodes show a random series of arc marks. These marks did not prevent the electrodes from holding off 1.06 MV/cm on the next series. The low probability of arcs initiating from previous arc is similar to the behavior observed with the 8 cm electrodes. There were two arcs near the edges because the 2.5 mm gap Chang curve used for these shots gave a uniform E-field out to ~ 2 mm of the edge before it dropped off.

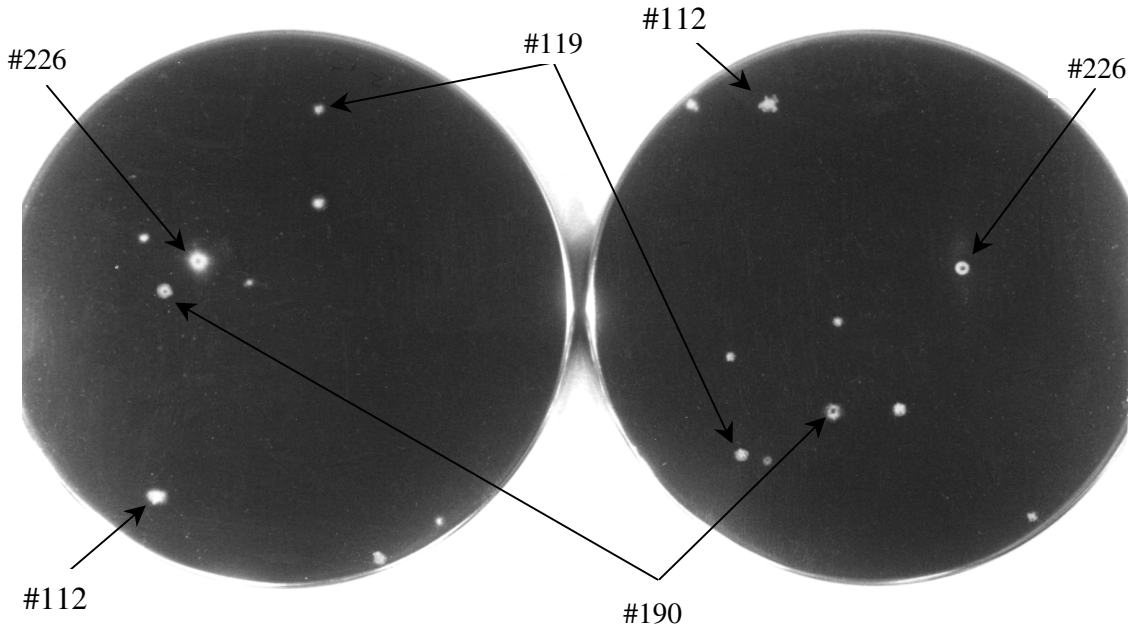

Figure 38. Photograph of 12-cm-diameter EBEST + HVFF electrodes taken after shot 226 in the upper plot of Fig. 41. The location of the last arcs from the 2nd, 3rd, 4th, and 5th shot series are labeled. The cathode was rotated 67.5° between each of these shot series.

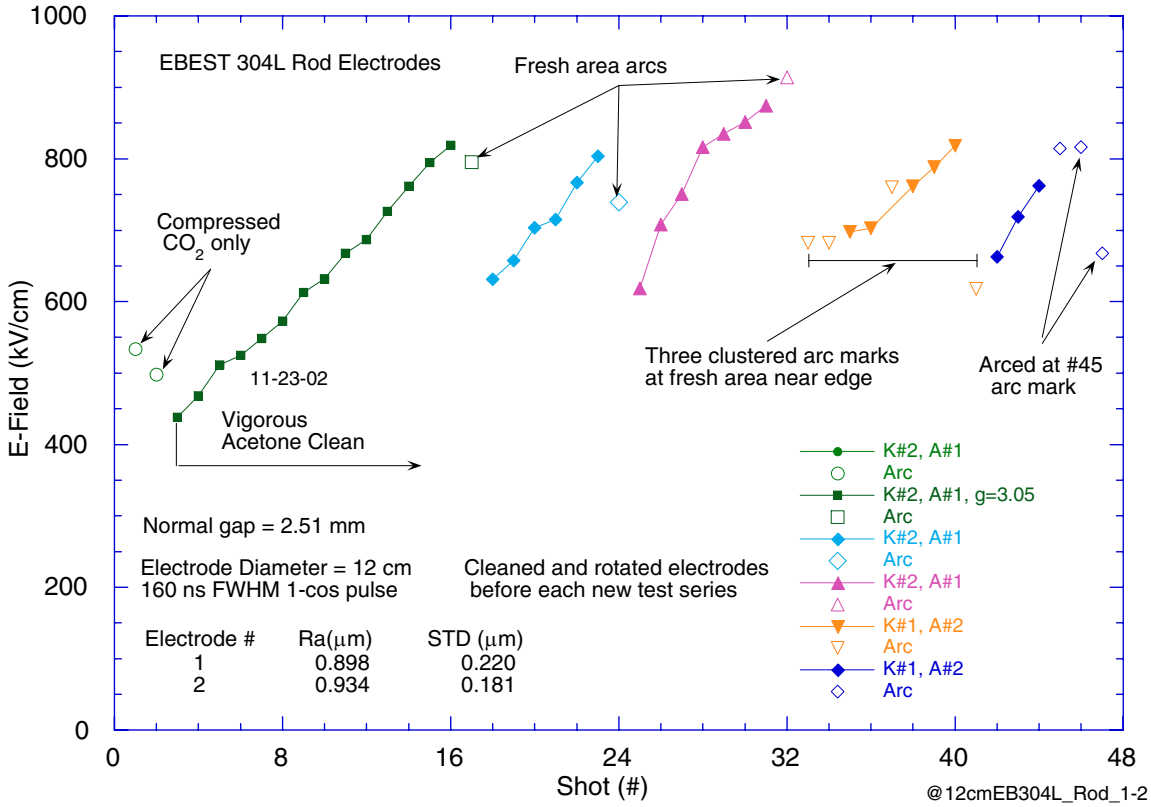

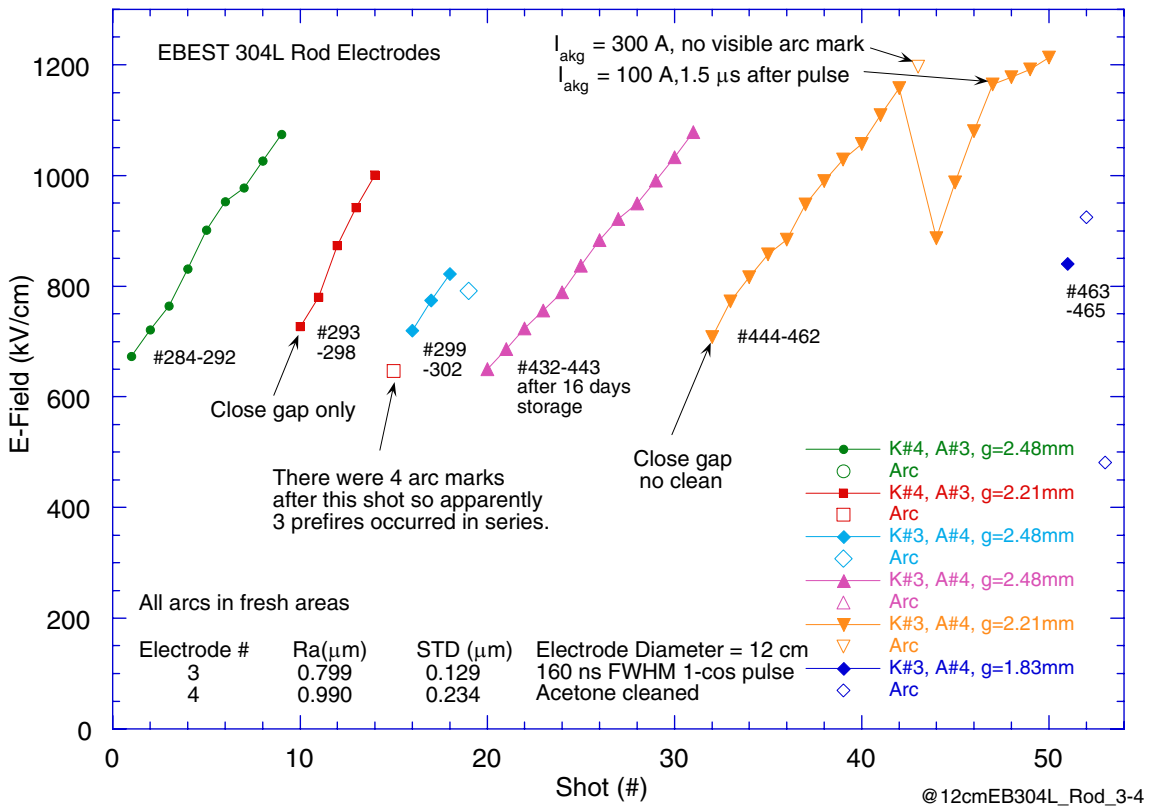

Figure 39. High voltage breakdown data for 12 cm EBEST 304L rod stock electrodes.

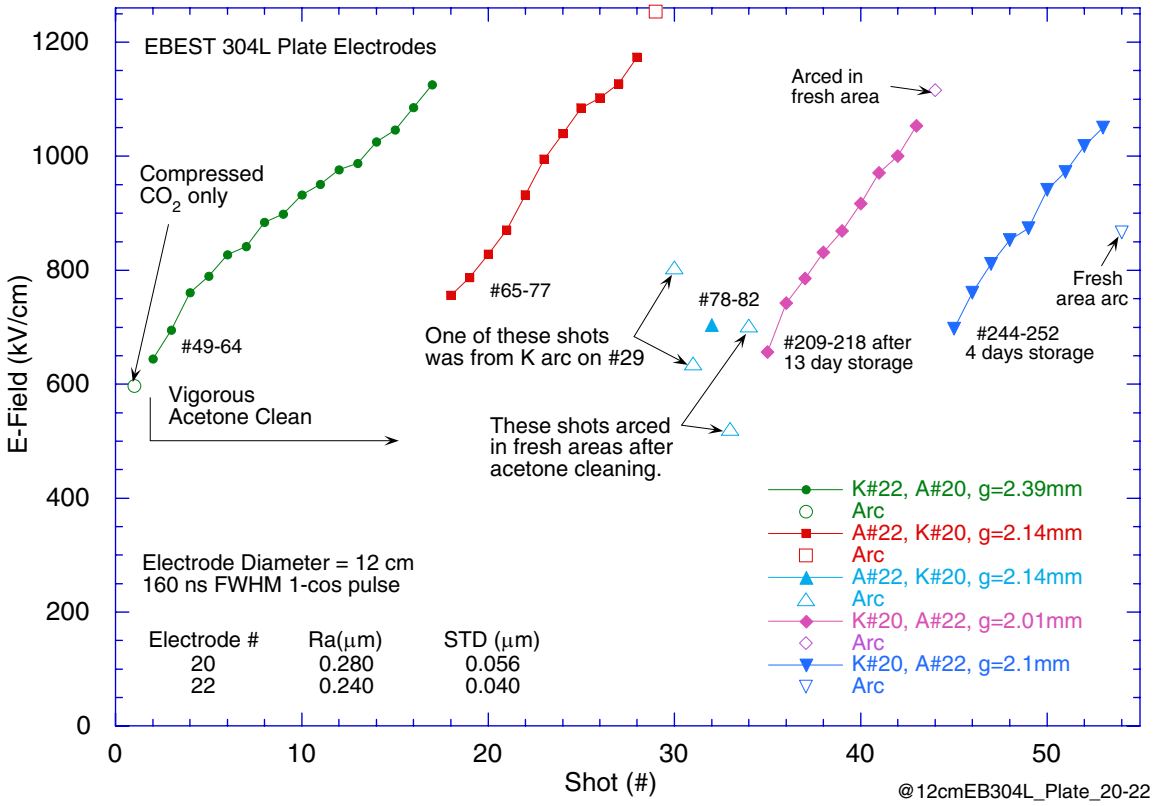

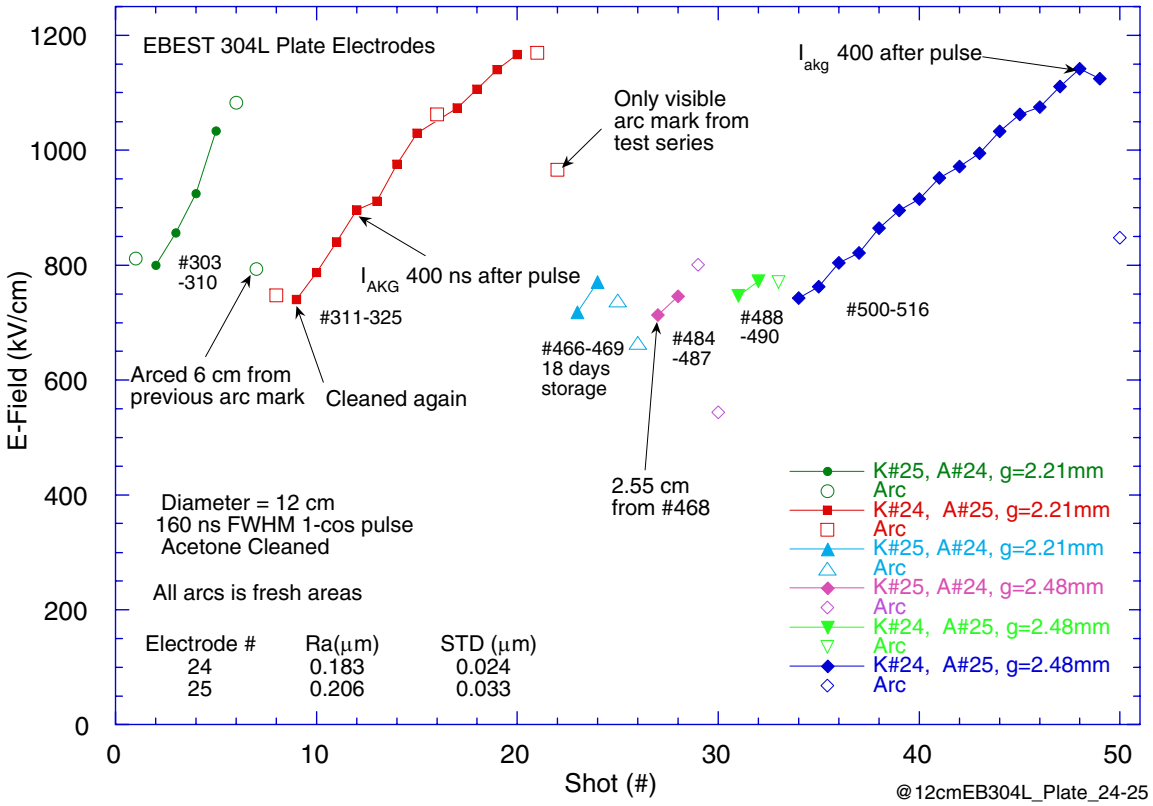

Figure 40. High voltage breakdown data for 12 cm EBEST 304L plate stock electrodes.

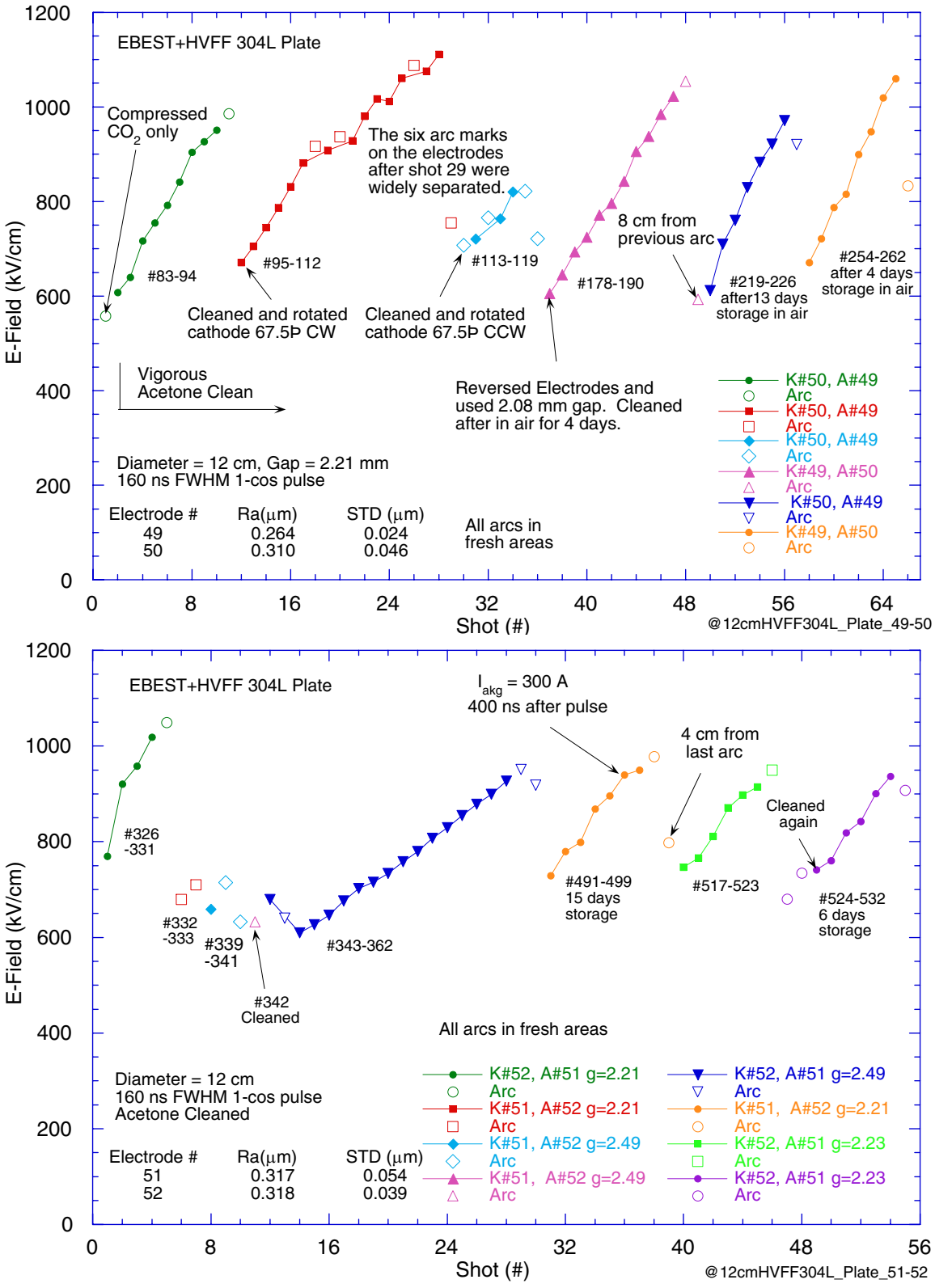

Figure 41. High voltage breakdown data for 12 cm EBEST + HVFF 304L plate stock electrodes

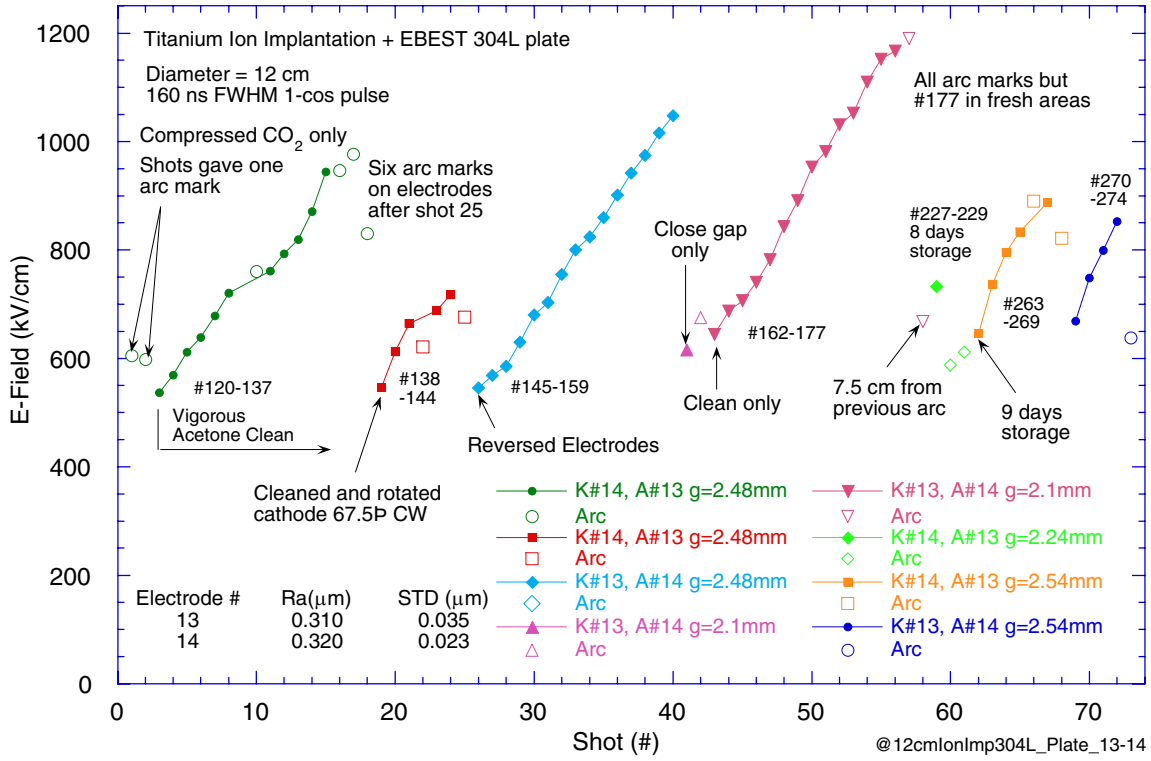

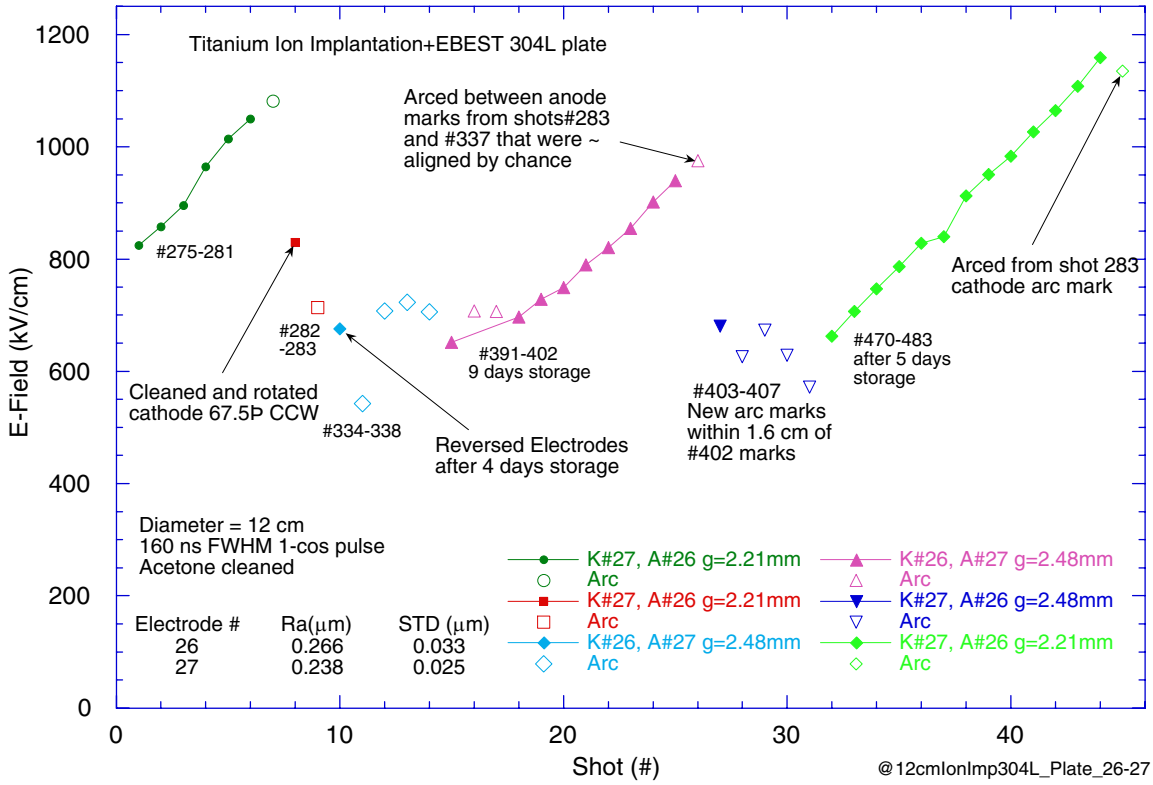

Figure 42. High voltage breakdown data for 12 cm Titanium Ion Implantation + EBEST 304L plate stock electrodes.

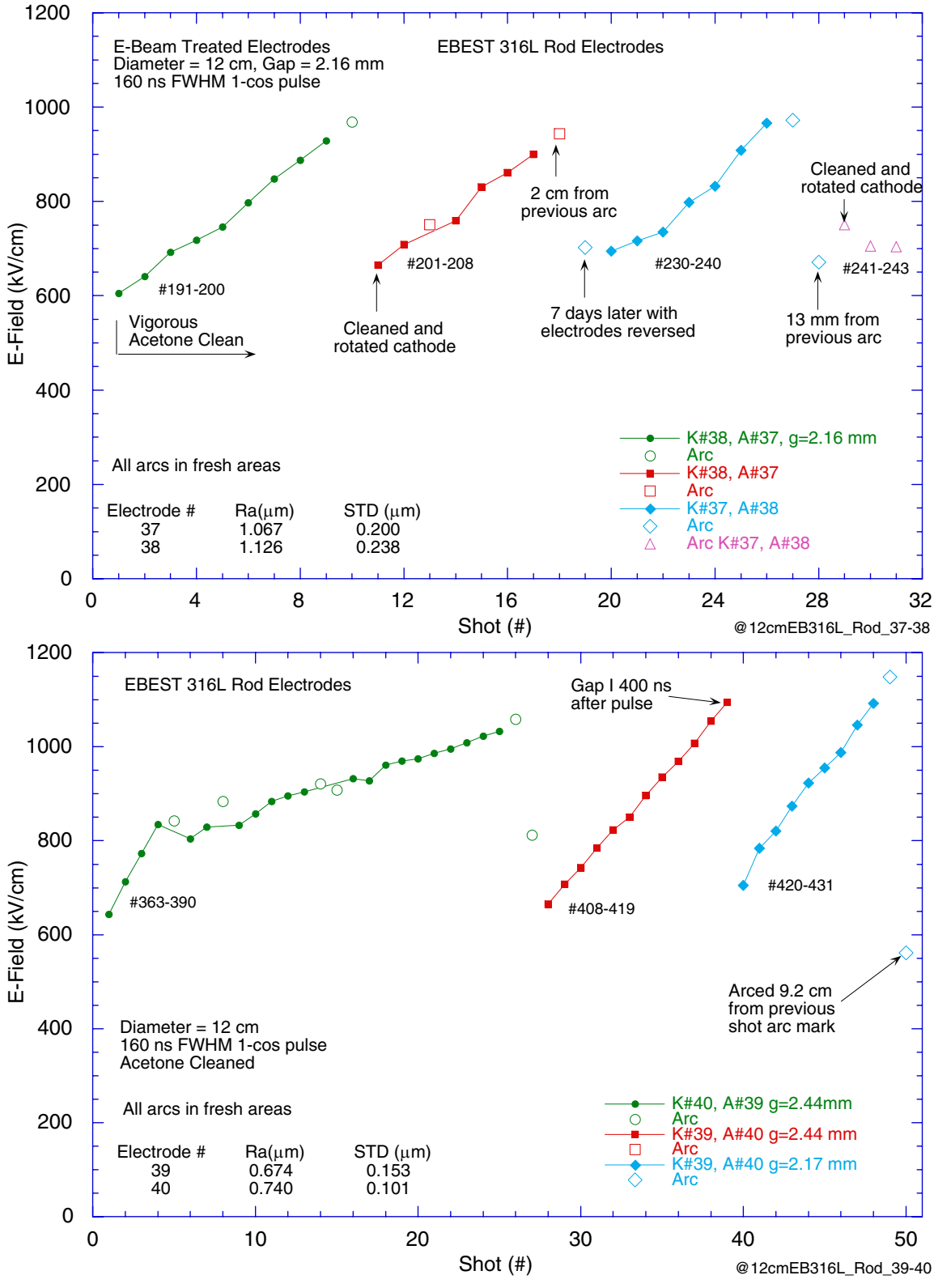

Figure 43. High voltage breakdown data for 12 cm EBEST 316L plate stock electrodes.

Large Gaps

In April 2003 we installed the LIVA that doubled the voltage so could test with 5 and 7.25 mm gaps. It was realized at the beginning of these higher voltage tests that the Chang curves of the 12 cm electrodes were mistakenly cut for a 2.5 mm gap. To correct this problem it was necessary to machine a 5-mm-gap Chang curve on the edges of the electrodes. This was done with a carbide tool bit ground to conform to the edge of a 17-cm-diameter electrode with the desired 5-mm-gap Chang curve. Some initial tests were done at 4.9 mm gap using EBEST treated 304L plate and HVFF 304L plate cathodes (see Fig. 45) with the 2.5-mm-gap Chang curve together with polished 316L anodes with the remachined 5 mm Chang curve edge. These tests give reference data for unmodified EBEST electrodes. Proper 5 mm Chang curves were later cut and polished on all the electrodes tested. We saw no evidence of preferential arcing from the machined edges or difference in hold-off due to surface contamination caused by machining the new edges. One new pair of each electrode type was tested at the higher voltages.

The breakdown results are generally much lower for larger gaps with peak E-fields of only ~ 0.75 and 0.58 MV/cm for the 5 and 7.25 mm gaps, respectively. These results are summarized in Fig. 44. The individual data for the shots taken with the EBEST machined and HVFF 304L plate stock electrodes are plotted in Figs. 45, 47, and 48. These figures have annotations that describe circumstances encountered during the shot series. The range of the repeated tests are shown with pointed arrows

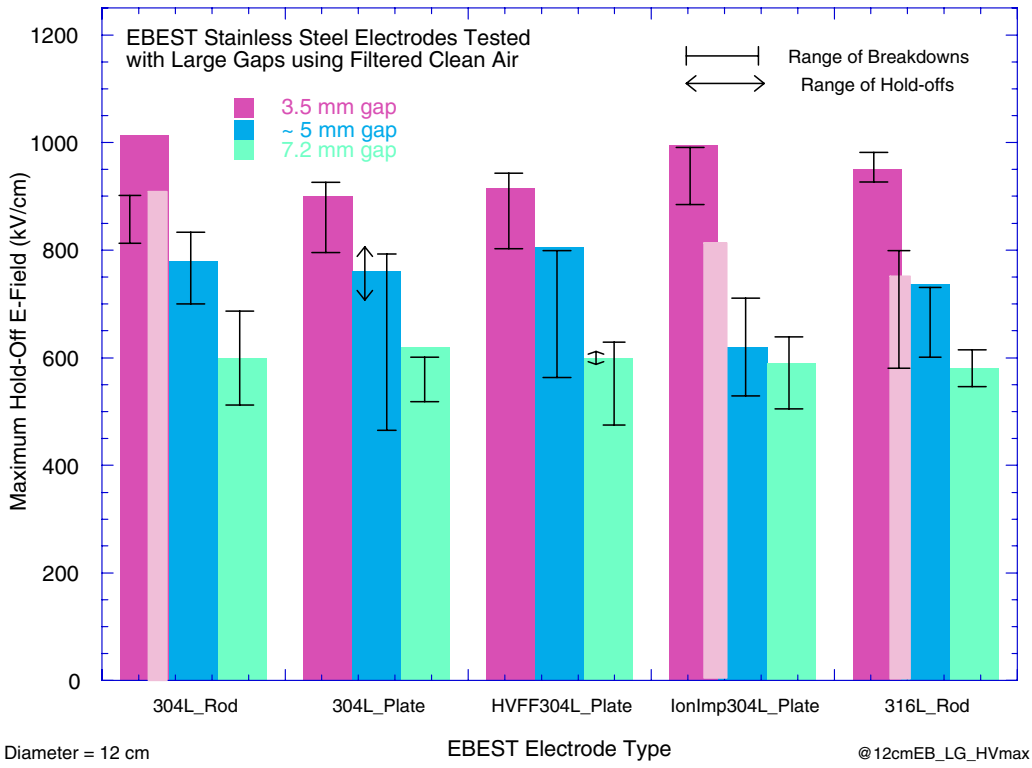

Figure 44. High voltage test results for large gaps using the LIVA based pulser. The bar graphs show the maximum hold-off. The error bars show the range of hold-offs for multiple test series and breakdowns for individual test series in Figs 45, 47 and 48.

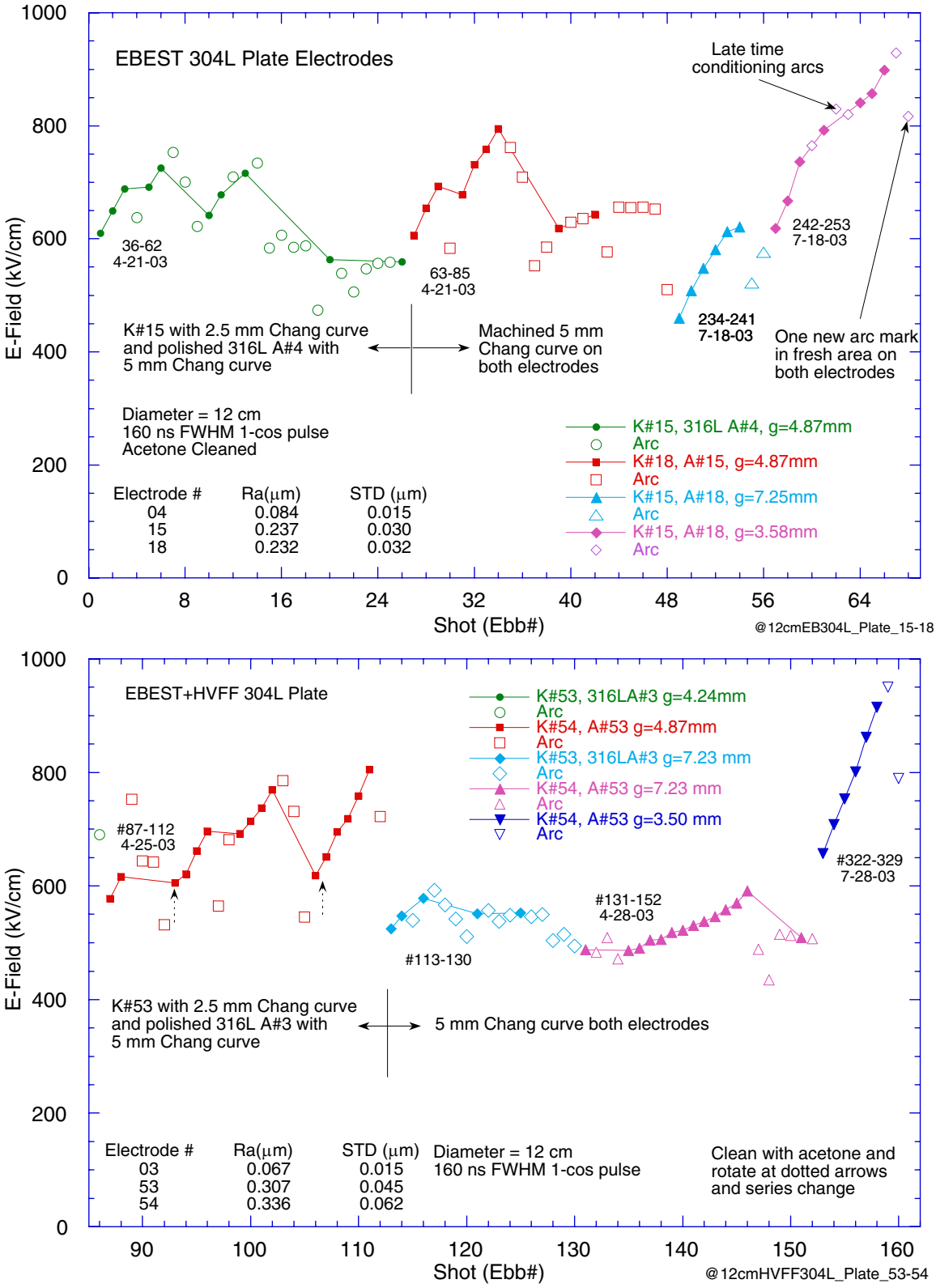

Figure 45. High voltage breakdown data for 12 cm EBEST (machined and HVFF) 304L plate stock electrodes with large gaps. The initial tests used cathodes with 2.5 mm Chang curves and 316L anodes with 5 mm Chang curves.

The waveforms for shot 152 and 329 (last shots of 4th and 5th series lower Fig. 45) in Fig. 46 show the jump in current that occurred late in time on about half of the EBEST and bare stainless steel shots. These shots had 3.5 and 7.2 mm gaps. The figure also shows a temperature calculation using the Child-Langmuir current density and surface electron stopping power for stainless steel obtained from Spencer [46]. This jump typically occurs when the calculated anode temperature reaches ~ 800 °C and probably occurs when ions are emitted from the anode. At his time the space charge limited beam flow becomes bipolar. Blaugrund [47] observed this with electron beam pinches when the anode temperature reaches 400 °C. Sanford [48] observed that anode plasma forms on metals at about 400 °C. For most shots it was possible to get a good fit at 400 °C if the incident beam radius was expanded by ~1 mm. This seems reasonable for space-charge induced expansion across a 7 mm gap but too large an expansion for a 2 mm gap. Therefore we are perplexed at why the jump occurs at such a high temperature for small gaps.

We noticed very little arc damage on either electrode when we used 7.5 mm gaps. The cathode arc marks appeared as pits a few μm diameter. Most anode marks appeared as a dendrite damage patterns. These type patterns were observed on anode #53 after shot 152 (pink triangle symbols in lower graph of Fig. 45) and are shown in Fig. 46.

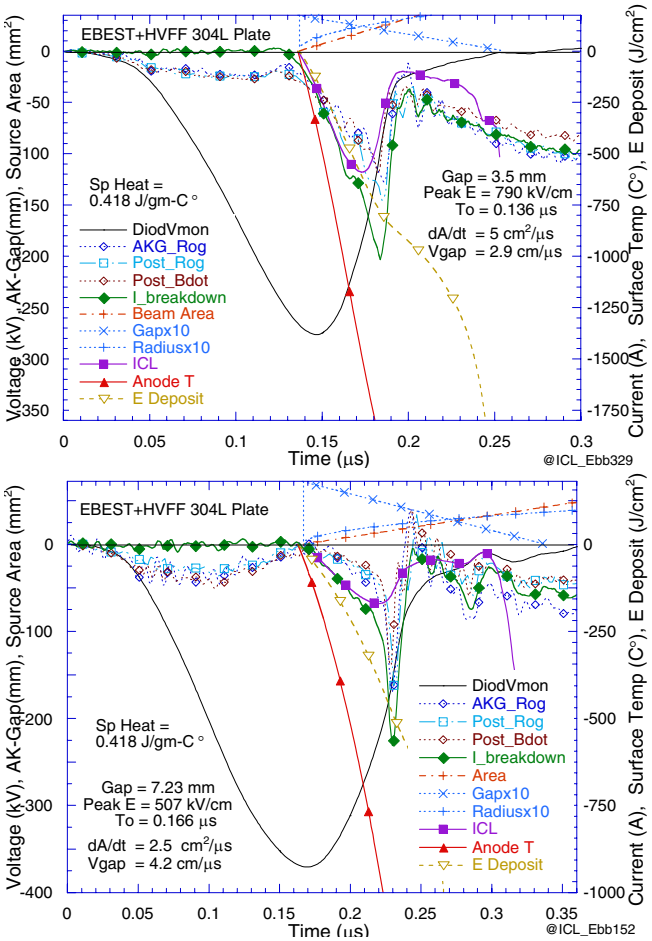

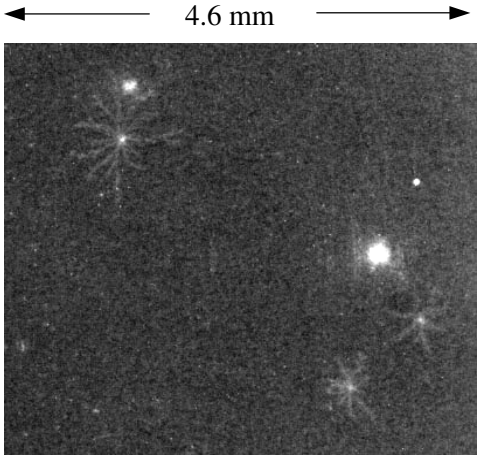

Figure 46. (left) The electrical waveforms for shots 329 and 152 using EBEST + HVFF 304L plate electrodes. The data include anode temperature calculations based up the Child Langmuir space charge limited currents ICL. (upper right). Dentrite patterns observed on the anode after shot 152 with EBEST + HVFF 304L plate stock electrodes.

The individual breakdown data for Ti ion implantation + EBEST 304L plate electrodes are shown in Fig. 47. The initial tests with 5.15 and 7.25 mm gaps showed rather low breakdown fields. As with the other 12 cm EBEST electrodes tested the breakdown fields increased when tests were performed with smaller gaps. A photo of the electrodes taken after the 4th shot series shows the arc marks that had accumulated on the electrodes. The photo shows the concentric marks that occurred near the edges of the electrodes where the 5 mm Chang curves were machined. The locations of the marks are well separated from the machining marks indicating this modification did not influence the breakdown results. The same was observed on other modified 12-cm-electrode edges.

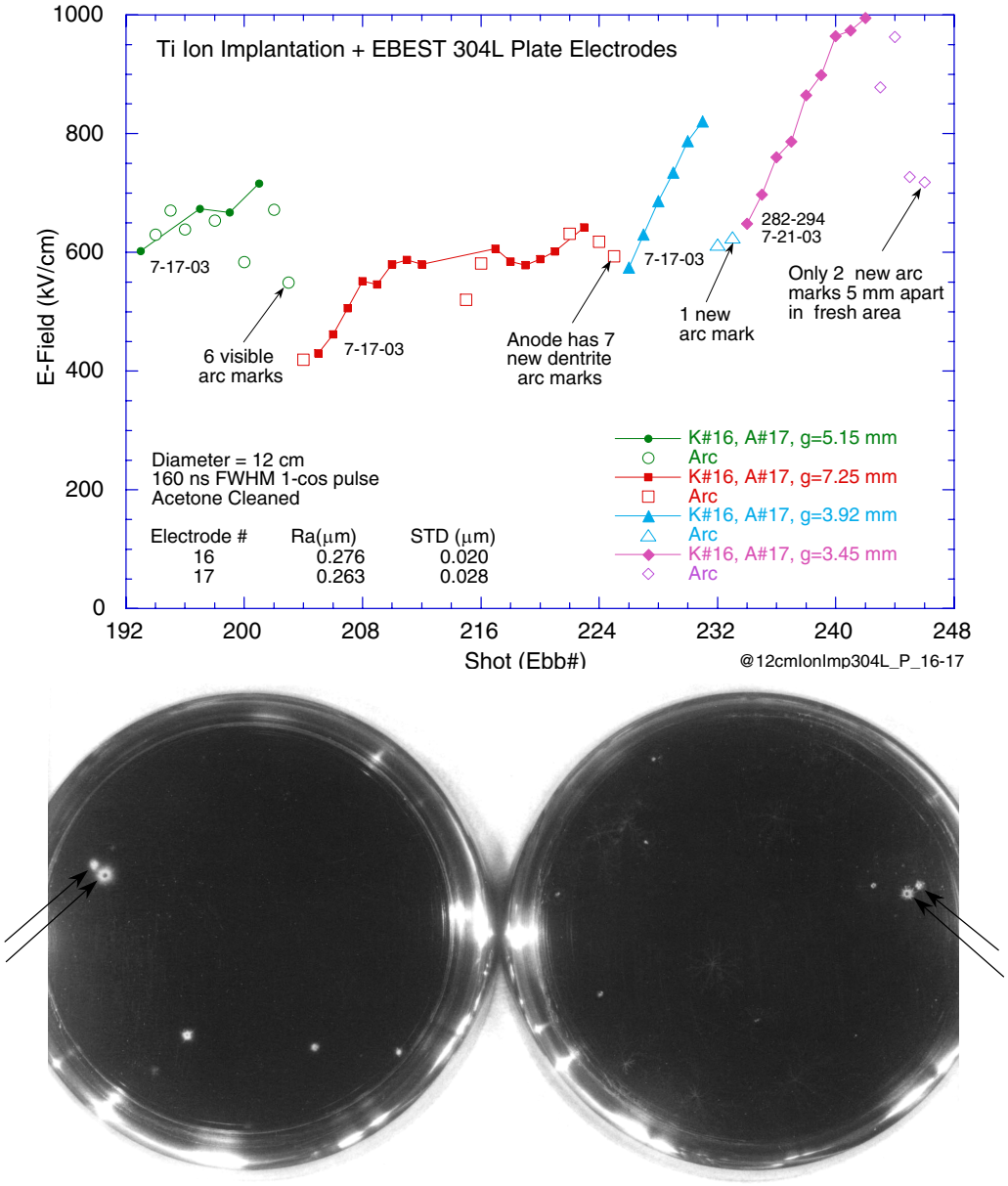

Figure 47. High voltage breakdown data for Ti ion implantation + EBEST 304L plate stock electrodes with large gaps. The photo shows the electrodes after the last test, Ebb394. The arrows indicate the location arcs on the last series. Cathode #16 is on left.

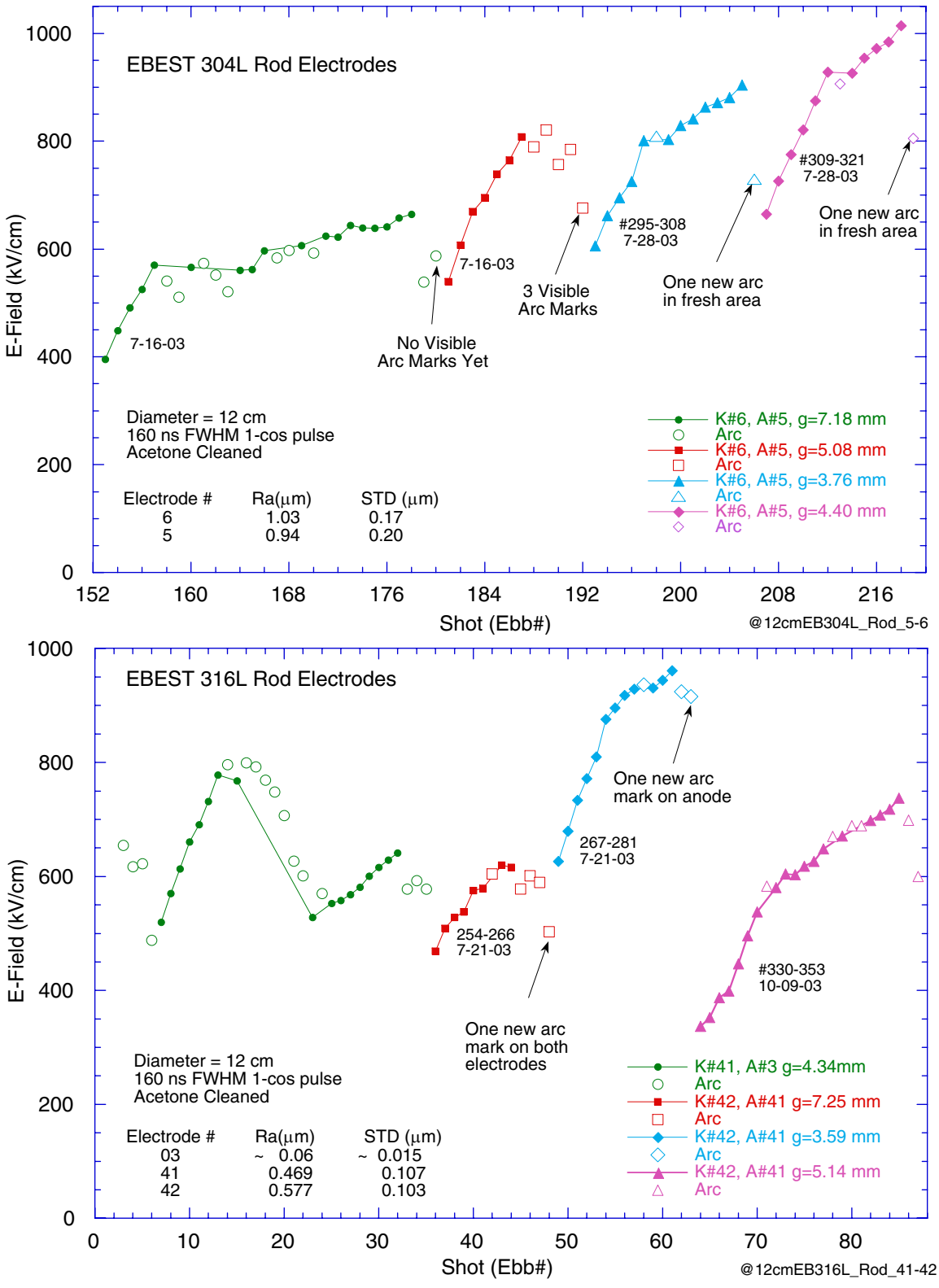

Figure 48. High voltage breakdown data for 12 cm EBEST 304L (upper) and 316L (lower) rod stock electrodes with large gaps.

Discussion

Our simple Child-Langmuir current model fits to the shape and amplitude of the breakdown currents are reasonably good and in some cases excellent. This gives some credence to our assumptions of how the anode and cathode plasmas evolve during breakdown. These fits indicated that a cathode plasma generates the current for the first ~ 50 ns of each breakdown. Later anode plasma is probably formed and the beam assumes bipolar flow. There was a large shot to shot variation in the breakdown current waveforms with all electrode types but not much variation between the electrode types. The CL current model parameters listed in Fig. 49 for 304L rod and HVFF 304L plate stock electrodes illustrate this. The former electrodes had the roughest surface with the highest crater density and the later the smoothest surface with the fewest craters. The craters are produced by dielectric inclusions that evaporate during the EBEST process and ranged from 10 to 0.1/mm^2 for the two electrode types represented. These are listed in Table 1 with the roughness values.

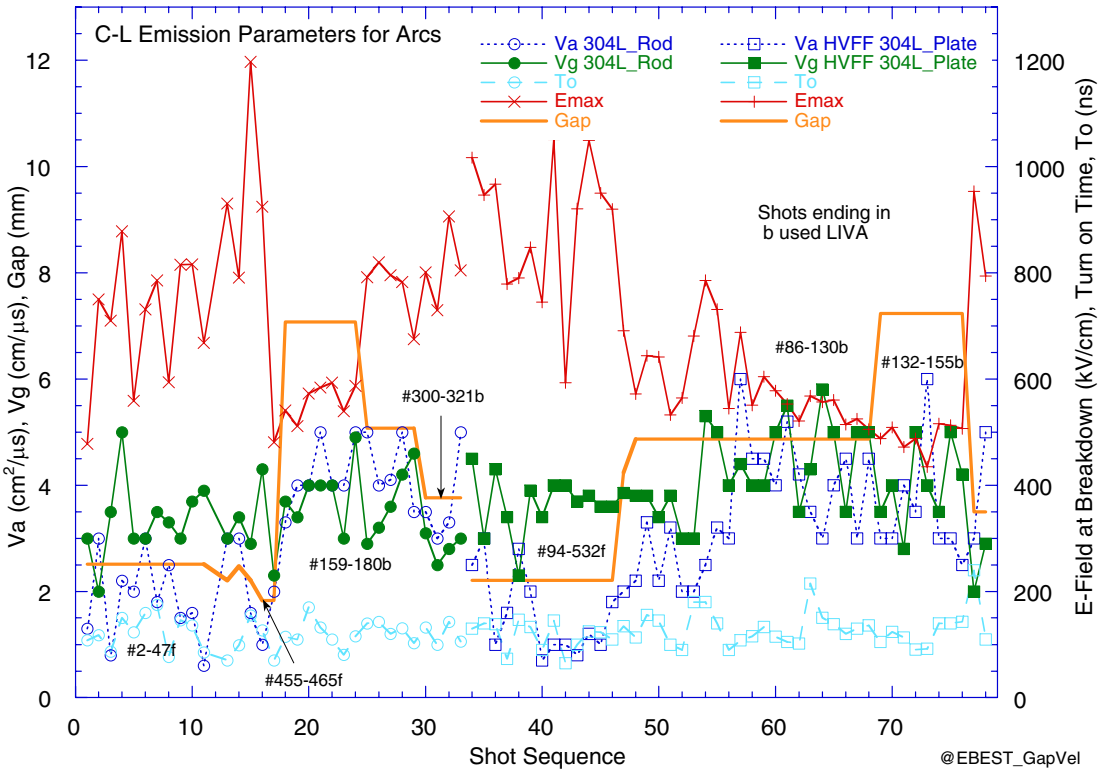

Figure 49. The CL model fit parameters of the breakdown shots for EBEST 304L rod and HVFF 304L plate stock electrodes listed in the previous plots of the individual breakdown data.

The mean values of the Child-Langmuir parameters and breakdown voltage for a number of different electrode types are listed in Table 2 and plotted in Fig. 53. The data for the EBEST stainless steel show the mean gap closure, Vg, beam source area expansion rates, Va, and turn-on time, To, agree within the standard deviation for the two stainless steels. The same was true for the other stainless steel surface types tested. The data also show there is a slight tendency for Vg, to scale with gap, Va to scale almost linearly with gap, and To to be independent of gap.

Type #	Electrode Type	Gap mm	Va $cm^2/\mu s$	Vg cm/μs	Ebreakdown KV/cm	To ns	Vbreakdown kV
1	EB 304L rod SS	2.5	1.99±0.82	3.30±0.67	764±176	120±34.9	191
2	EB 304L rod SS	5	4.32±0.66	3.60±0.70	773±56	127±16	386
3	EB 304L rod SS	7.1	4.19±0.61	3.86±0.59	561±31	119±27	398
4	EB HVFF 304L Pl ate	2.2	1.57±0.79	3.65±0.57	890±133	125±27	196
5	EB HVFF 304L Pl ate	4.89	3.55±1.09	4.27±0.81	591±76	132±31	287
6	EB HVFF 304L Pl ate	7.23	3.50±1.10	4.0±0.75	491±27	118±21	355
7	Sanded 316L Plate	2.3	1.28±1.6	2.97±0.76	833±118	124±23.5	192
8	T4 Al	3.5	3.36±1.24	3.24±0.36	515±70	135±30	180
9	T4 Al	7.4	4.46±2.4	4.08±0.66	424±89	150±37	313
10	T8 Al	3.7	2.48±0.72	3.22±0.65	425±69	138±42	157
11	T8 Al	7.4	2.93±1.35	4.48±0.61	461±63	154±27	341
12	T5 Anodized Al	2.2	4.17±2.09	5.26±0.65	906±2.69	144±36	193
13	T1 Anodized Al	4.5	4.04±1.14	3.48±0.68	908±159	146±22	409
14	T3 Anodized Al	4.5	2.83±1.16	3.47±0.54	813±211	124±39	366
15	T5 Anodized Al	4.5	3.02±1.12	3.47±1.34	766±28	121±32	345

Table 2. The mean and standard deviation of the Child-Langmuir current model breakdown parameters for different electrode types and gaps.

Our experimental highest hold-off results for the 12 cm EBEST and polished stainless steel electrodes appear to approximately follow the Cranberg [16] scaling law $V_b \propto d^{1/2}$ for the "total voltage effect". The average of these data are shown in Fig. 50 where the scaling law is arbitrarily set at 1.1 MV/cm for a 2-mm-wide gap. This scaling law arises for mechanisms that respond to the E-field at the initiating surface and the voltage across the gap. This is the case for breakdowns caused by the impact of micro-particles accelerated across the AK gap if three criteria are met. The criteria are that: 1.) charge density (Q/A) of the particle is proportional to the E-field at the surface, 2.) breakdown occurs for particle energy density (U/A) greater than a well defined value, and 3.) time is available for the particle to cross the gap during the voltage pulse. Latham [4] indicates (Eq. 7.6) that the charge on a spherical particle resting on a planar surface is given by $Q = 6.6\pi\varepsilon_0 r^2 E$. Also the particle energy per cross-sectional area gives in impact velocity of $v = C \cdot (3/2\rho r)^{1/2}$, where C is a constant and ρ is the particle density. The threshold velocity for graphite particles to vaporize on impact is estimated by Gray and Stinnett [21] to be 12 km/s. Smith and Adams [49] found that iron particles impacting at 10 km/s result in plasma production. Similar velocities are quoted by Latham [4]. These limits are for ~ 1-μm-diameter particles. These criteria give guidance to the likelihood of micro-particle initiated breakdown.

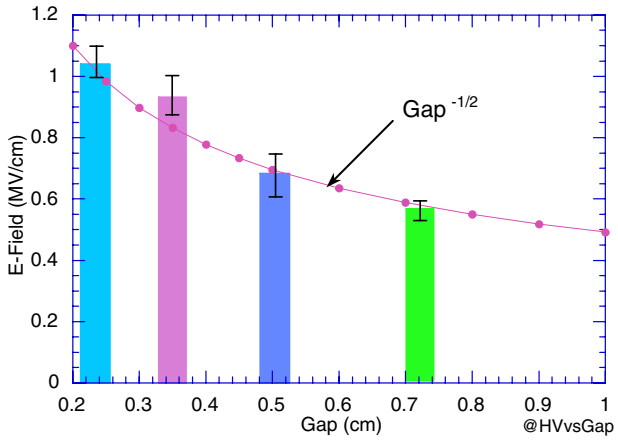

Figure 50. The mean breakdowns for the 12 cm SS electrodes plotted with a $gap^{-1/2}$ scaling.

The impact velocities, transit times, and critical velocity for vaporization of graphite particles accelerated across 2.5 and 5 mm gaps by the typical breakdown E-fields of1 and 0.7 MV/cm are shown in Fig. 51. The plots show impact velocities and times for enhancements of 1, 10, and 100. The critical velocity occurs at an enhancement of ~ 80 based on Gray's estimate for 1-μm-diameter graphic particles. Only particles with radii < 0.05 μm and enhancements > 100 have transit times less than our ~ 160 ns acceleration pulse. Note that the same particle size gives the same velocity when the voltage $\propto g^{1/2}$. Also a 1 MV/cm field with 5 mm gap gives the same result for a factor of two larger particles. Iron particles, which are more likely to be present after an arc, have factor of two longer transit time and 50% lower critical velocities. Since the measured value for plasma production for iron is ~ 10 km/s the enhancement would need to be ~ 150.

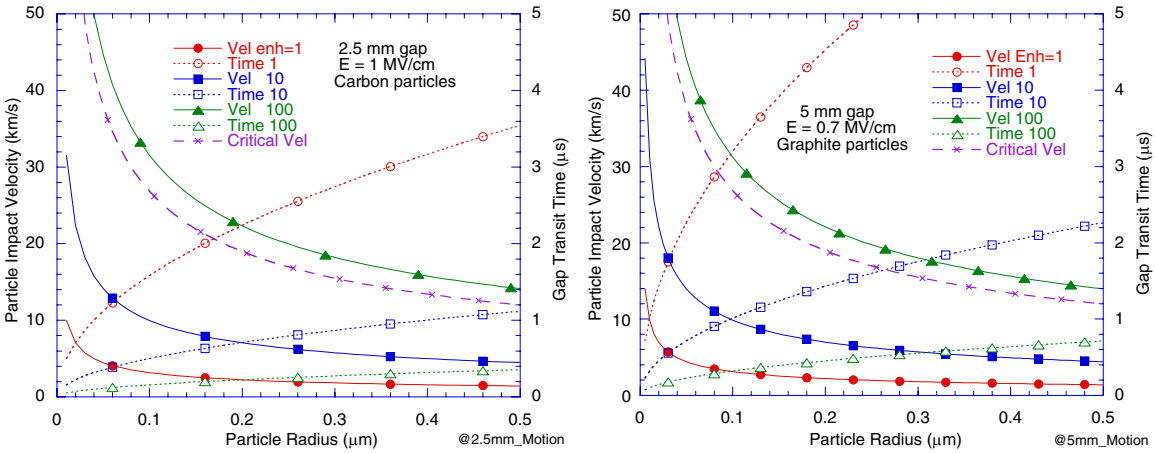

Figure 51. The impact velocities, transit times, and critical impact velocity for spherical graphite particles accelerated across 2.5 and 5 mm gaps. The red, blue, and green curves were calculated using Latham's charge formula with charge enhancements of 1, 10, and 100 respectively.

There is a lower limit to particle size set by attractive forces holding particles to the electrodes. The van der Waals force between particles and the electrode surface must be smaller than the electric-mechanical force pulling particles from the surface. According to Latham [4] and Gray [20] the minimum radius is: $r_m \geq 2A_0 / \pi\varepsilon_0 E^2$, where A_0 is the van der Waals constant of 0.2 N/m. For E = 1 MV/cm the minimum radius is about 0.5 μm. However, Latham [4] states that the van der Waals constant is considerable reduced in ~ 10^{-5} torr vacuum so this radius is an upper limit. The required small particle size and high enhancement for micro-particle inducted breakdown with 160 ns pulses push this mechanism into a regime that, except for Gray and Stinnett, has not been considered in the past where most studies of micro-particle induced breakdown used 1 to 10 μs pulses.

At first sight this mechanism seems so unlikely that we look at it more deeply for lack of a better explanation. We make an attempt to show how it could happen based upon the plots in Fig. 52. The calculated transit times shown in the left plot of Fig. 52 assume a charge enhancement of 100 and voltage scaling as gap$^{1/2}$. Note that the impact velocity is the same for all gaps and the transit time is proportional to gap. The final velocity remains constant because the particle energy scales as the gap voltage times the charge, which increases with E-field.

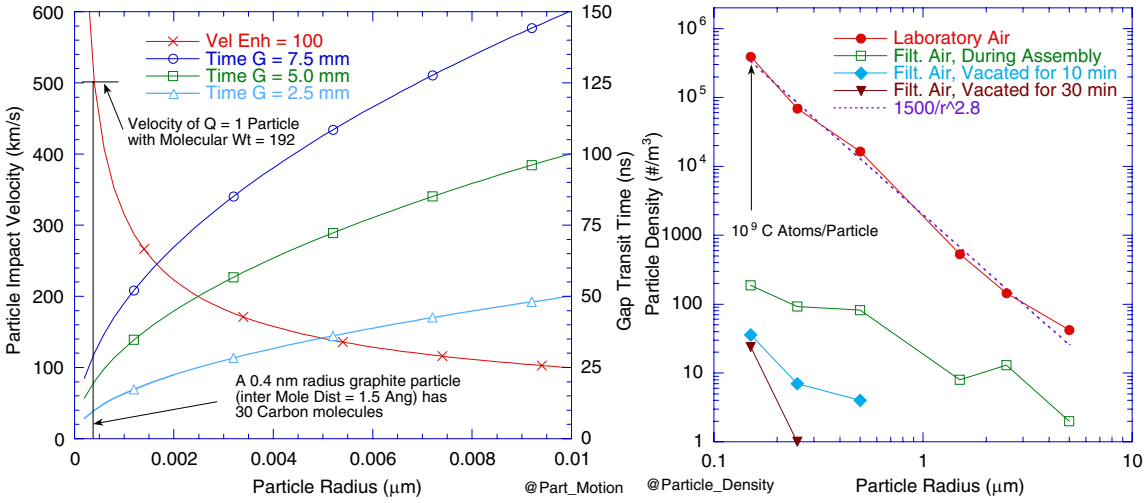

Figure 52. (left) Calculated particle impact velocities and transit times for 2.5, 5 and 7.5 mm anode-cathode gaps. The voltage was taken be 250 kV for the 2.5 mm gap and to scale as the square-root of the gap. (right) The particle density in the measurement interval for the: 1.) laboratory environment, red curve, 2.) during cleaning and assembly of hardware with rubber gloves and lint free lab jacket used, green curve, 3-4.) with the clean air tent vacated and filtered for 10 and 30 minutes, blue and brown curves, and 5.) an empirical scaling as $2000xR^{-2.8}$, purple curve.

Figure 52 shows that the particles would need to be < 0.01 μm in diameter to cross the gap while the voltage was applied. A larger charge enhancement would allow for larger particles to participate in the mechanism. The particle count density measured in the lab and filtered air tent are shown in the right plot of Fig. 52. Note that our filter system primarily removed particles > 0.3 μm so the density of particles less that this diameter probably remained very high. This argument would be very convincing if the turn-on time varied with gap size according to the transit times shown in Fig. 52. The delay should be at least 50 ns longer for a 7.5 compared to a 2.5 mm gap. However this is not the case as illustrated by Fig. 49. Also Table 2 shows mean delay, To, and other CL parameters for the gaps and electrode types listed in Table 2. The time, Tnorm, is the time after 100 ns (V = 0.6Vmax) that particles would initiate a breakdown if normalized to a 5 mm gap and 300 kV voltage. The Tnorm values are actually inversely related to the calculated values for micro-particle induced breakdown shown in Fig. 52.

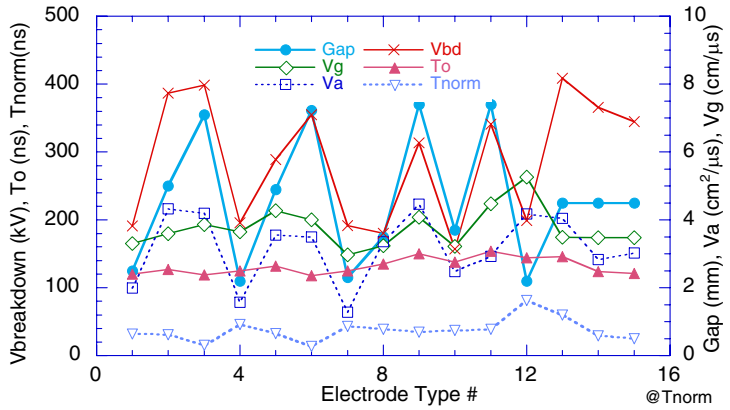

Figure 53. The mean Va, Vg, To, and breakdown voltage, Vbd, plotted with gap for different electrode types. Tnorm is a normalized delay time to produce breakdown for particles emitted when 0.6Vmax. It is specified by the formula:

$$T_{norm} = (T_o - 100) * (5/G) * (V_{bd}/300)^{1/2}$$

We are therefore forced to conclude the particles need to be << 1 nm, have enhancements > 1000, or have a launching mechanism that favors earlier launches for larger gaps. It is difficult to envision an earlier launching mechanism so we first consider how particles with such small size could possibly dominate the breakdown mechanism. The EHD mechanism for generating extremely small metal droplets with high enhancements and velocities > 10^5 m/s discussed by Gray [20] is intriguing but the mechanism requires a molten surface to allow the droplets to be generated and pulled from the anode. However it isn't obvious how this anode could melt so quickly before current flows in the diode. Amore likely scenario involves molecules with about 10 atoms that happen to acquire a single electron charge. They would have an effective enhancement of ~ 300 and cross our 2.5 and 7.5 mm gaps in 8 and 18 ns. They might initiate a breakdown but should still show a measurable 10 ns difference of breakdown time in Fig. 53. Larger particles with >1000 enhancement would cross faster and not show a measurable delay. However their impact velocity would be far above the threshold for plasma production and a wider range of particles would cause breakdown, leading to preferential breakdowns with smaller gaps. All these arguments seem to rule out the micro-particle breakdown mechanism for our short pulse experiments.

Latham has a brief discussion of the physics of breakdowns for pulsed voltages in Section of 2.6.2 of his book [4]. He references Lloyd and coworkers [50,51] for work with vacuum switches that show a distinct $V_b \propto d$ for gaps < 1.5 mm and $V_b \propto d^{1/2}$ for gaps > 2 mm where the pulse length is much too short for particles to cross the gap. They suggest that the large-gap breakdowns are the result of a trigger mechanism associated with the launching of the micro-particles. However Latham states that the events could be the result of a thermal instability following the rapid switching on (within 10's of ns) of a more complex non-metallic electron emission mechanism associated with insulating micro-inclusions on the surface of the cathode. The argument seems improbable in the light of our experiments where we little difference in hold-off of EBEST + HVFF 304L plate electrodes that have a factor of 100 lower inclusions density compared to EBEST 304L rod electrodes (see Table. 1). Also we see reduced hold-off from electrodes with molten metal blow-back debris after an arc that can be recovered from by simply cleaning the electrode surfaces. Jimenez [3] indicates metal particles are accelerated from anodes.

Electrons or ions released from the background gas could build-up charge on dielectric particles or inclusions and initiate cathode plasma. This effect should scale with vacuum pressure and gap but we saw no effect on breakdown with 10^{-7} to 10^{-6} Torr vacuums. Another possibility is leakage electron from the cathode striking dielectric particles and initiating charge build-up by a mechanism that is related to the gap voltage. The current density from background gas or the cathode required to charge-up and flashover a dielectric is ~ 1 A/cm^2 and would be measurable. Also we see no reason why the charge build-up would be proportional to the energy of leakage electrons. Other pathological effects such as UV-radiation from partial breakdowns on the support rods or the slightly faster rise times that occur with the larger gaps seem unlikely explanations also.

VII. 12 cm Machined and Polished Stainless Steel Electrode Tests

Air Purity Tests with Polished 316L Stainless Steel

It has often been noted in the literature, that polished metals, including stainless steel, have excellent hold-off characteristics. Mahner and colleagues [32] obtained scanning anode probe plots of pre-emission sites from chemically polished R_a = 10 μm and diamond turned R_a = 6 nm copper. The plots show a factor of ten fewer pre-emission sites per unit area with the diamond turned samples. Otsuka and colleagues [52] obtained 3 MV/cm hold-off fields with diamond turned, R_a = 50 nm, oxygen-free copper after about 50 electrical conditioning shots. The electrodes were 2.5 cm diameter with hemispherical tips. The electrical pulse was 700 μs FWHM. They also observed that hydrogen annealing reduced the number of conditioning shots required to attain stable hold-off to ~ 10 but that the maximum hold-off dropped to 2.5 MV/cm.

We tested polished 304L plate and 316L rod electrodes in June and November 2002 prior to testing the Russian EBEST electrodes. Three 304L rod and nine 316L plate electrodes were retained from Russia or testing. The polish was obtained by polishing on a lathe with 1-μm-grit diamond polishing paste and also by wet or dry sanding with 2000 grit silicon carbide sandpaper. We either blew a flushing of acetone from the surfaces with compressed CO_2 or just dusted the surfaces with CO_2 after wiping off the acetone with the laboratory wipers. The two polishing methods and CO_2 applications gave similar hold-off results to within 10%. These tests showed that the high-voltage hold-off improved when the electrodes were carefully cleaned in a filtered air environment. The summary data in Fig. 54 shows this improvement. Individual data for the 304L plate and 316L rod electrode tests are shown in Figs. 55 and 57.

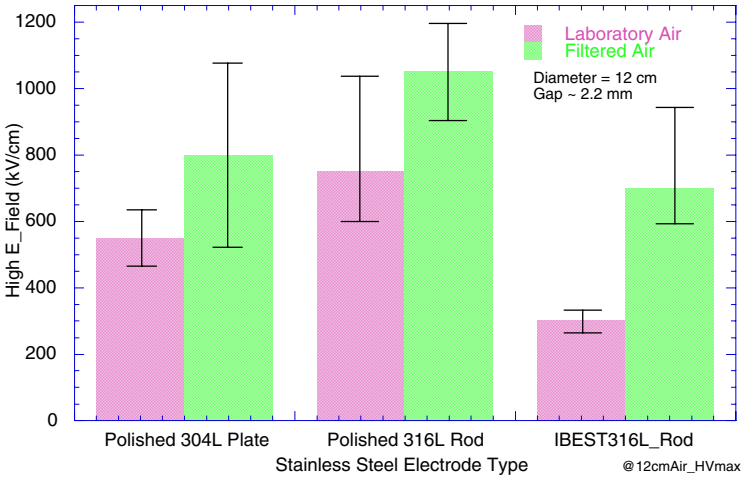

Figure 54. A summary of the hold off data for polished 304L plate and 316L rod cleaned in laboratory and filtered air. Some comparison data obtained with a 5 J/cm^2, 50 ns, 800 keV, nitrogen beam treatment is shown as IBEST.

The cathode arc marks on many of these shots showed interesting patterns similar to the mark illustrated in Fig. 56 for shot plt142. Both photographs were taken of the same arc location but with different illumination. This shot was taken with new 304L plate cathode # 63.

We also observed the large increase in the hold-off of ion beam treated stainless steel when tests were done after cleaning in the clean air environment. The poor hold-off of IBEST electrodes was previously attributed to emission from chunks of copper debris that were melted from the diode electrodes on some shots. This debris is difficult if not impossible to remove so perhaps the very rough surface generated by the ion beam made it difficult to clean the surface in laboratory air where air born particles constantly landed in the craters of the surface. With filtered air few air born particles are present so careful cleaning can eventually remove most of the particles from the surface craters.

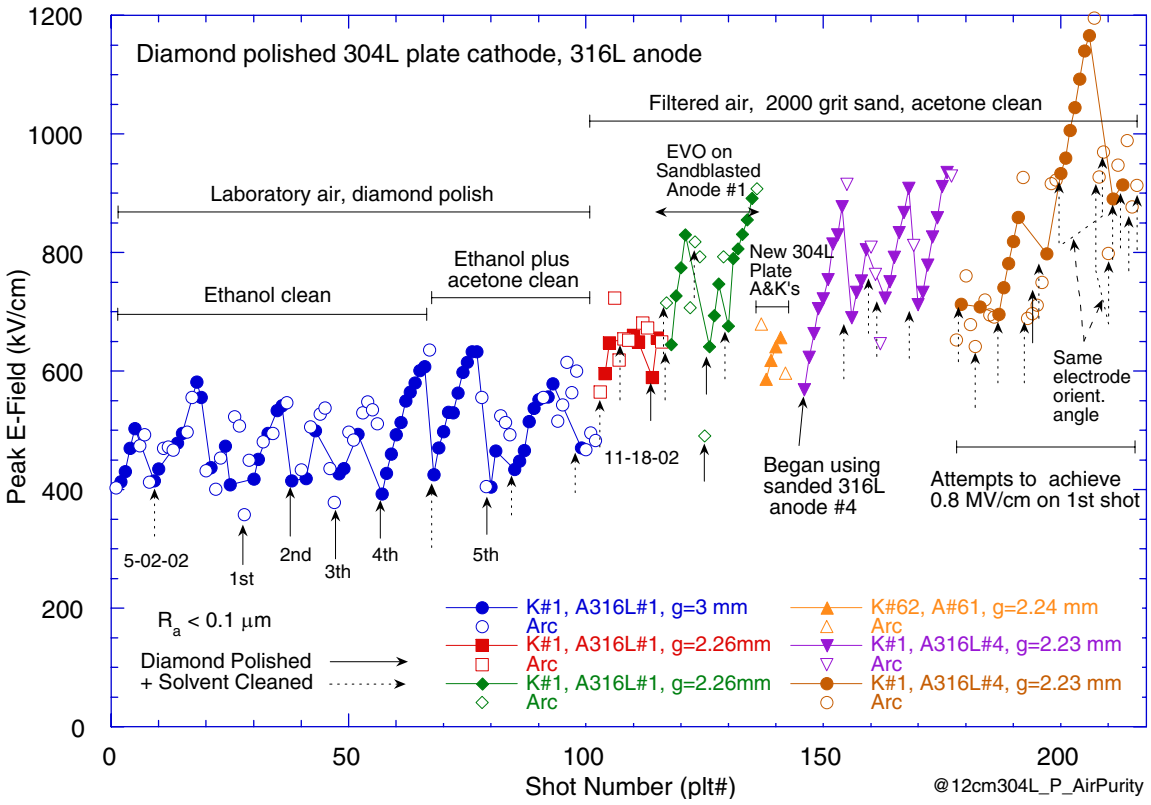

Figure 55. The electrical breakdown data for polished 304L plate cathodes acquired with various cleaning procedures.

During the preliminary tests with polished electrodes we attempted to improve hold-off performance by RF discharge cleaning. Tests were done with 2000 grit sandpaper polished 316L plate electrodes. The gap was opened to 1.2 cm prior to the test shot and the chamber filled with ~ 20 mTorr argon. The gas was then excited to a purple glow with 200 W of 14 MHz power applied to the gap. This was sufficient power to heat the electrodes significantly as noticed by touching. In each case the hold-off field dropped from ~ 800 to 500 kV/cm. We attribute the drop to a brownish color film that was deposited on the electrodes from hydrocarbons liberated from the plastic parts in the chamber. However the drop could also have been due surface contamination that occurred during the more difficult installation procedure. The procedure involved installing a RF-cable assembly and using an arm operated through a vacuum feed-thru to lower the gap to 2.3 mm.

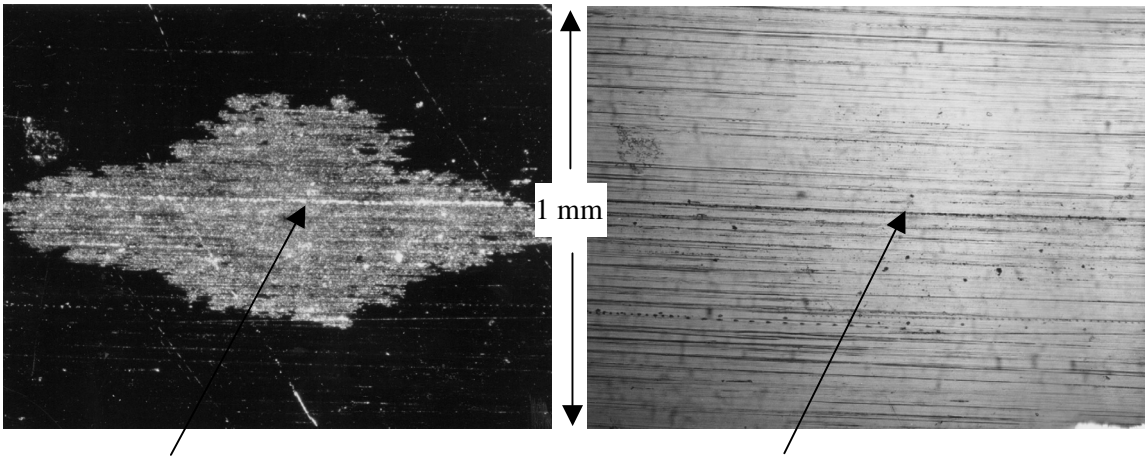

Figure. 56. Photographs of the cathode arc mark from shot #plt142. The arrow points to the location of the arc. The photo on the left was taken with grazing incidence light from a fiber optic light source. The photo on the right was taken with nearly normal incidence source projected through the microscope lens.

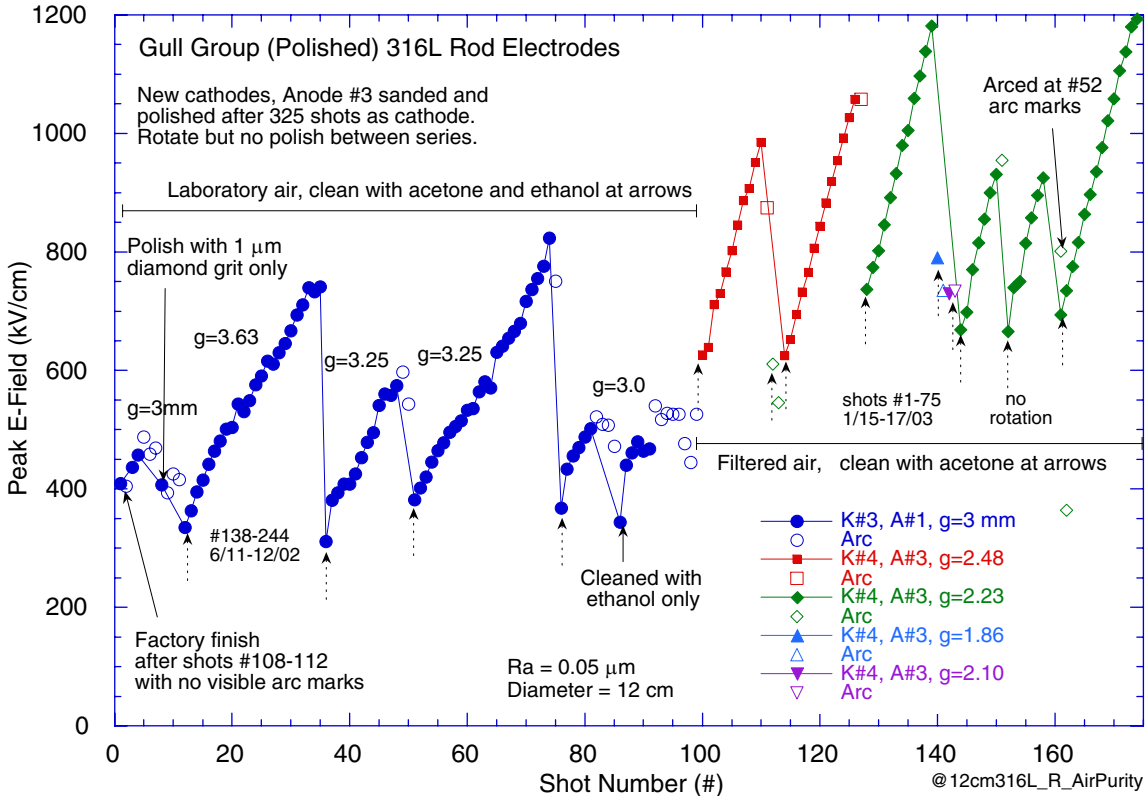

Figure 57. The electrical breakdown data for polished 316L rod electrodes cleaned in laboratory and filtered air.

The data obtained with new Gull Group cathodes comparing laboratory and air are somewhat compromised for two reasons. First we switched to acetone only with the filtered air and second we used smaller gaps. The acetone seemed to give a qualitative improvement in hold-off. More importantly the change of gap also gave an increase to

hold-off. This change occurred because it was necessary to use a 2.2 mm gap to get breakdown with the filtered air because we were still using the pulser without LIVA which was limited to 265 kV. In retrospect the "total voltage effect" scaling produces a 16% higher hold-off E-field for the smaller gap. Therefore the nearly 50% improvement we observed would have been only about 30% at the same gap spacing.

Machined 316L Electrode Surface Quality

We also tested machined 316L rod electrodes with different R_a values with the clean filtered air. These results are summarized in Fig. 58 and the voltages and CL parameters for breakdown shots are shown in Fig. 59. They show that with machined surfaces, hold-off decreases with increased roughness. This is different from EBEST electrodes that have nearly constant hold-off for R_a varying from 0.2 to 1 μm. The reason for this difference could be that, although EBEST electrodes have a rougher surface, the surface features are longer wavelength with few if any micro-protrusions. This assumes that classical breakdown from electron emission and subsequent exploding cathode "whiskers" are important for machined surfaces.

There is also the possibility that small burrs on the machined surfaces retain cleaning wiper lent and make it more difficult to clean the surface. It this is the case one might expect the gap closure to change with the surface roughness. However this was not the case as shown by the CL fit parameters for breakdown shots with the various machined surfaces. The gap closure velocities plotted in Fig. 59 are relatively independent of machined roughness and have a value of ~ 3 cm/μs which is similar to EBEST surfaces with the same gap.

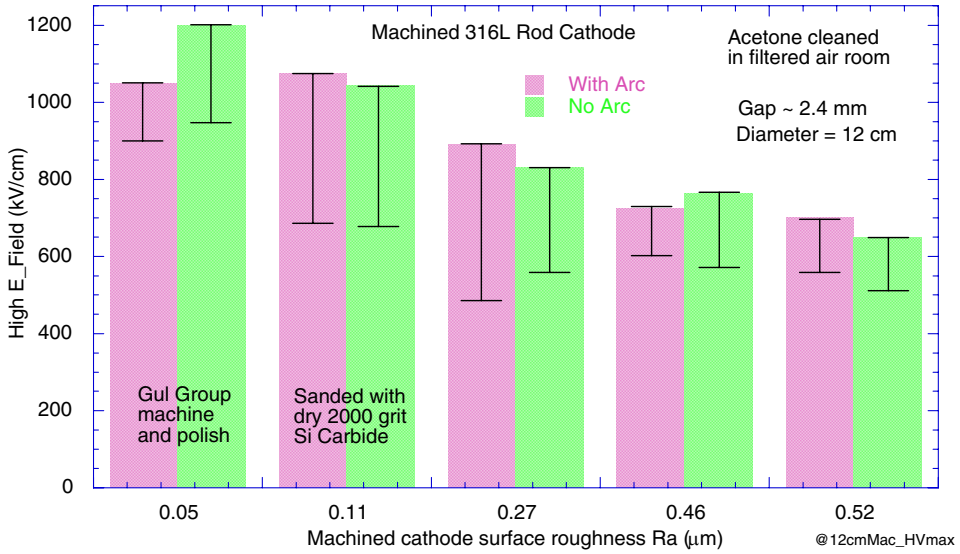

Figure 58. Maximum high voltage hold-off achieved for machined 316L rod cathodes with difference surface roughness. The anode was a polished 316L. The error bars show the range of hold-offs and breakdowns from multiple tests. The breakdown voltages are shown in Fig. 59.

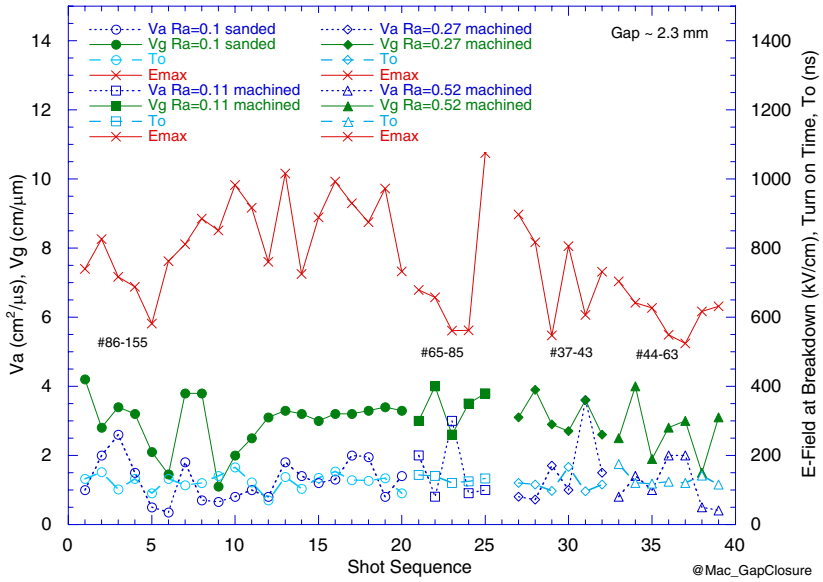

Figure 59. The gap closure velocity and plasma area expansion rates for breakdown shots with machined 316L electrodes.

Extended use Breakdown

We obtained extended use data with polished 316L rod electrodes during a 120 shot radiation survey series. These shots were fired with 7.08 mm gap and most of the shots were fired at our maximum pulser voltage to generate a high x-ray yield. The data demonstrate that the hold-off for polished stainless steel reaches a stable value of about 650 kV/cm under these conditions after a large number of breakdowns. The data were acquired with polished 316L electrodes #3 and #4 (R_a = 0.067 and 0.084 μm) that had previously been used as anodes for the initial large gap tests of EBEST electrodes shown in Fig. 45. Those shots were fired with a 4.87 mm gap and caused the arc mark damage shown in Fig. 60. Note that anode #3 shows the dendrite (Lictenburg) patterns typical of large gaps whereas anode #4 shows the conventional melt arc marks typical of medium and small gaps. It is very surprising that there is difference in the patterns on the two because the breakdowns occurred at similar voltages.

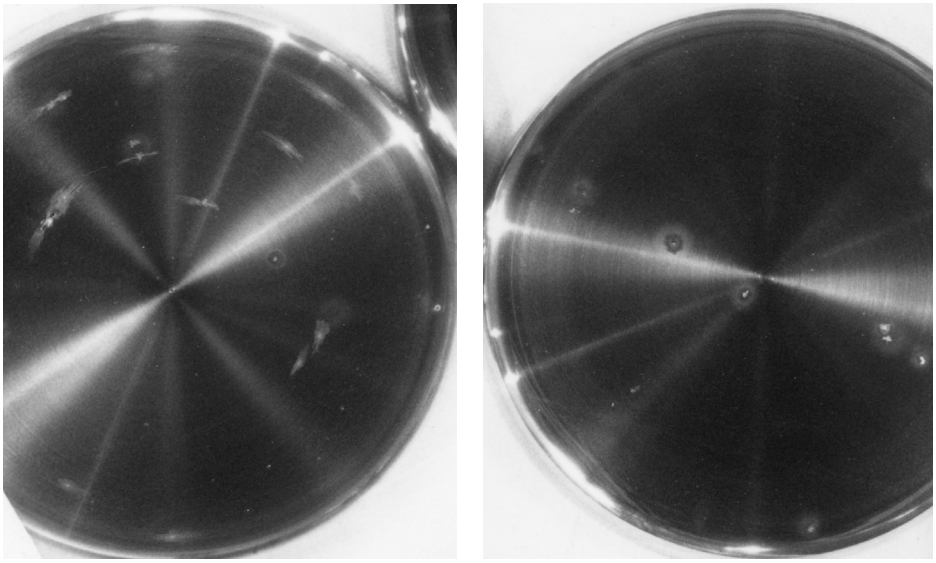

Figure 60. The arc marks on 316L anodes #3 (left) and #4 (right) that occurred during the preliminary shot series shown in Fig. 45.

The breakdown results for the radiation survey series are shown in upper Fig. 61. Note that the breakdowns occurred consistently at 630 ± 50 kV/cm, after the initial shots where the pulser charge voltage was increased from 55 to 87 kV. A photograph of the electrodes after the series is shown in lower Fig. 61. It shows that the breakdowns are randomly located across the electrode surface and not correlated with marks from the previous shot series. There are many new small pit marks on the cathode and the arrow points to an area with a high concentration of just discernable marks.

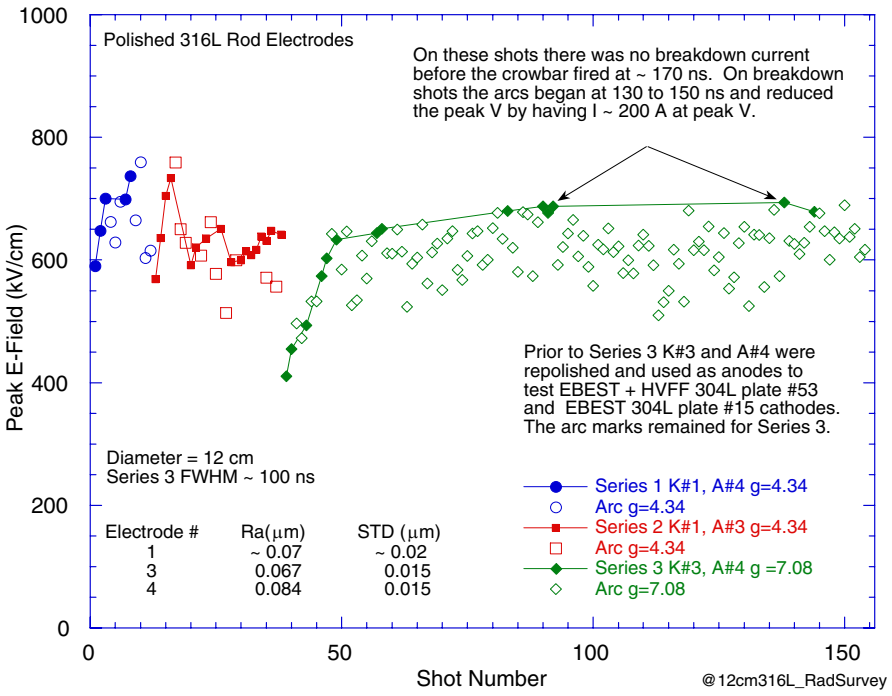

Figure 61. (upper) Electrical breakdown data for polished 316L rod stock stainless steel electrodes. Shots for the radiation survey, Series 3, are shown in green. (lower) The 316L electrodes after the radiation survey. The arrow points to an area on the cathode with many small pit marks from the arcs.

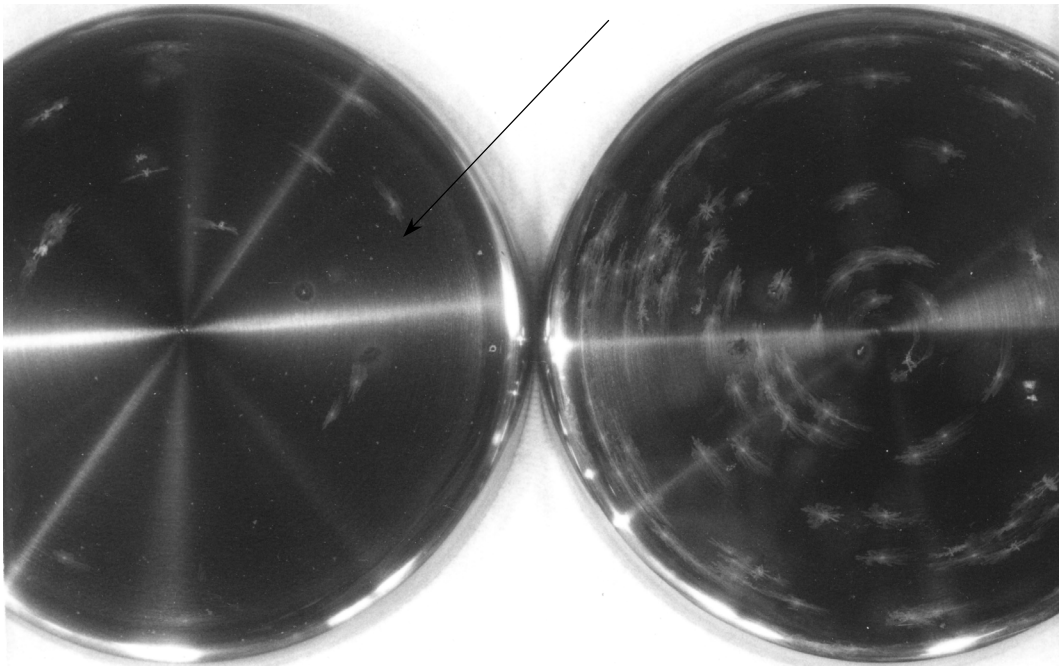

Cathode #3 Anode #4

The electrical waveforms for shot 108 taken near the end of the radiation survey test are shown in Fig. 62. The current does not show the jump late in time current that was observed for many of the EBEST electrode shots. Although some of the shots in the first half of the series showed the jump those in the second half did not. This could be due too conditioning of the cathode, which delayed turn on and resulted in insufficient time to heat the anode. There might have been a small increase of Vgap with higher E-field but the spread in data such as shown in Fig. 59 make it difficult to be sure. The Varea values for the highest voltage shots in the radiation survey series were ~ 7 $cm^2/\mu s$. This is nearly twice the typical values for EBEST tests and may indicate the presence of more than one arc.

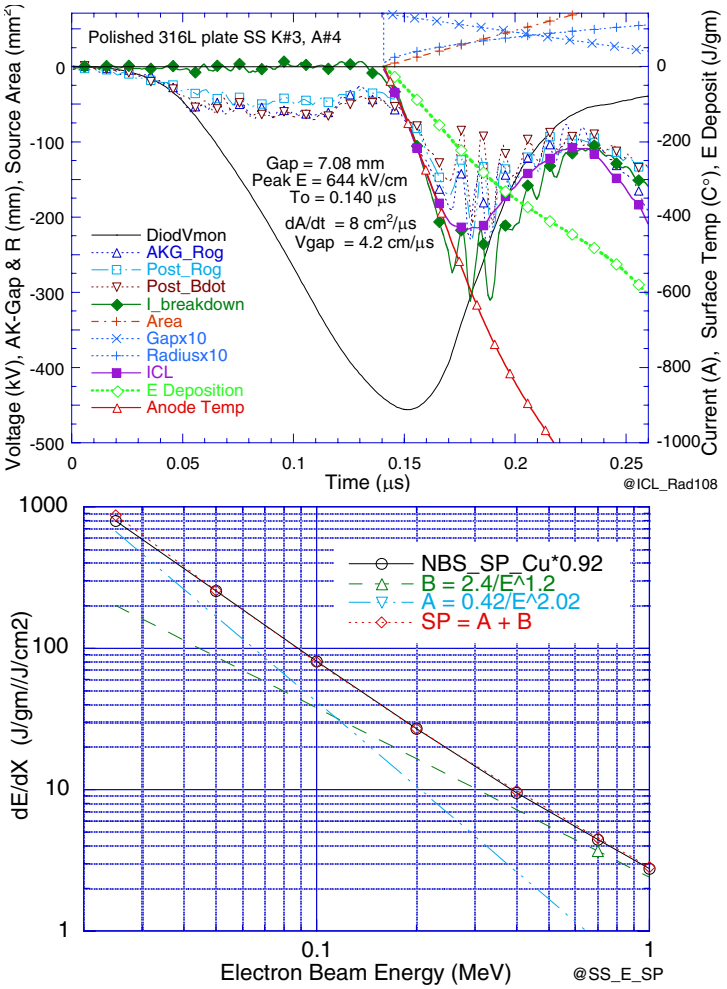

Figure 62. (upper) Electrical breakdown data for shot 108 with polished 316L rod stock stainless steel electrodes acquired at the end of the 125 shot radiation survey series. (lower left) The electron beam surface stopping power extrapolated from the copper data in the Spencer Monograph [46]. The analog expressions for A and B were used in the Kaleidagraph graphics program to calculate the temperature.

The highest hold-off E-fields occurred when the crow-bar fired at ~ 170 ns. On these shots the FWHM was only ~ 110 ns. If the crow bar had not fired there is a good chance the gap would have arced. Shots that began to arc at 125 ns registered 300 A at peak voltage which dropped the voltage by 70 kV. Shots with later onset of breakdown gave progressively higher voltages with lower current and greater tendency for current oscillations. The ringing current observed was due to a partial firing of the crowbar switch that sets up an oscillation between the crowbar circuit inductance and support assembly capacitance. This behavior is shown upper Fig. 62.

VIII. 15 cm Aluminum Electrode Tests

The purpose of this test was to evaluate the 2-mils-thick (50 μm) hard-anodized coatings used on the aluminum grading rings in the Z-accelerator vacuum-stack. Preliminary results of the tests have been described by Johnson [53]. The anodized coatings were formed on 15-cm-diameter 6061-T651 aluminum electrodes by Anadite Inc. [54]. A medium quality, R_a ~ 0.6 μm, and coarse, R_a ~ 3 μm, machined surface, with and without an industrial standard etch, were the planned base surfaces for the coatings. The coating types tested are listed in Table 3 with the typical R_a obtained. The purpose of the etch was to improve the bonding of that anodized coating to the surface. The coarse machined surfaces were tested to determine if the hold-off capability of the coatings would degrade with a very poor machine surface. Tests were also performed on bare aluminum, surfaced finish types T4 and T8, as a reference.

Table 3. Aluminum coating specifications.

Type	Initial R_a μm	Final R_a μm	Etch	Anodized Coating
T1	0.57	1.60	Yes	Yes
T3	0.65	1.40	No	Yes
T4	0.7	Same	No	No
T5	1.55	1.85	Yes	Yes
T7	2.60	2.90	No	Yes
T8	3.25	Same	No	No

Ten anodes of each type were ordered from Gull Group [38] with a 5-mm-gap Chang curves and delivered with roughness from 23 to 130 μinch. The electrodes were then shipped to Anadite to have the coatings formed. They measured their coating thicknesses to range from 2 to 2.2 mil. These values were checked by Jeff Gluth at SNL who measured thickness to be 65 to 75 μm (~ 2.8 mil). The etch was measured by Anadite to increase R_a on T5 surfaces by 0.1 μm. The initial machined and final coated roughness and coating thickness measured at SNL for the electrodes tested are plotted in Fig. 63.

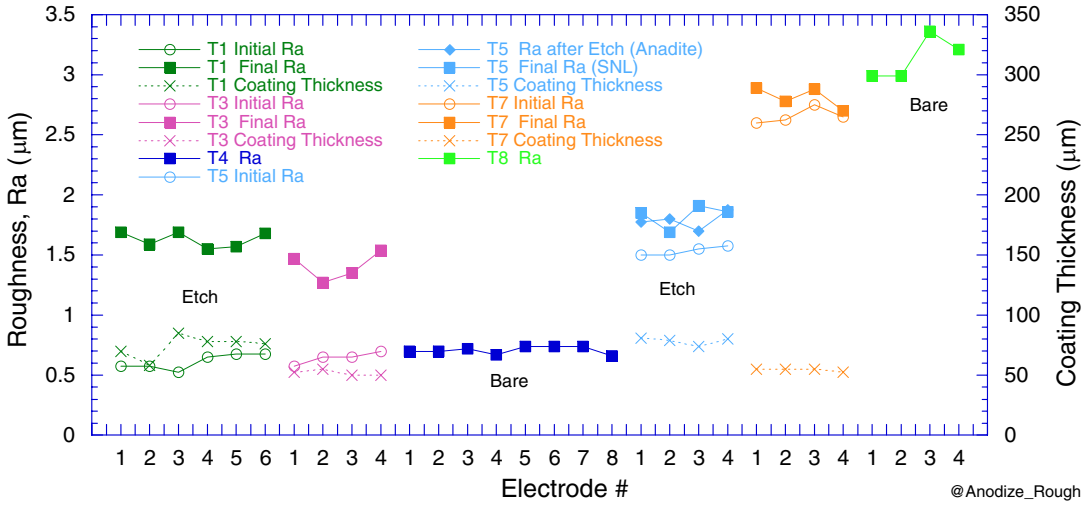

Figure 63. The surface roughness and anodized coating thickness of the electrodes tested.

Tests were also performed with British EVO 191 industrial cleaner applied on the electrode surfaces. The polymer based liquid, EVO 191, is composed of toluene/ethyl acetate/hexane, mixed by volume as 55%/35%/10%. We tested the British AWE formula [55], which is EVO 191 mixed 50/50 with Dow Corning 704 diffusion pump oil. It had been reported to us that optimum hold-off should be expected ~ 2 hrs after application but we observed good results with 2 hr to 12 hr pump downs.

Anodized Coating Tests with Small Gaps

Data were first acquired for anodized aluminum with ~ 2 mm gaps before the LIVA become operational because larger gaps failed to breakdown. The variation in breakdown E-field was larger than observed for stainless steel so it is difficult to give a precise number on the hold-off fields. This is evident in the large spread in the observed breakdown and hold-off E-fields that are plotted with the summary of these results in Fig. 64. Even with the large variation we are able to conclude that new anodized aluminum coatings displayed peak hold-off E-fields of ~ 1.4 MV/cm which is ~ 40% higher than was typical for the best stainless steel treatment. Unfortunately, the hold-off decreased significantly when arc marks accumulated on the electrode surfaces. Large arcs that resulted in a significant amount of aluminum debris on the cathode could result in a 50% reduction in hold-off. On the positive side, small pit marks on the cathode coating from the arc current caused only ~ 20% reductions. Also we did not see a significant difference in the hold-off characteristics of the anodized coatings on the smooth (T1,T3) compared to the rough (T5,T67) initial surfaces. These hold-offs decreased by 30% after an accumulation of arcs. The plot shows the hold-off of EVO coated bare aluminum to be about 30% lower than the value for anodized coatings. The individual breakdown results for T1 electrodes are shown in Fig. 65.

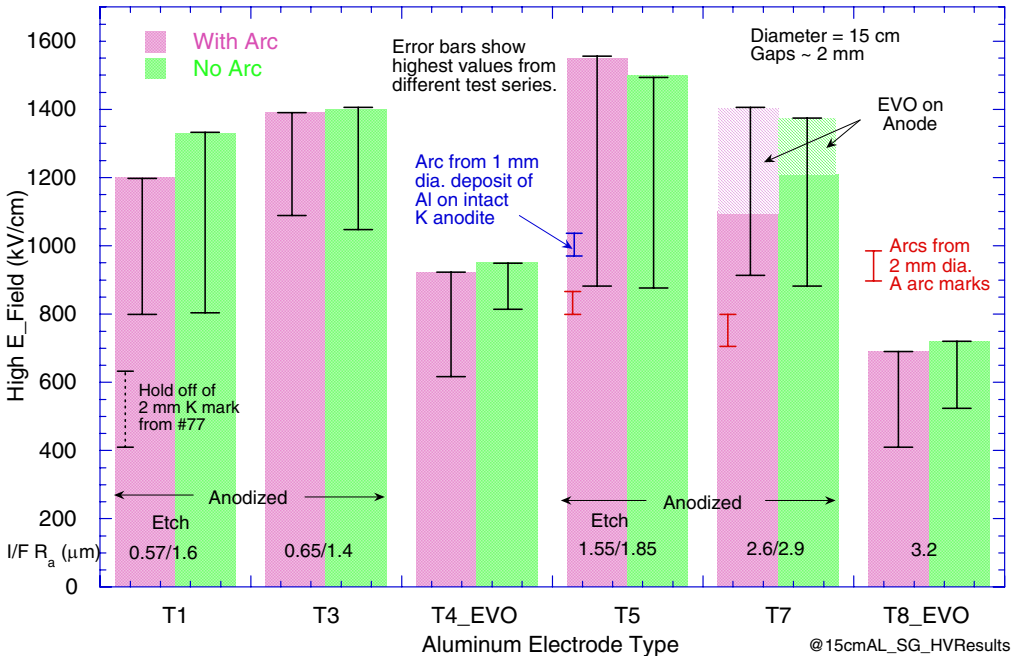

Figure 64. A summary of the test results for anodized and bare aluminum with small gaps.

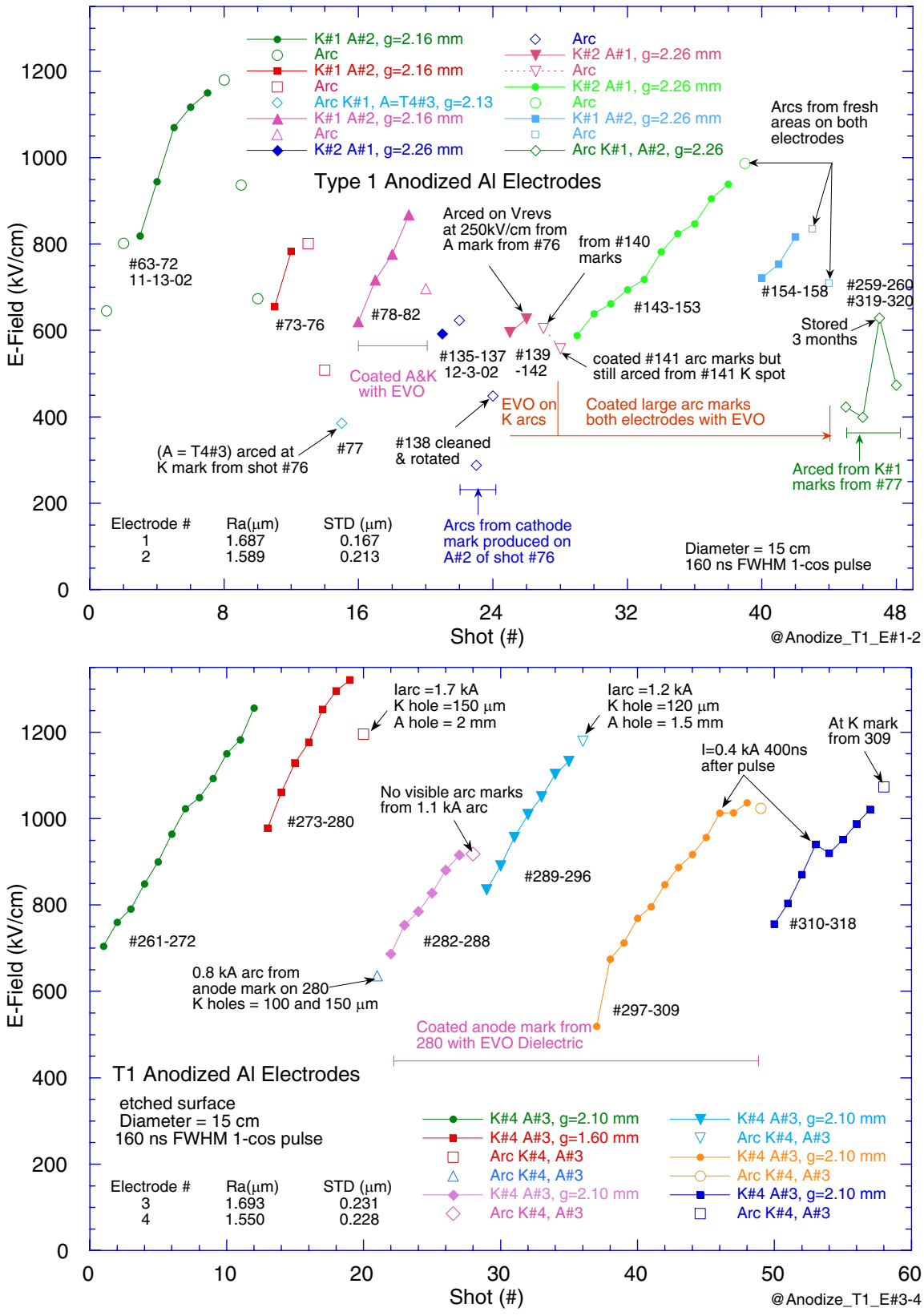

Figure 65. Breakdown data for T1 anodized aluminum anodes #1 to #4 acquired with small gaps.

The breakdown plots in Fig. 65 are annotated in similar manner to the stainless steel breakdown plots to indicate where arcs occurred and other relevant information. With anodized aluminum previous arc marks on either the anode or cathode were likely points of origin for new arcs. Fig. 66, which shows the damage patterns on new T1 electrodes #1 and #2 after shot 76, illustrates this. Note that 6 breakdown shots had already occurred. The initial tests for electrodes 1 and 2 were disappointing in that the hold-off E-field dropped from 1.15 to only 0.37 MV/cm after breakdown shots 70 and 71. It is assumed that breakdown on shot 72 occurred at the same location as shot 71. Scrutiny of the arc marks in Fig. 66 shows that the cathode damage marks were minor pits. The arc indicated from shot 70 was sufficient to melt the aluminum and remove the anodized coating from ~ 0.5-mm-diameter area on the anode. The anode mark labeled 71 was ~ 2 mm wide and located 7.5 cm from arc from shot 70. The electrodes were then cleaned with acetone, in the same manner as the stainless electrodes, and returned to the test chamber after a 67.5° rotation. The subsequent shot series 2 in Fig. 65 then gave breakdowns labeled 75 and 76 in Fig. 66 that occurred from the previous anode arc marks. This demonstrated that anode arc marks are an important potential source of new arcs. We then fired one shot with a bare T4 aluminum anode #3 that had been used for 61 shots (see upper Fig. 79) and accumulated 5 severe and 6 minor arc marks. The purpose of this shot was to determine if arcs on bare aluminum would self-heal like stainless steel and not produce later arcs. The arc on shot 77 occurred from cathode mark labeled 70 in Fig. 66 showing that cathode arc marks can also be an important source of new arcs. The breakdown occurred at only 0.38 MV/cm and we concluded that the small amount of aluminum debris on the cathode surface from shot 70 was sufficient to ruin the hold-off of the coating. This breakdown was actually far below the typical value for bare aluminum so there must have been a sharp edge in the debris.

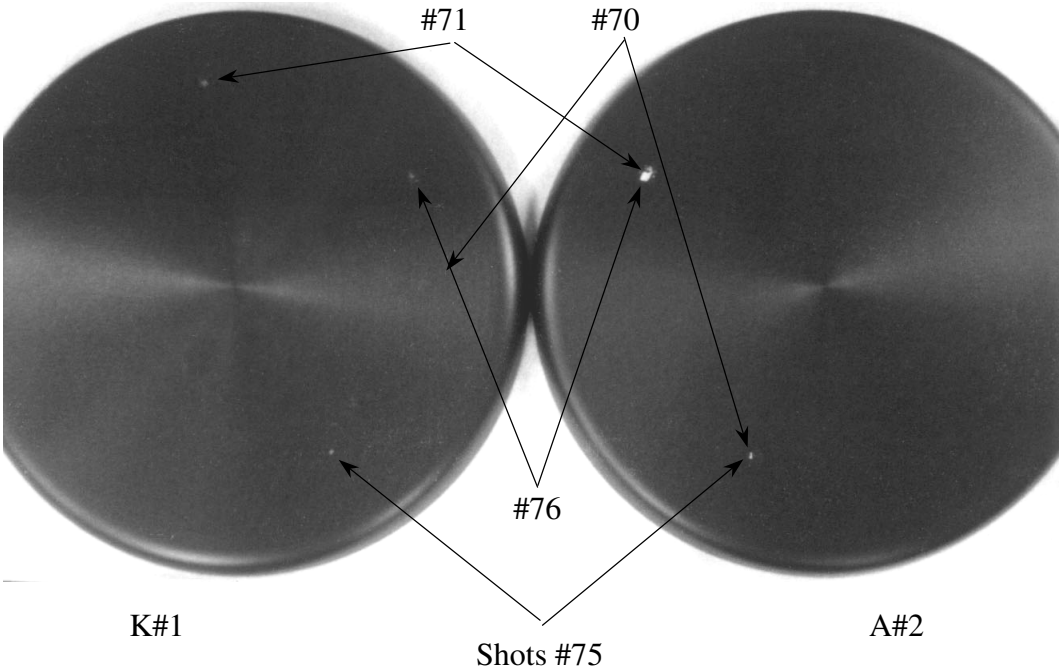

Figure 66. The damage patterns on anodized aluminum electrodes 1 and 2 after shot 76. The cathode, K#1 was rotated 67.5° counter clockwise in photo after shot 72.

The electrical data for T1 electrode breakdown shots 70 and 75 are shown in Fig. 67. These occurred at end of the 1st and 2nd shot series after several successful hold-off shots. The first shot gave the highest breakdown with these electrodes, the second was ~ 400 kV/cm lower. The current fit parameters indicate current source area growth rates, Va, of 0.5 and 0.9 cm/μs, and gap closures, Vg, of 2 and 3.3 cm/μs. These low Va values are typical of the breakdowns of anodized aluminum with high hold-offs (see Fig. 79). The Va's are smaller than the typical value of 3 $cm^2/\mu m$ observed 4 mm gaps (see Fig. 75) as was noted with stainless steel. Both shots show a jump in the diode current late in the pulse that was observed on about half of all anodized and bare aluminum, and various stainless steel electrode tests. This jump is again suggestive of a change to bipolar space-charge limited current flow that occurs when anode plasma has formed and protons counter flow in the gap. There was a significant jump variation in the timing of the jump with respect to the calculated anode temperature but it typically occurred when the calculated temperature was between 1000 and 2000 °C. It is possible that the jump occurs when the anodized coating melts at ~ 2000 °C. If this is true the dielectric surface has a different plasma formation behavior than bare metals that emit ions above ~ 400 °C.

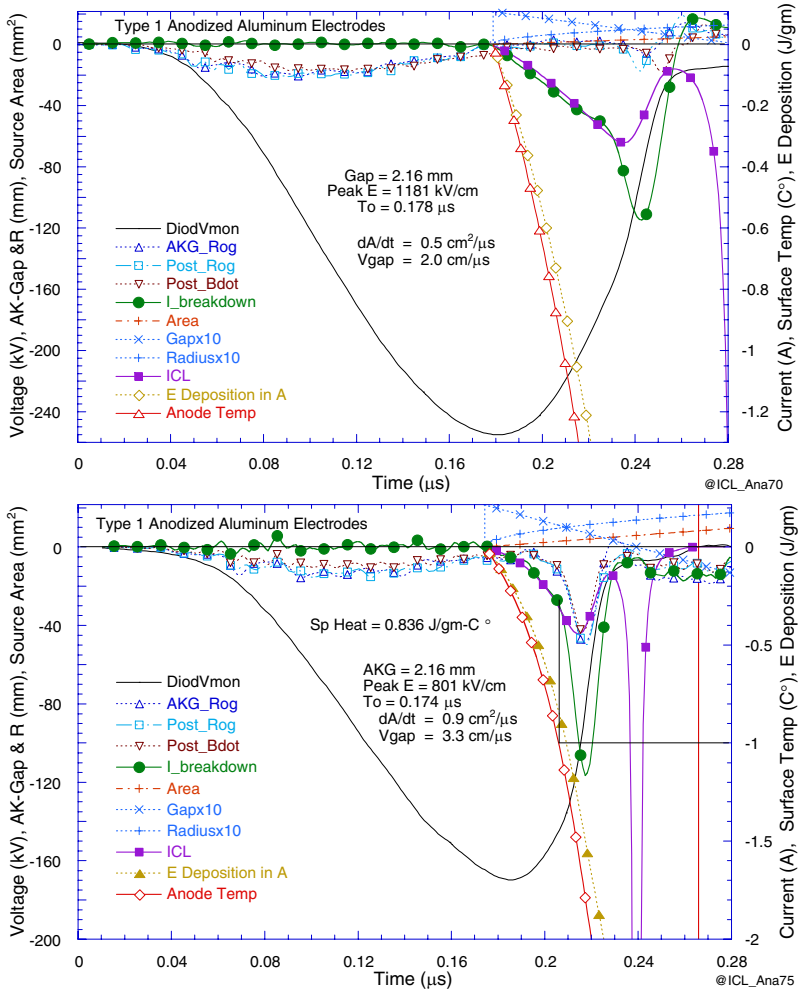

Figure 67. Electrical data from T1 anodized aluminum shots 70, 75. The purple curves are calculated Child-Langmuir space-charge limited currents for a linear area growth and gap close rates. The anode temperatures calculated from the CL current density. The surface stopping power for normal incidence electron on aluminum oxide was used in the calculation.

After the shot 77 we applied EVO only to the cathode arc marks. This prevented emission from the previous arc marks and shot 82 arced in a fresh area. The electrodes were again tested 4 weeks later in reverse order without EVO. In this test arcs originated from the severe mark on cathode #2 created by shot 76 when #2 was the anode (see 2 mm mark on #2 in Fig. 66). The annotations in Fig. 65 describe the remaining tests with these electrodes. We continued tests with EVO on cathode arc marks. Unfortunately the crowbar did not fire so the anode initiated an arc from #76 (enlarged by shot 77) on voltage reversal at 0.25 MV/cm. We then coated the arc marks on both electrodes with EVO and noted hold-off to 0.9 MV/cm with arcs initiating in fresh areas of the electrodes. This showed that electrodes with several EVO coated arc marks would give a hold-off close to that of a new anodized coating. (Later tests with EVO on T4 and T8 bare aluminum electrodes gave hold-offs of ~ 900 and 700 kV/cm as shown in Fig. 85. Similar results were obtained with EVO coated sandblasted stainless steel. The EVO beaded up on machined SS and the hold-off dropped.) Finally the electrodes were tested again after an additional 3 months storage and observed to breakdown from # 77 arc marks at ~ 0.5 MV/cm. These tests show that the arc mark from shot 77 was not pacified was oxide buildup over this time duration. There were no arcs initiated from the small cathode pit marks generated on shots with T1 electrodes #1 and #2.

Later tests with T1 electrodes #3 and 4 shown in lower Fig. 65 generated several ~ 100-μm-wide pit marks in the cathode surface coating but these electrodes still supported hold-off E-fields of ~ 1.1 MV/cm when the anode arc mark from shot 280 were coated with EVO. Shot 318 arced from cathode pit mark on 309 at 1.07 MV/cm giving an indication of the hold-off strength of a cathode pit mark. Prior to the EVO coating the anode mark from 280 caused shot 281 to arc at 0.61 MV/cm. The damage spots from shot 280 are shown in Fig. 68. The molten and/or vaporized aluminum deposited on the cathode is clearly visible. There is a small pit mark at the center of the deposit. However there is no other damage to the anodized coating under the deposited aluminum.

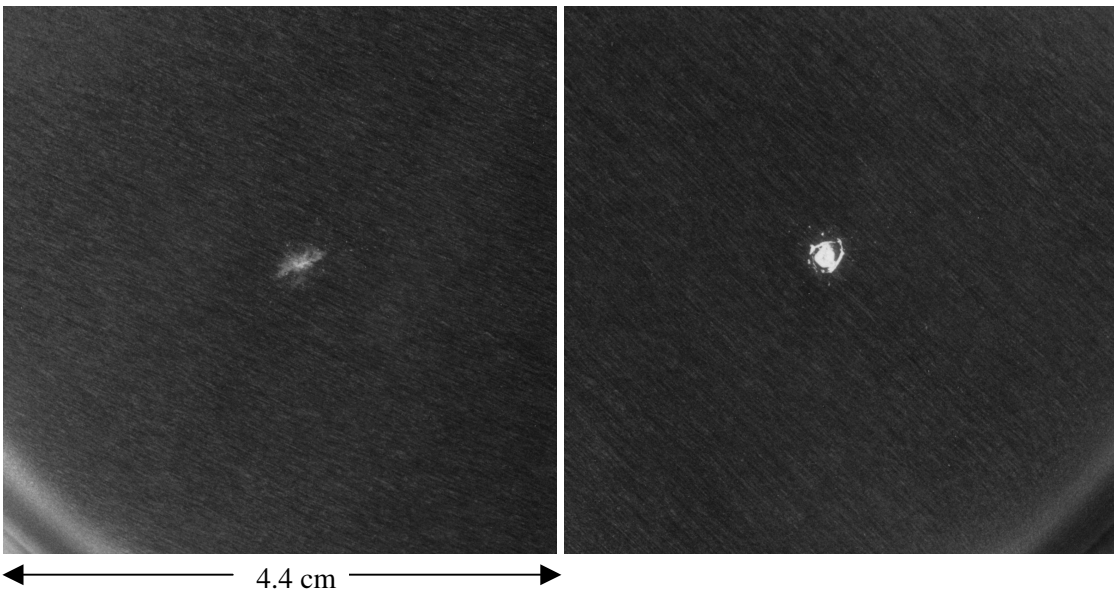

Figure 68. The damage from the arc that occurred on T1 electrodes shot 280 is located at the center of each photo. Cathode #4 is on left and anode #3 is on the right.

The current traces for shot 280 are shown in upper Fig. 69. This shot was taken with the smallest gap tested of 1.6 mm and has the high gap closure velocity of ~ 4.0 cm/μs typically observed for the breakdowns in lower Fig. 65. The Child-Langmuir parameters for the small gap anodized aluminum shots are plotted in lower Fig. 69. A comparison for typical anodized aluminum gap closure velocities in this figure to those for stainless steel shown in Figs. 49 and 59 points out that the gap closures are about 1.5 cm/μs faster for anodized aluminum under similar conditions. The EVO does not further increase the gap closure velocity. The area expansion rates have a much larger variation than the values for bare aluminum and anodized coating tested with larger gaps presented later.

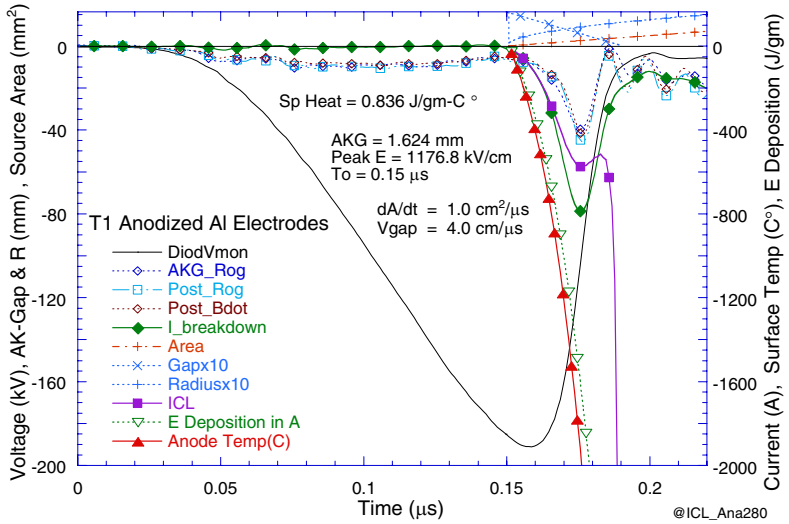

Figure 69. (upper) The voltage and current traces for shot 280. This shot produced the arc damage shown in Fig. 68. (lower) The Child-Langmuir space charge limited current flow parameters for anodized aluminum shots with small gap shots.

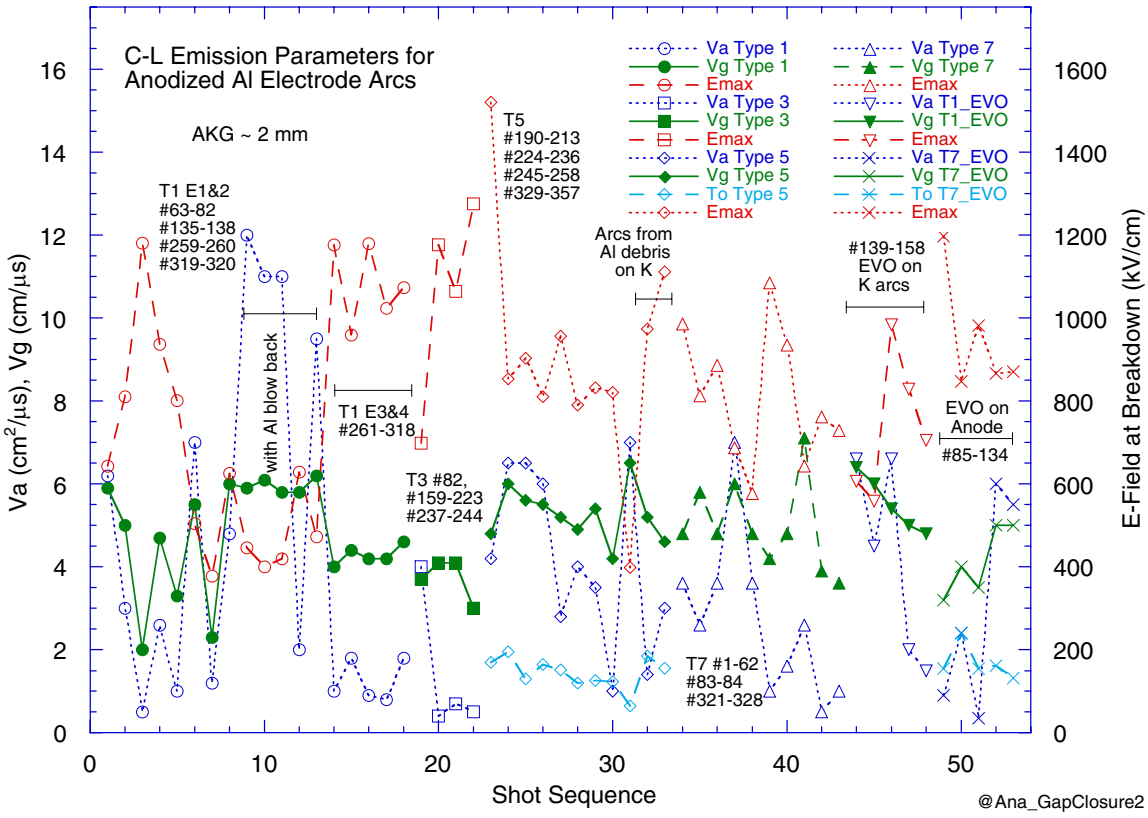

The hold-off data for shots with T3 (no etch) electrodes 1 and 2 are shown in upper Fig. 70. The breakdown shots with these electrodes produced similar damage to those for the T1 electrodes but did not produce such a precipitous drop in hold-off. Some of the damage mark sizes are indicated in the figure annotations. The hold-off for cathode pits marks was similar to the results for E#1 and #2 with shot 189 registering a pit generated arc at 1.07 MV/cm. The electrical waveform data for shot 223, that ended the 4th test series, are shown in lower Fig. 70.

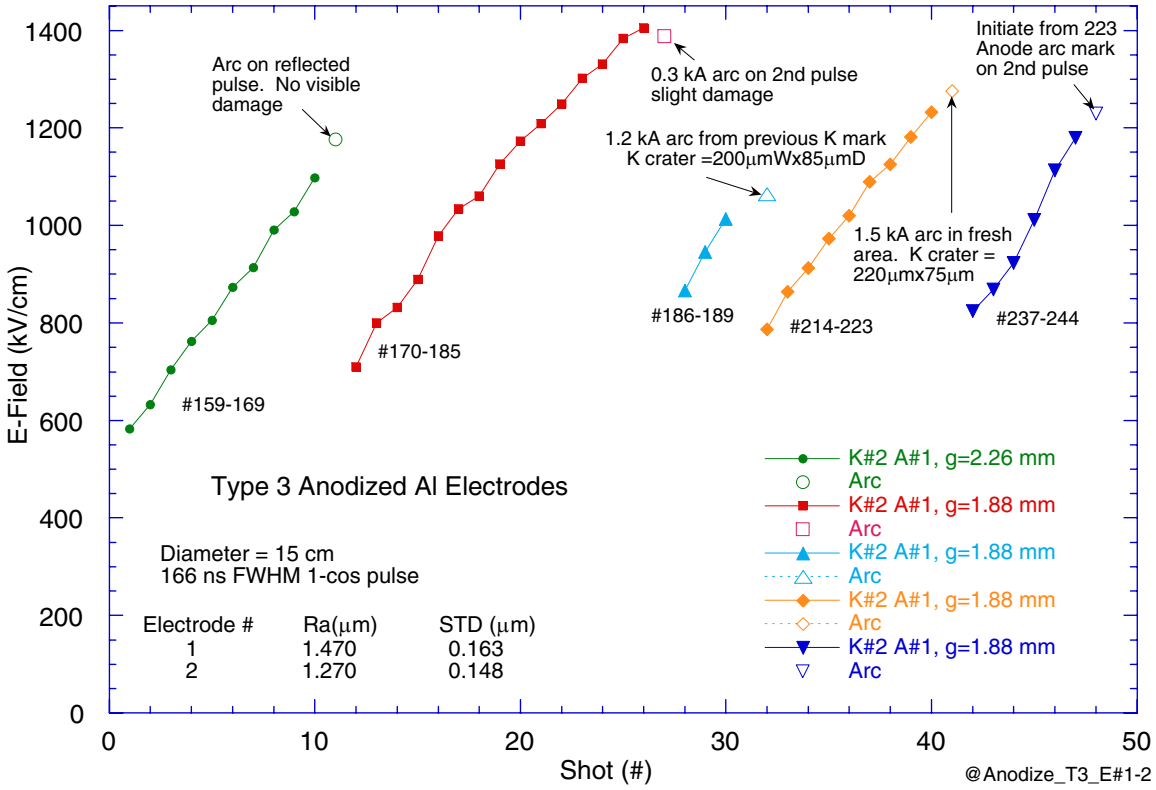

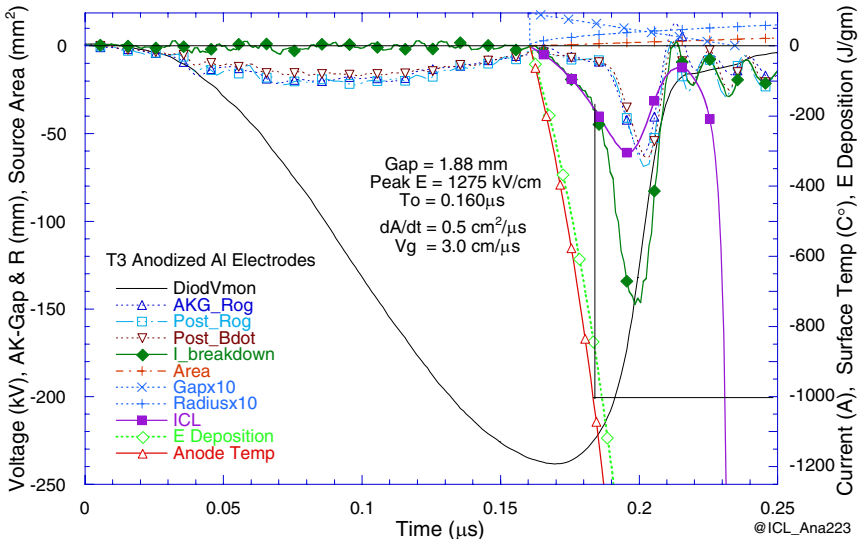

Figure 70.
(upper) Breakdown data for T3 anodized aluminum electrodes K#2 and A#1 acquired with small gaps.
(lower) Electrical data from T3 shot 223. See Fig. 67 for a description of the waveforms and calculations.

The damage observed on the electrodes after shot 223 are shown in Fig. 71. Note that the anode damage on shot 189 has one large central melted region surrounded by several smaller pit marks. This indicates a filamentary structure to the current flowing to the anode. After the cathode was rotated 67.5° the cathode pit mark from shot 185 initiated a second arc on shot 189. After the cathode was again cleaned and rotated the gap sustained a breakdown at 1.28 MV/cm from a fresh area on both electrodes. Surprisingly the ~ 2-mm-diameter melt region on the anode from shot 223 did not cause new breakdowns until the E-field was increased to 1.22 MV/cm and then the breakdown did not draw measurable current until the second pulse. These data indicate that the non-etched electrodes may be capable of better hold-off after damage than the T1 etched electrodes. However we hasten to draw this conclusion because of the limited amount of data. There was little difference between the damage patterns for anodized etched and machined surfaces.

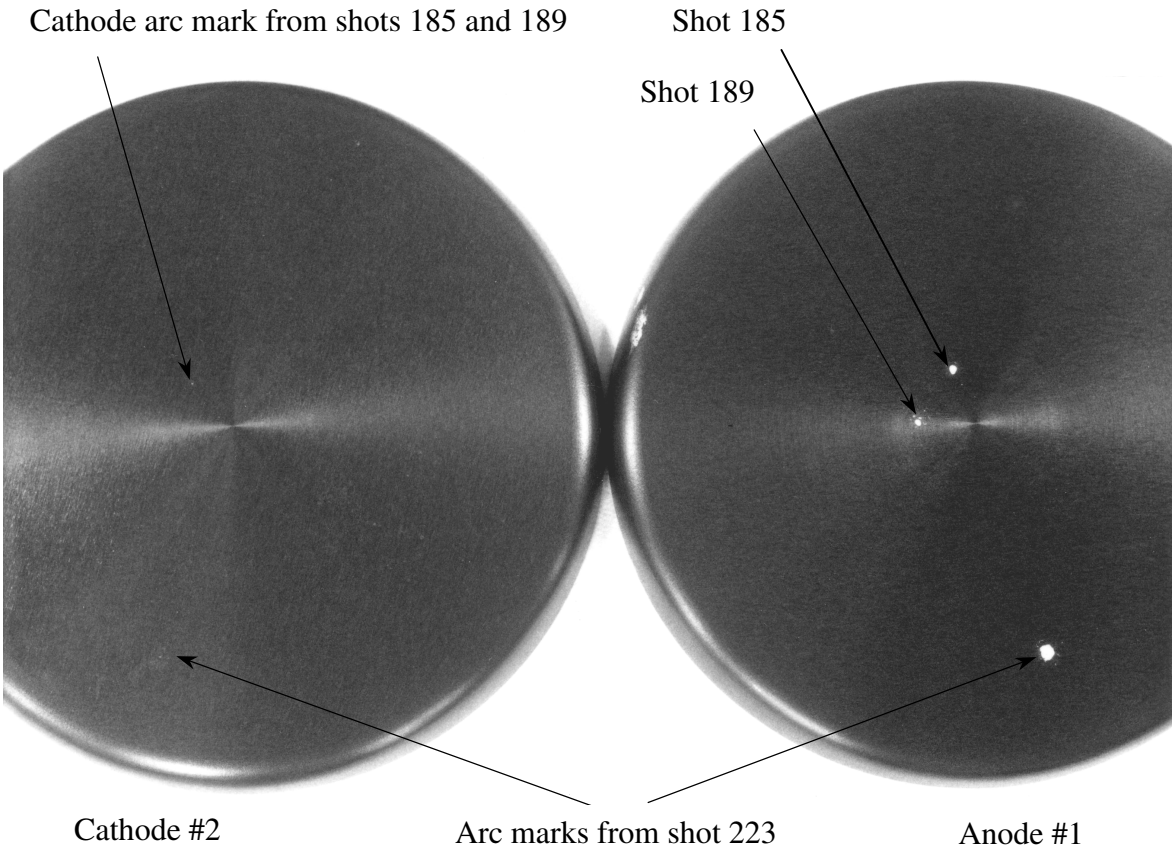

Figure 71. The appearance of T3 electrodes after shot 223, which was the last shot of series 4 shown in Fig. 70.

Close up photos of the cathode arc marks from shots 189 and 223 are shown in Fig. 72. These photos show typical cathode arc marks in the form of a pit burned through the anodized coating that in this case did not cause much more than 10% reduction in hold-off. These holes are 85 and 75 mm deep which is only slightly deeper than the depth of the anodized coating.

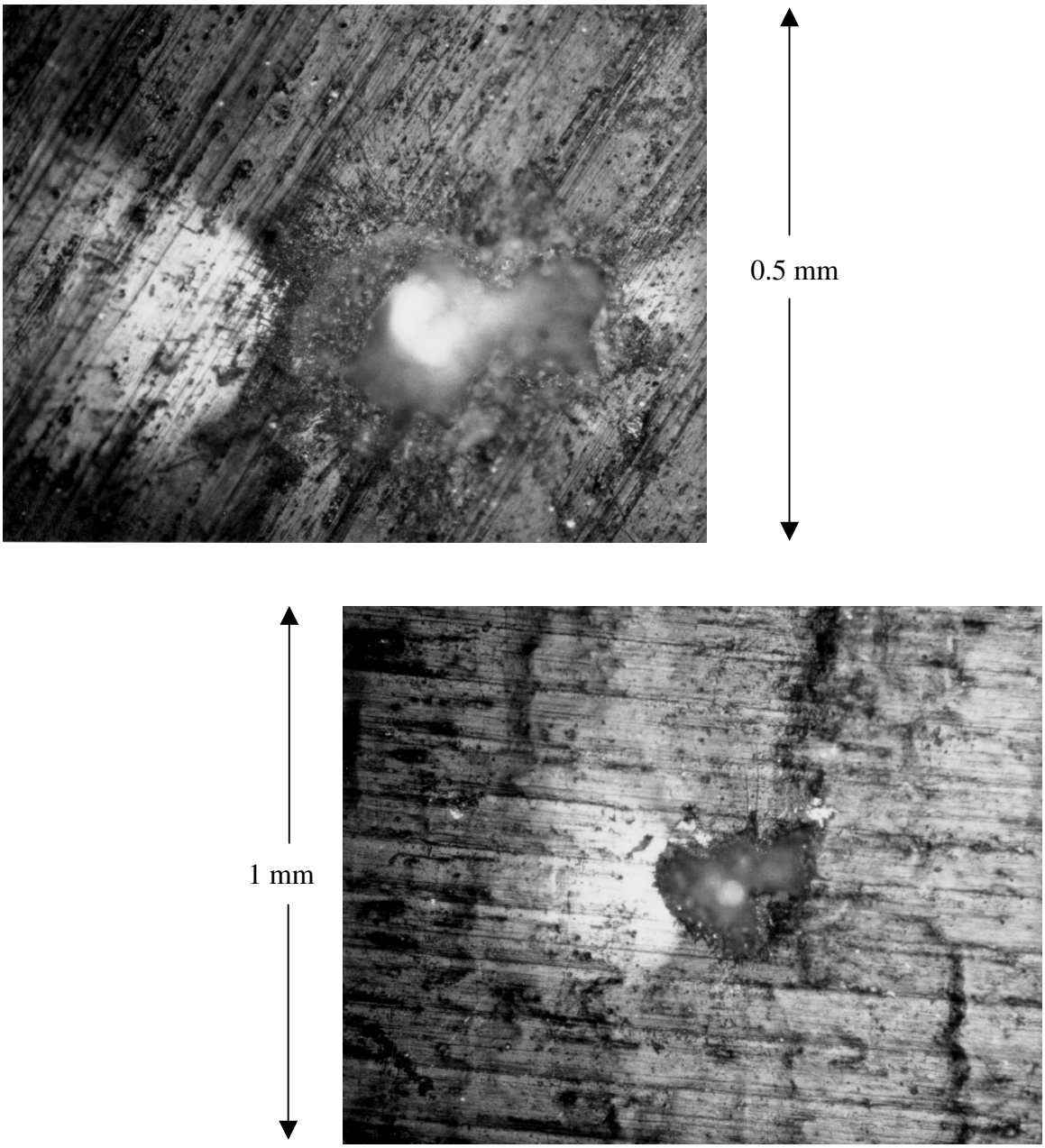

Figure 72. (top) Cathode arc mark from shot 189. This mark is ~ 85 μm deep.
(bottom) Cathode arc mark from shot 223. This mark is ~ 75 μm deep.

Anodized Coating Tests with Large Gaps

A summary of the breakdown data obtained for anodized aluminum using the LIVA pulser with large gaps is shown in Figure 73. The data show about the same hold-off as was observed for the 2 mm gaps. This would indicate that the hold-off is not dependent gap and responding to the "total voltage effect" as was observed with stainless steel. Unfortunately we did not have enough voltage to achieve breakdowns with 7.5 mm gaps with anodized aluminum where the "total voltage effect" was most obvious with stainless steel. The plot also shows data for diamond polished and machined aluminum that does show reduced hold-off with larger gaps.

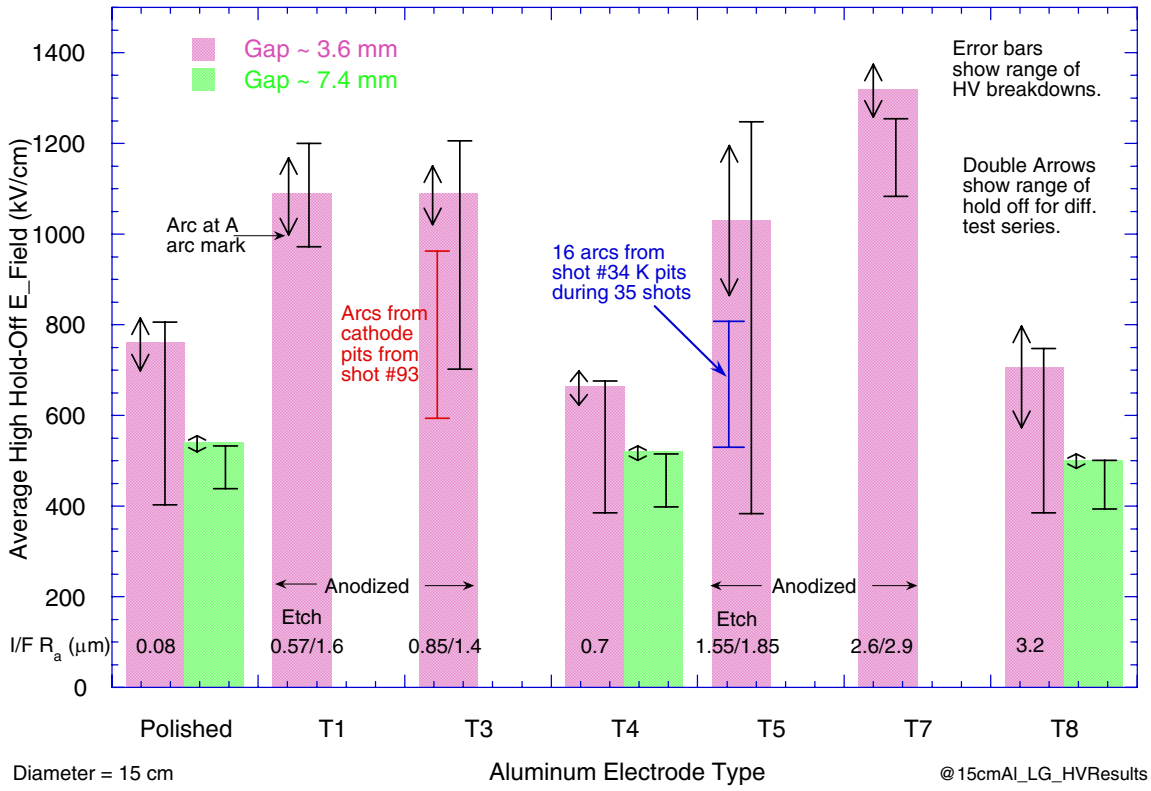

Figure 73. A summary of the test results for anodized and bare aluminum with large gaps.

The breakdown data for larger gap T1 and T3 electrodes are shown in Fig. 74. The arc on T1, electrodes #5 and 6 used on shot175 resulted in a 4-mm-wide region of melted aluminum debris on the cathode. This still allowed a hold-off of ~ 1 MV/cm on the next series after the cathode was rotated. Surprisingly the 3-mm-wide crater in the anode did not produce a breakdown. Coating these arc marks with drops of EVO allowed the electrodes to hold-off 1.1 MV/cm. Again there is not much difference in the nature of the damage or breakdown thresholds for the T1 and T3 electrodes for these ~ 4-mm-gap shot series.

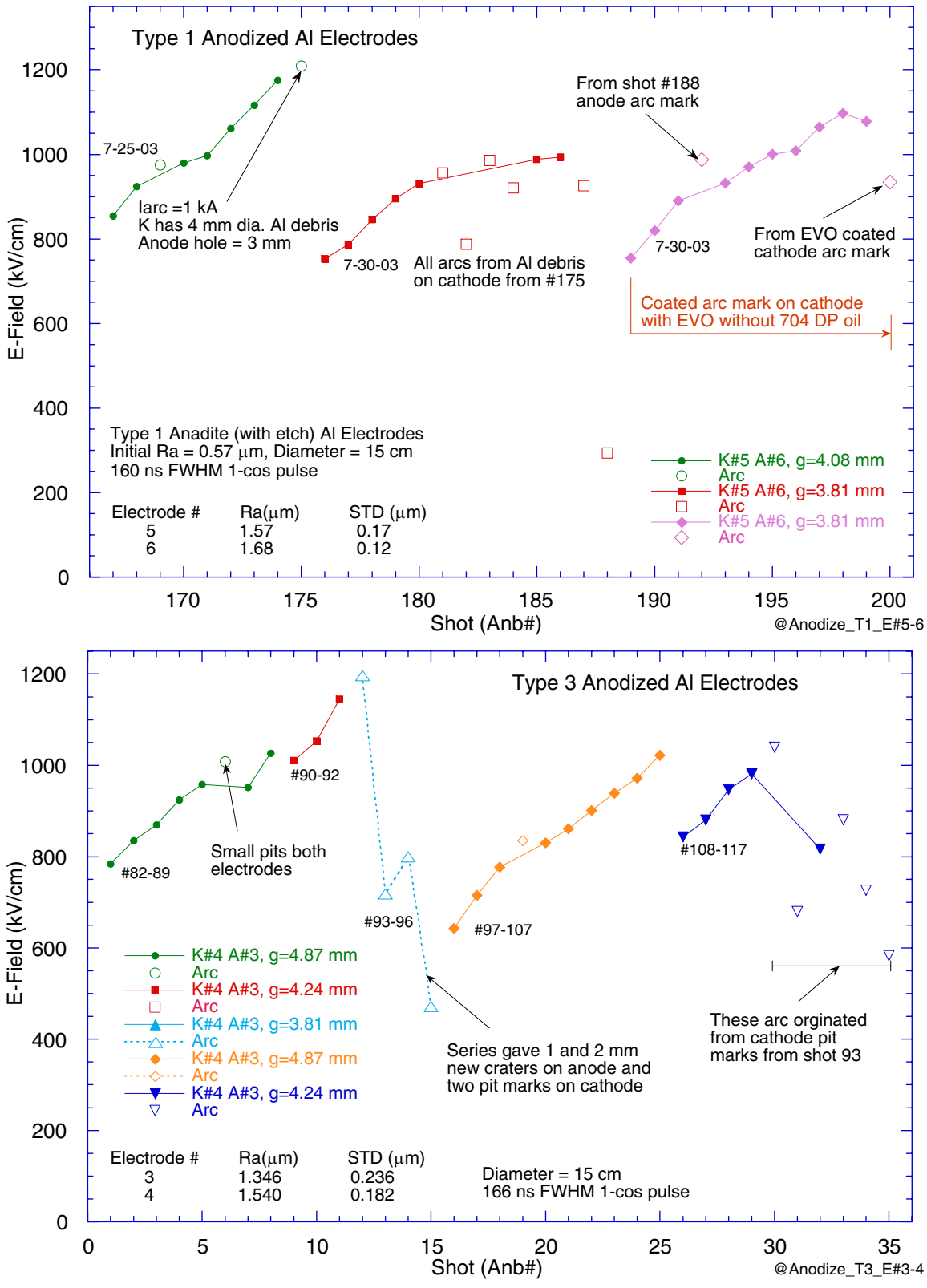

Figure 74. Breakdown data for T1 and T3 anodized aluminum electrodes acquired with large gaps.

The gap closure was relatively independent of gap so the current traces did not rise as fast with large gaps. This is illustrated by the waveforms for T1 and T3 shots Anb181 and Anb112 in Fig. 75. Also the voltages are higher so the heating occurs slower and jump of current typically occurred well after the peak of the current and is consistent with the anode being heated to ~ 1000 °C. The CL current parameters for large gap anodized aluminum tests are shown in Fig. 75. A comparison to Fig. 68 shows that the Vg is about 1 cm/μs smaller for the large gap shots, whereas, Va is 1 cm^2/μs larger.

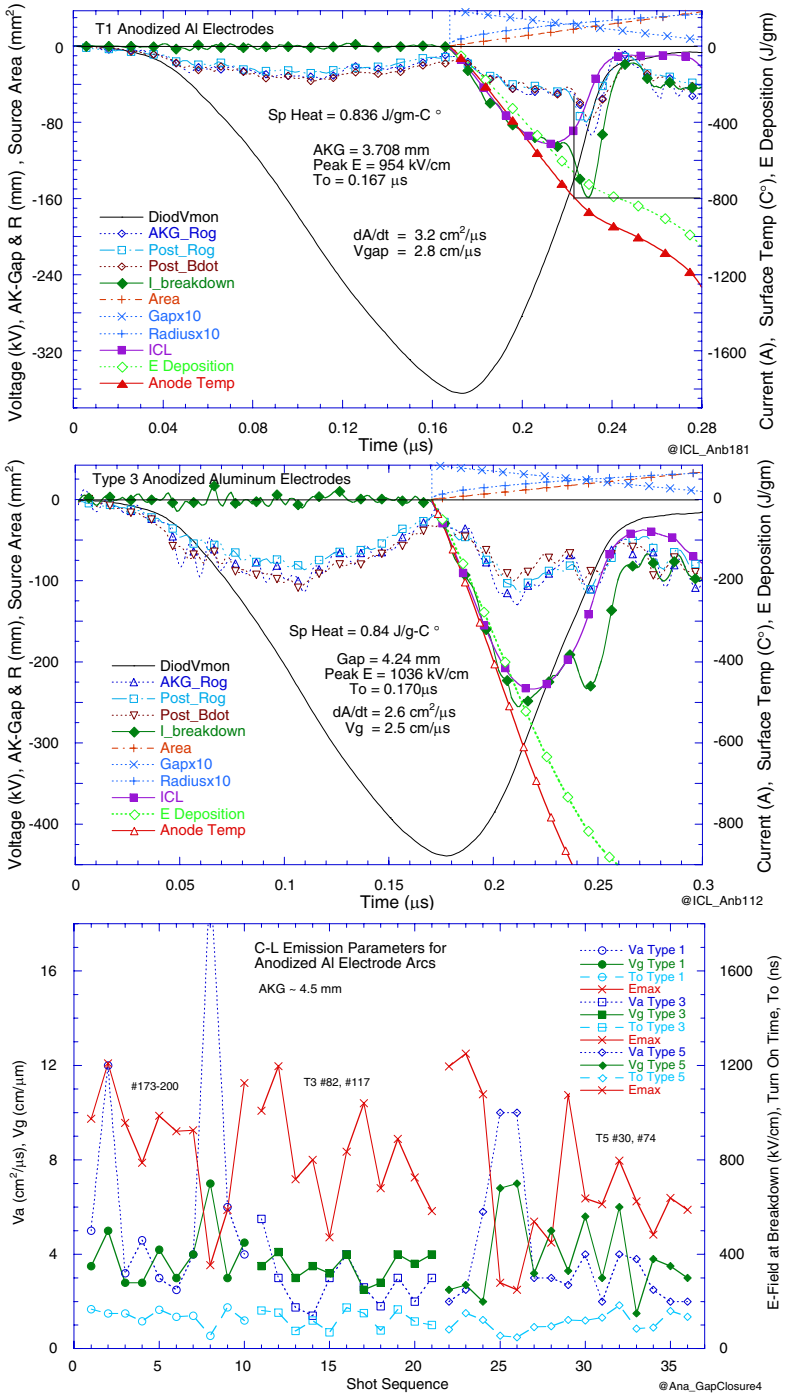

Figure 75. (upper) The current and voltage waveforms for T1 and T3 anodized aluminum shot Anb188 Anb112 taken with large gaps. (lower) Child-Langmuir parameters for anodized aluminum electrodes tested with large gaps.

Rough Surface Anodized Aluminum

The summary plots in Fig. 64 shows that the T5 electrodes tested had the highest E-field hold-off of the anodized coatings but had more variation in hold-off. This should not be surprising because the T5's only had slightly higher roughness compared to the T1's (see Table 2). Damage to a T5 electrode pair K#4 and A#3 from shot 34 is shown in Fig. 76. We did not notice a significant difference to the damage patterns with the rougher surfaces. The electrical breakdown data for T5 and T7 electrodes with large and small gaps are shown in Figs. 77 and 78. The T7's had 1 μm larger R_a than the T5's and also 10% lower peak hold-off E-fields. This may indicate that R_a larger than ~ 2 μm is detrimental to hold-off.

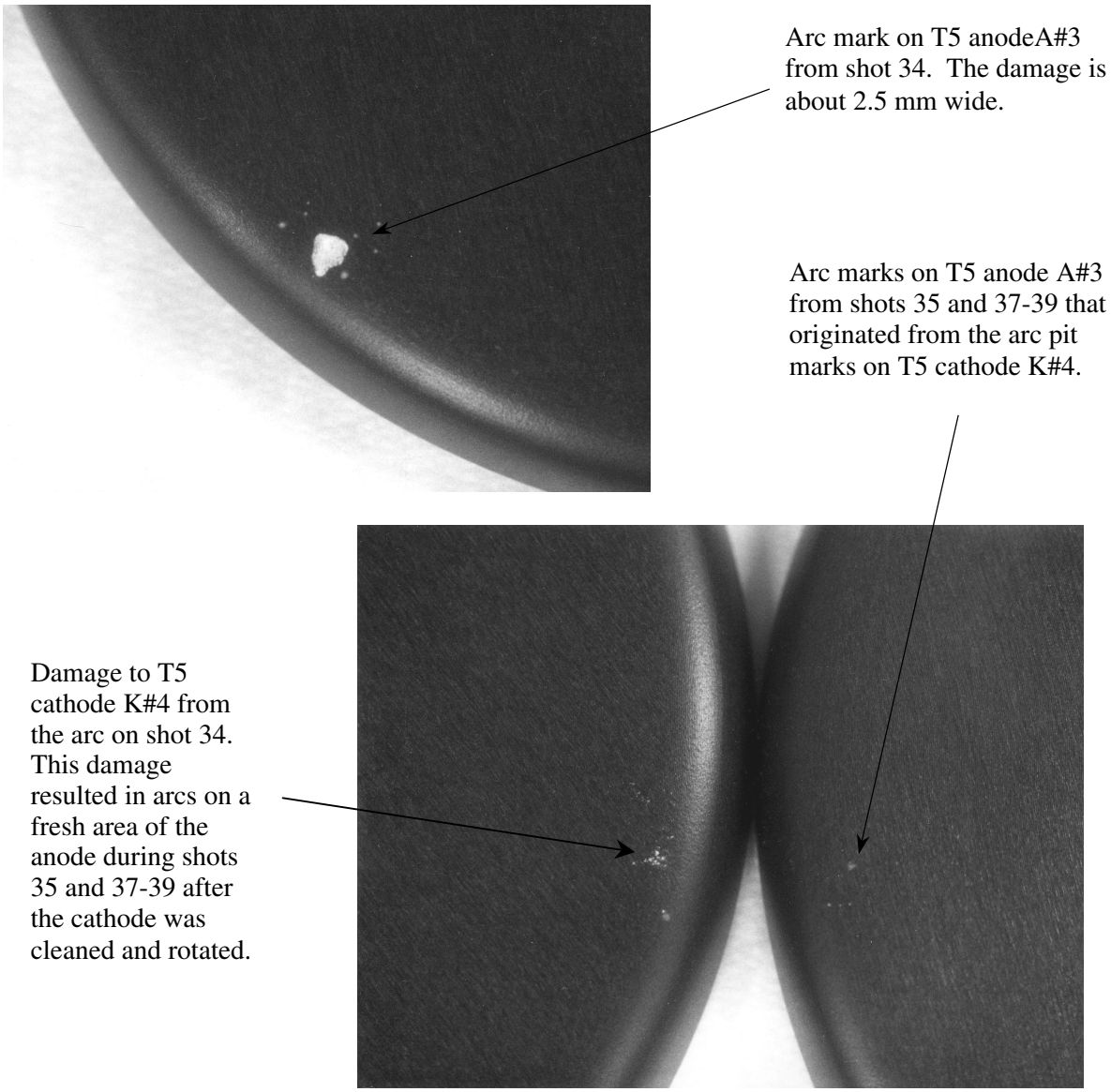

Figure 76. Damage patterns on T5 electrodes #3 and 4that occurred during the 3rd large gap shot series with these electrodes. The damage most likely occurred on shots Anb34.

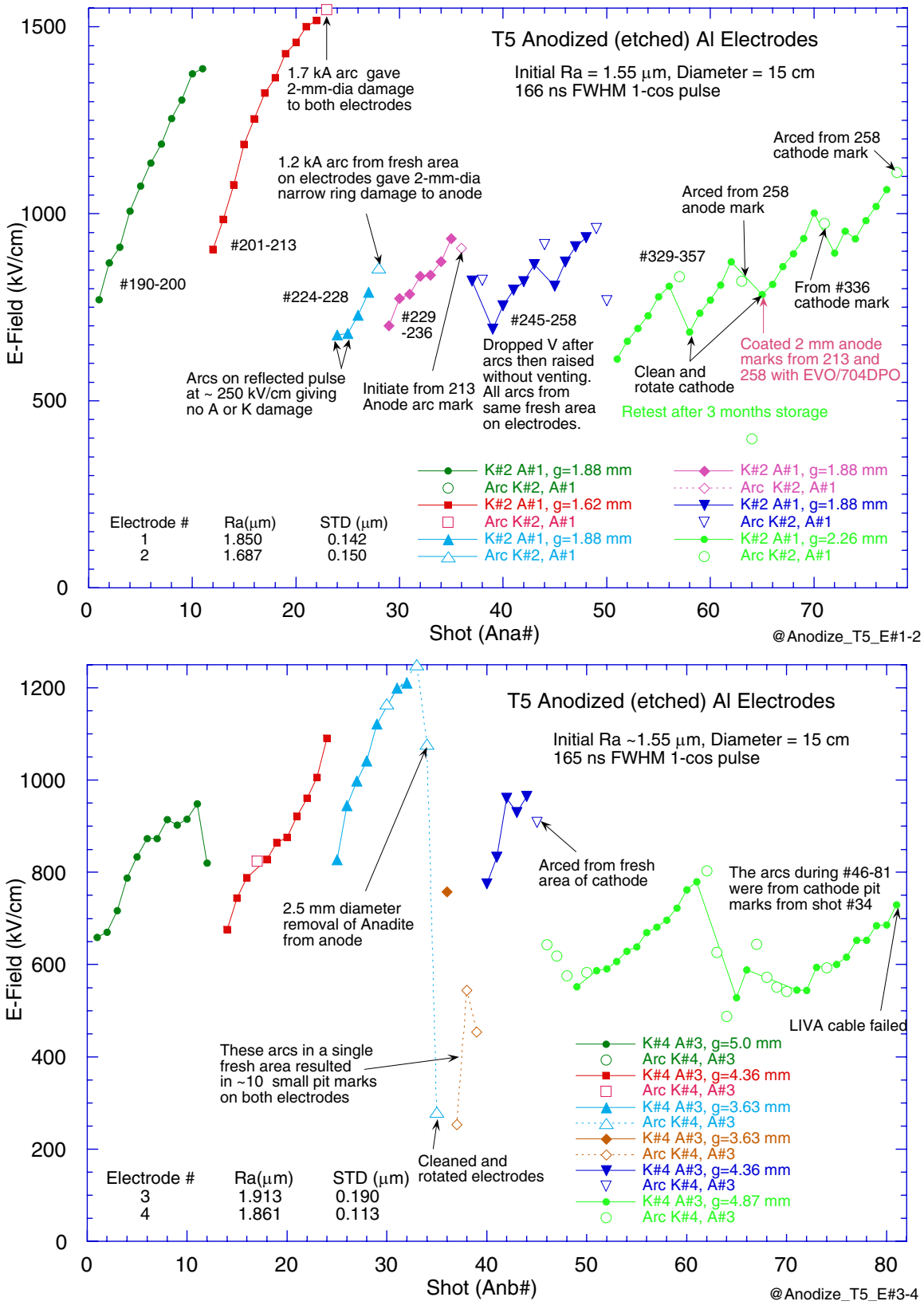

Figure 77. Breakdown data T5 anodized etched Al electrodes tested with small and large gaps.

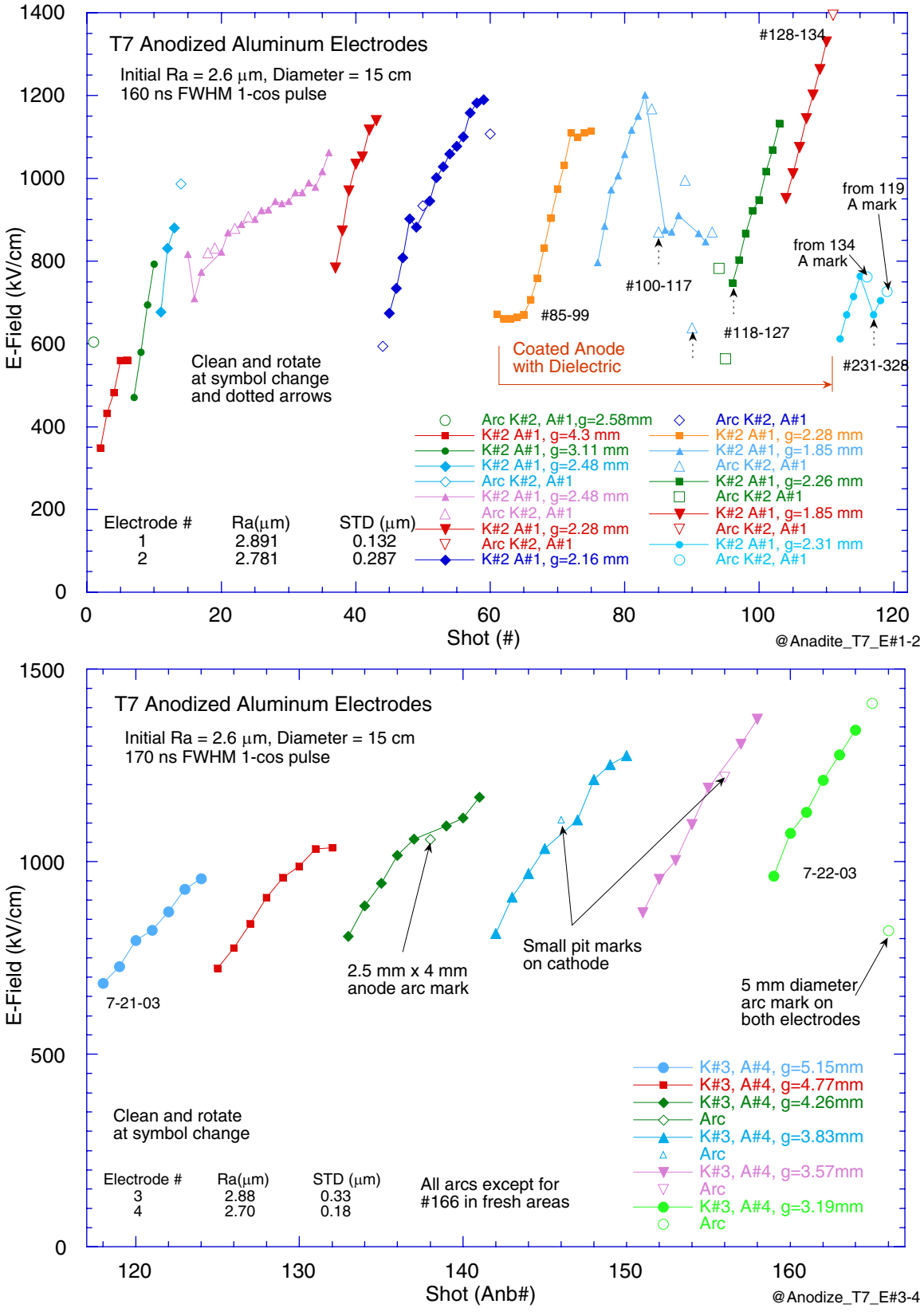

Figure 78. Breakdown data for T7 anodized Al electrodes tested with small and large gaps.

Bare Machined Aluminum

A summary of T4 bare aluminum tests is plotted in Fig. 73 with the anodized large gap data. The breakdown threshold in these tests was about half the value for anodized aluminum. These tests were primarily with larger gaps because the hold-off E-field for bare aluminum was low and the large gaps minimized damage. The summary data show a drop in hold-off with large gaps similar to stainless steel. The last data in the experiment were taken with particular attention to confirming the hold-off E-field scaled as $g^{-1/2}$. This will be described later with the comparison of the hold-off for diamond polished and the very rough T8 electrodes.

Our initial tests with aluminum were conducted in October 2002 to get baseline data for the T4 electrodes. We were not expecting gap dependence so did not make a concerted effort to look for it. The data for T4 electrodes #1 and #2 are shown in upper Fig. 79. These electrodes were cleaned in laboratory air because the filtered air system did not become operational until 11-08-03. They showed reluctance to breakdown on the first two series with our available voltage. We therefore closed the gap twice in moderate amounts until shots 33 and 34 showed strong arcs. We then switched electrodes to test if the anode damage would self heal from the arc melting process as was observed with stainless steel. This appeared to be the case because the subsequent test showed hold-off to about 540 kV/cm.

We next tested electrodes #3 and #4 with the filtered air. Expecting much improved hold-off we starting testing with a factor two smaller gap and avoided a long series of electrical conditioning shots. This test gave one hold-off shot at 410 kV/cm but the next broke down at 510 kV/cm. Examination of the electrodes showed three arc marks located in a 1-cm-wide region of the anode. One of these is presumed to be from the single prefire shot that occurred during this shot series. We then cleaned and rotated the electrodes and fired successful hold-off shots up to 650 kV/cm with increasing gaps. The exception was the 7^{th} series where the electrodes were reversed. Based on our final understanding of how bare metal hold-off responds to gap it is surprising that the 8^{th} series, with the largest gap at 3.48 mm, reached the highest hold-off E-field. This is remarkable in that the many arc marks from the earlier series did not contribute to the breakdowns. Perhaps this was due to electrical conditioning from the previous tests. These marks are shown in the Fig. 80 photograph of T4 electrodes #4 and #3 taken after shot Alm163. The data also suggest that arcs on aluminum electrodes are self-healing as with stainless steel.

The data acquired with T4 aluminum using larger gaps are shown lower Fig. 79. The tests with E#6 and E#5 are inconclusive. These tests were made when we were measuring hold-off with minimal and no electrical conditioning. The results show hold-offs about 500 kV/cm independent of gap from 3.6 to 7.4 mm gaps. Nearly all the arcs were in fresh areas. Our last two test series were done in Sept. 2003, the end of the experiment, and show hold-offs of 550 and 700 kV/cm for 7.3 and 3.5 mm gaps, respectively. These results appear prominently in Fig. 73.

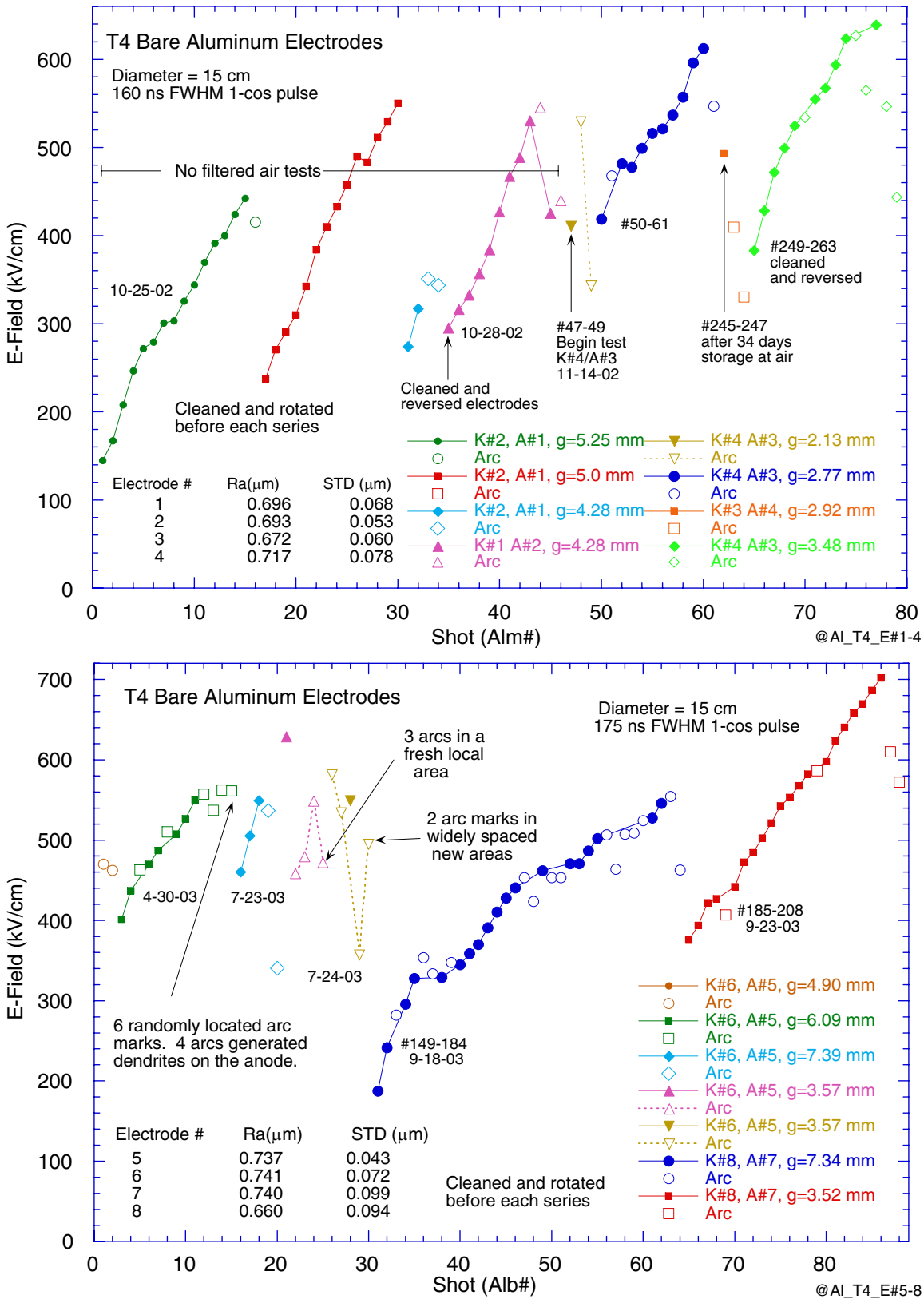

Figure 79. Breakdown data for T4 bare aluminum electrodes #1 to #8.

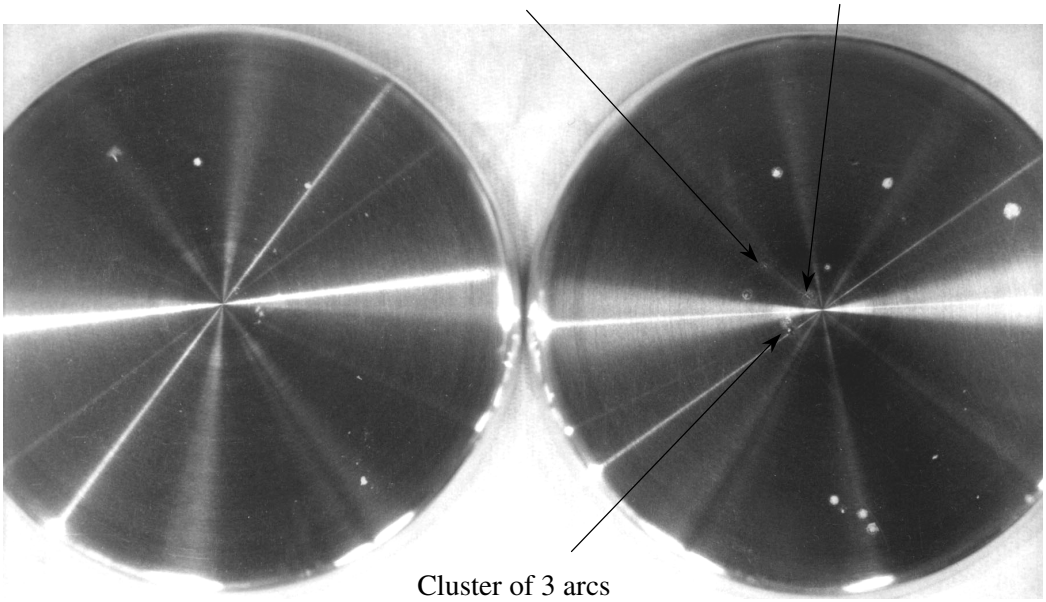

Figure 80. A photo showing bare aluminum type T4 electrodes K#4 (left) and A#3 (right) taken after shot Alm263. The arrows show the location of the arcs during the 8th test series in upper Fig. 79.

The dendrite type anode damage patterns typically observed with large gap shots are shown in Fig. 81. They radiate out from central melted region at the core of the arc. Apparently the fast rise of the arc current causes the current to concentrate in a gaseous cloud on the surface of the anode near the arc. The dendrite traces would be evidence of filamentation of the current in the gas cloud or resultant plasma.

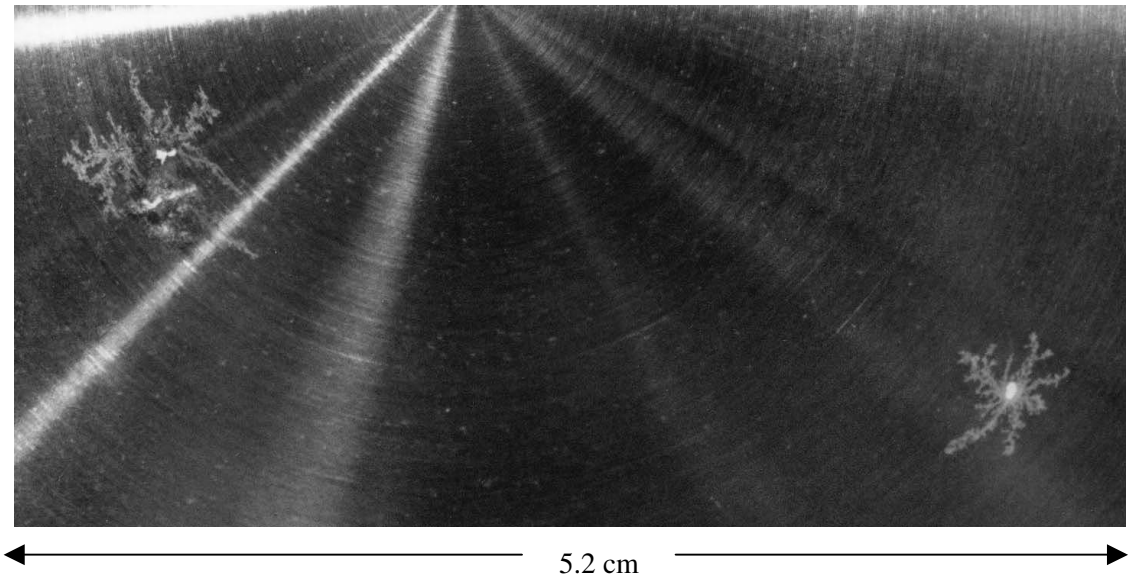

Figure 81. A photograph of two arc marks with dendrites (upper left and lower right) that appeared on aluminum T4 anode #5 during the 2nd test series, shots #3-14 (Fig. 79 lower). The anode-cathode gap was 6.09 mm.

The current traces for T4 bare aluminum electrode shots with 2.8, 3.57, and 7.34 mm gaps are shown in Fig. 82. The shots have current jumps that occurred when the calculated anode temperature reached 400 to 600 °C. This same temperature range was also observed with the rougher T4 and polished bare aluminum electrodes. The jumps occurred on about half the shots, as with other electrode surface types, but the onsets were typically at a factor of two lower temperature. With bare aluminum the jump occurs near the 400 °C temperature value others [47,46] note the onset of plasma formation and ion current from the anode. The CL current parameters for aluminum electrode test are shown in Fig. 83.

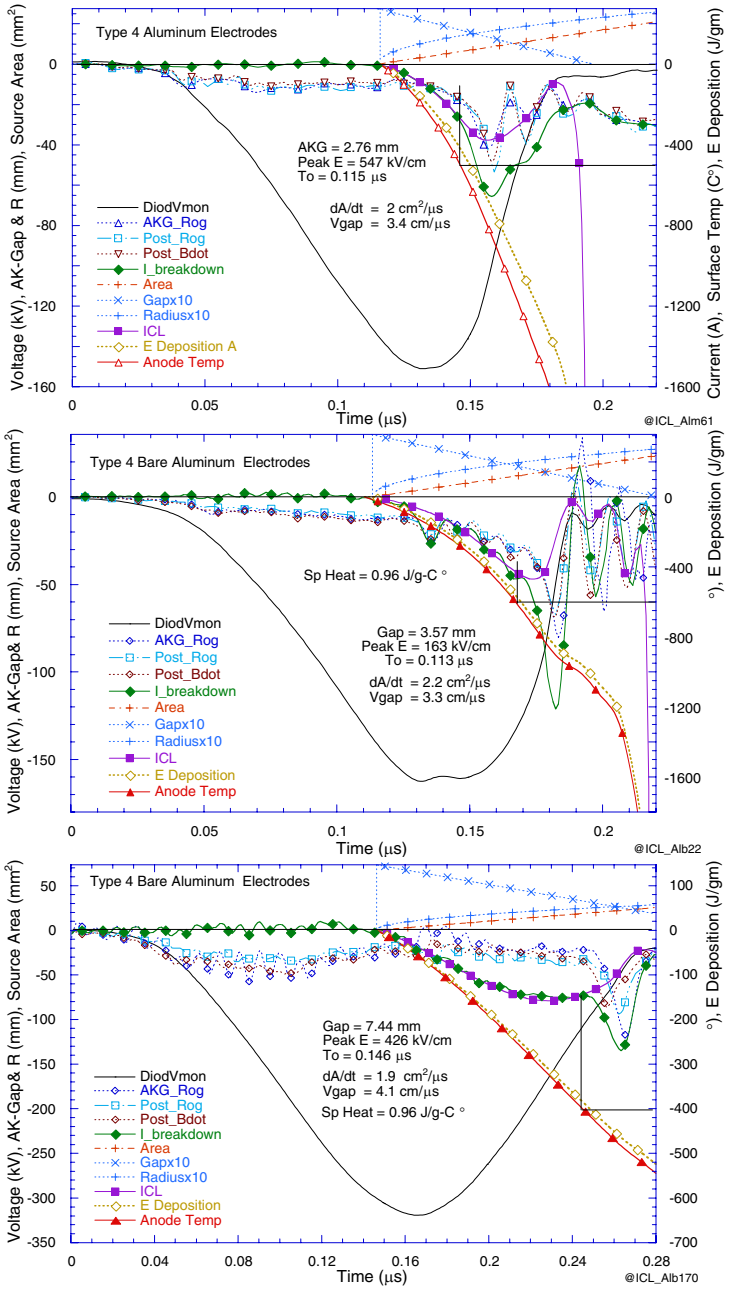

Figure 82. Electrical data from bare aluminum electrode shots Alm61 (upper), Alb22 (center) and Alb170 (lower) shown in Fig. 79. The olive green and red curves are the calculated energy deposition and anode temperature for the CL current density. The data demonstrate the difference in the calculated rise of the anode temperature for large and small gaps. The front surface electron stopping power used for the calculation is shown in the graph located below.

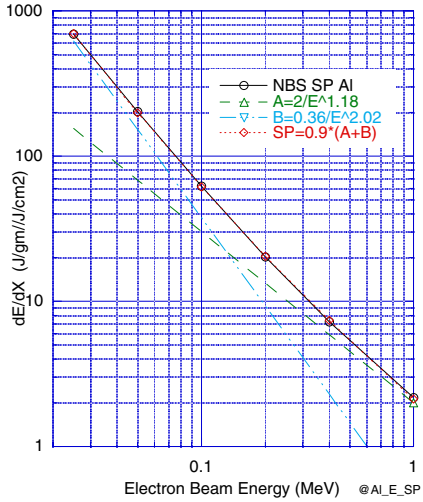

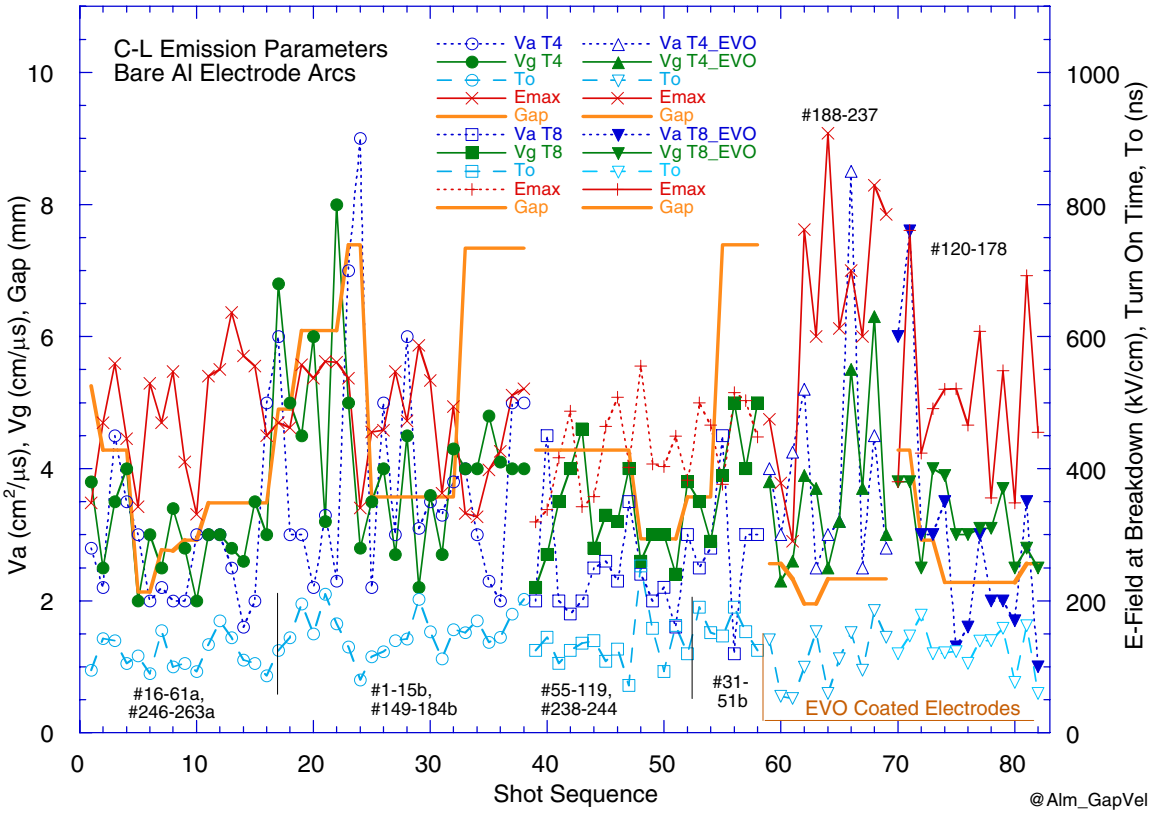

Figure 83. CL parameters for breakdown shots with bare and EVO coated aluminum electrodes.

The breakdown data for the last series of tests before the filtered air system became operational are shown in Fig. 84. These shots were fired with the rough surface T8 aluminum surface and EVO coated T4 and T8 electrodes because it was felt that these tests would not be help with cleaner air. The initial tests with T4 electrodes used a thin EVO coating and the hold-off was poor. Use of a thick glassy coating began with shot Alm192 and demonstrated hold-off to 800 kV/cm with 2.56 mm gap. A repeat series gave 950 kV/cm. This was nearly a factor of two improvement for electrodes #1 and 2 that gave hold-offs of only 500 kV/cm when tested earlier (see Fig. 79) without a coating. Further repeats with 2.33 and 1.95 mm gaps gave similar hold-offs of ~ 920 kV/cm. It was felt that the dielectric coating would probably work without electrical conditioning. Therefore we next fired a series of shots without the conditioning. These shots were fired at full pulser power, 265 kV max voltage, to determine the "real world" hold-off expected for a single shot pulsed power machine. These shots gave a 30% improvement over bare aluminum. However the results were mixed with the hold-off varying from 600 to 900 kV/cm. The CL parameters for bare and EVO coated electrodes shown in Fig. 83 indicate similar cathode plasma expansions velocities.

The breakdown data for the four times rougher T8 bare aluminum electrodes are shown in the lower plot of Fig. 84. The majority of data were taken without filtered air. The bare surface shots 51 to 119 initially showed breakdowns in the range of 330 kV/cm. Subsequent repeat shots in the 1st and 2nd series showed that electrical condition removed breakdown sites and the hold-off eventually reached 500 kV/cm. This is nearly the same

value as the first breakdowns with T4 electrodes. At this point we judged that the rougher surfaces gave ~ 20% reduced hold-off. We next fired shots 120 to 178 using the EVO coating. The results show that EVO gave a 30% improvement. The last shots were fired with clean air without electrical conditioning. The breakdown was again in the 400 to 500 kV/cm range.

The final series of tests in the experiment were conducted to obtain more data on the variation of breakdown for bare aluminum versus gap. We also did this comparison with diamond polished and T8 aluminum to get more data on the hold-off versus roughness. The data are shown in Fig. 85. The diamond polishing was done on T4 electrodes #1 and #2 after they had received a fresh machined surface with R_a ~ 0.2 μm. They were then sanded with 1000 and 2000 grit sandpaper and finally polished with 1-μm-grit diamond paste to a final $R_a = 0.08 \pm 0.01$ μm. The electrodes were then cleaned with acetone in an attempt to remove the residual polishing compound. The last polishing, prior to shot 244, was done with extreme care and gave a near mirror surface quality finish. The surface was buffed with acetone soaked Kimwipes while the electrodes turned on the lathe to enhance the removal of polishing compound.

We were over confident on our original test series with diamond polished Al when we began testing at 600 kV/cm with a 3.9 mm gap. This and subsequent shots broke down as we dropped the pulser voltage as follows; 40, 37, 34, and 30 kV. In each case the breakdown occurred after the peak of the gap voltage. We then doubled the gap after recleaning the electrodes and observed hold-off to about 500 kV/cm. The 3rd series where the gap was returned to 2.9 mm after cleaning and rotation of the cathode, achieved 820 kV/cm. The second polish again showed breakdown at about 450 kV/cm during two test series with ~ 3 mm gaps. A 6th test with 4.5 mm gap achieved 580 kV/cm. The third and super polish test was on 9-25-03. This showed an initial breakdown at 380 kV/cm that was similar to the hold-off of the previous polished surfaces. After second cleaning the electrodes held 695 kV/cm. The 8th test series with the 7.5 mm gap held 550 kV/cm.

The data for bare T8 electrodes #3 and #4 are shown in the lower Fig. 85. Initial tests in July 2003 gave a hold-off of only about 450 kV/cm for 3.5 and 7.4 mm gaps. Tests taken two months later achieved 720 and 805 kV/cm for the 3.52 mm gap and 510 kV for the 7.39 mm gap. This was a surprising result because we now had similar hold-offs for polished, T4 (see Fig. 79) and T8 electrodes. For all of these tests we used 1 and 2 kV pulser charge increments for the small and large gap shot to use the same E-field conditioning protocol for the gaps. It is difficult to explain how bare aluminum electrodes with R_a varying from 0.08 to 3.2 μm can have the same hold-off for the two gaps when our observations for machined stainless steel had lower hold-off for rougher surfaces. Perhaps there is a difference in the number of sharp metal burrs present on the stainless steel than the aluminum. The final conclusion one can glean from the T8 data is a reinforcement of our observations for stainless steel that the "total voltage effect" is not a statistical anomaly. The 2nd to 5th test series shown in Fig. 85 show the drop in hold-off with larger gaps too clearly.

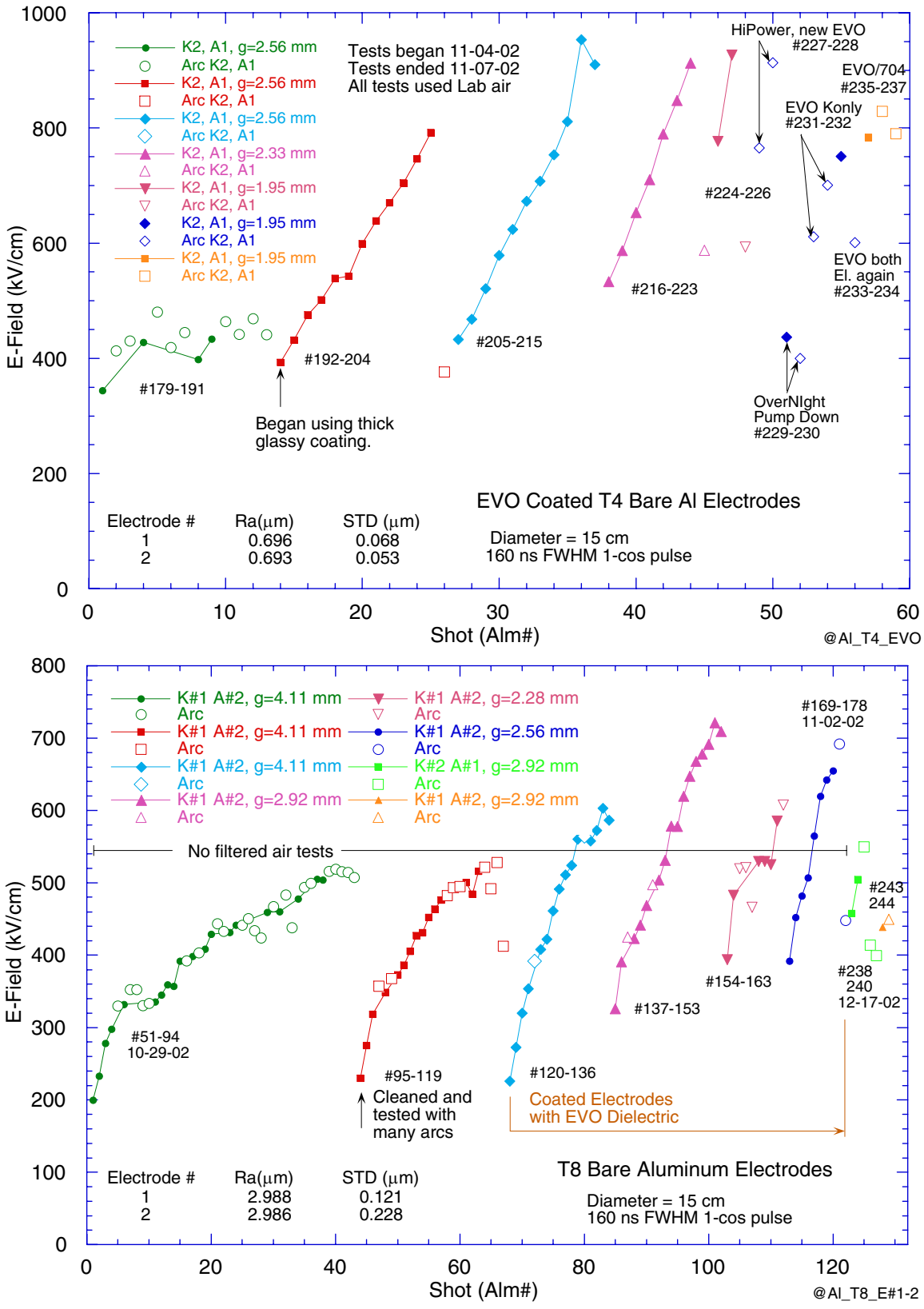

Figure 84. Breakdown data for EVO coated T4 and T8 aluminum electrodes tested with small gaps. Bare T8 aluminum electrode tests with large gaps are also shown in the lower figure.

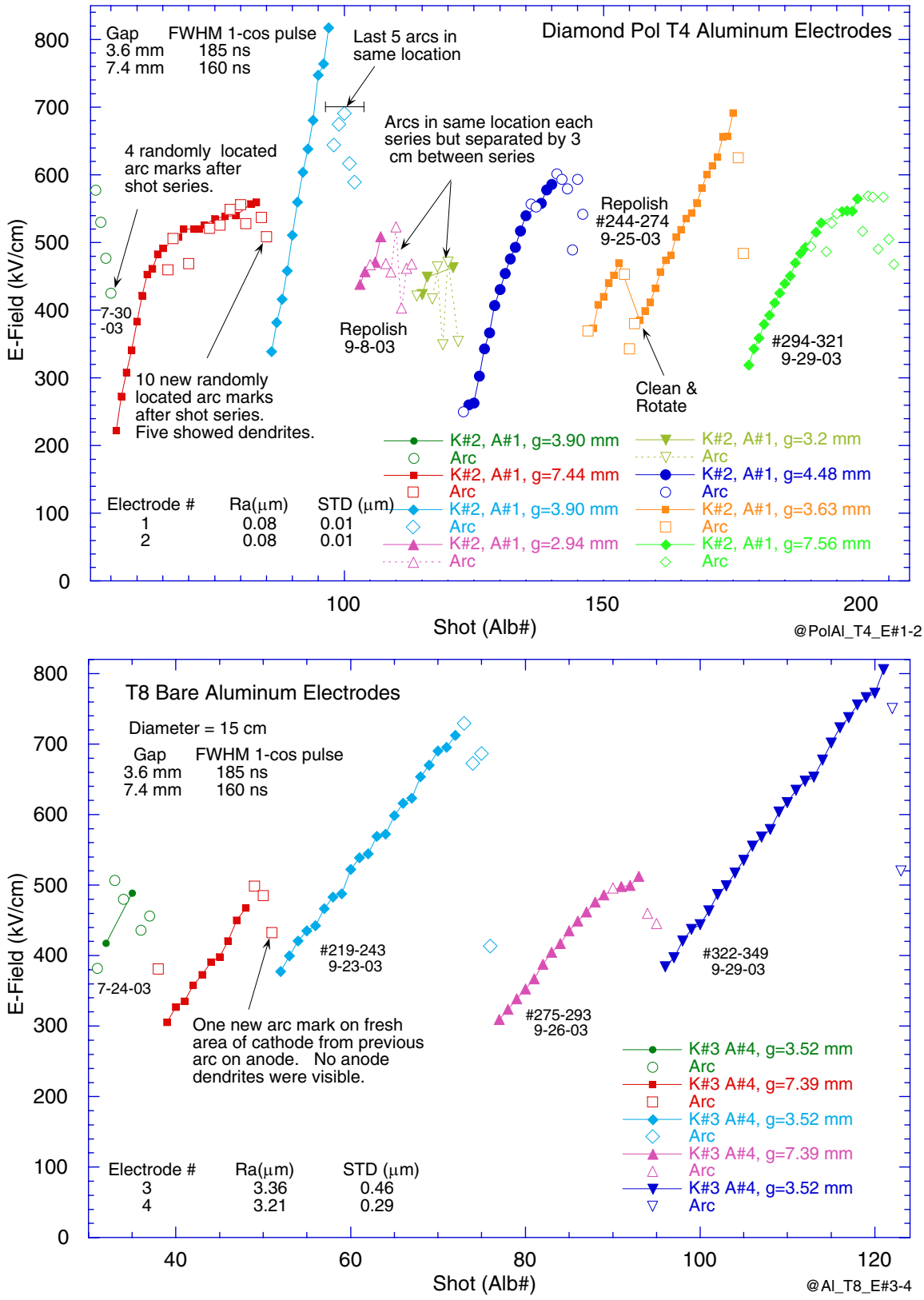

Figure 85. Breakdown data for bare diamond polished and T8 Al electrodes tested with small and large gaps

The electrical waveforms for polished aluminum shots from Fig. 85 are shown in Fig. 86. The data show a smooth current waveform for late turn-on shots. (The upper right current waveform shows ringing due to partial crowbar switch firing.) The earlier turn on shots show the current jumps and/or pulses described earlier for other electrodes. The traces show the jumps beginning at ~ 400 °C for the 3.6 mm gap but at only ~ 200 °C for the 7.6 mm gaps. The lower temperatures for the large gap shots casts doubt on our earlier conclusion that the jumps are a transition to bipolar current flow in the gap.

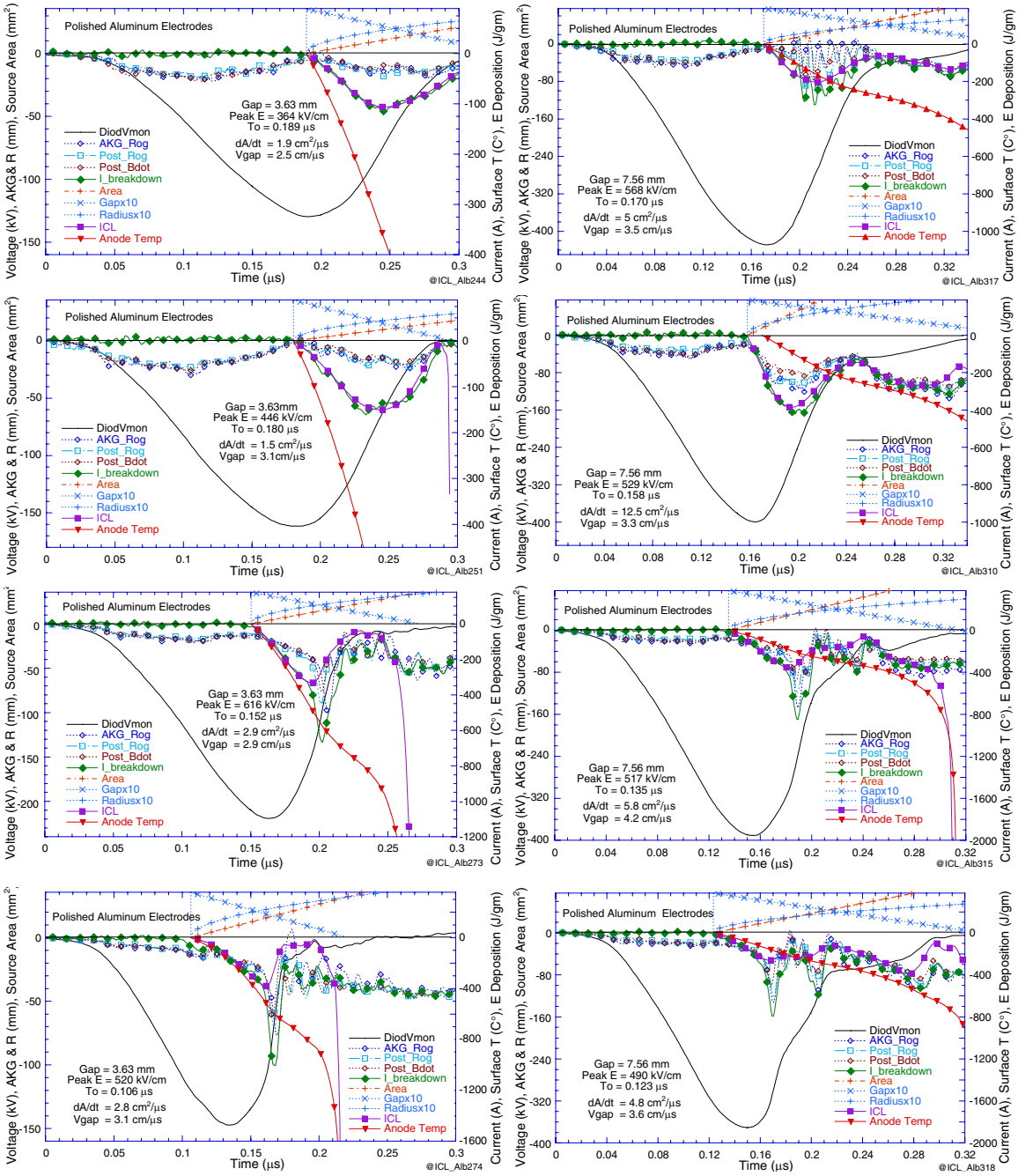

Figure 86. Electrical waveforms for shots with diamond polished Al electrodes with 3.63 and 7.56 mm gaps on the left and right. The upper shots have later turn-on times. The anode surface temperatures are calculated using specific heat of 0.96 J/g-°C.

Discussion

Anodized aluminum showed similar current jumps to those observed with bare metal surfaces but the temperature at the jump was ~ 1000 °C. This may be related to the high melting temperature of aluminum oxide of 2000 °C. The CL parameters for anodized aluminum shown in Figs. 69 and 75 have the same wide variation of values as bare metal surfaces. The gap closures for small gaps ranged from 4 to 5 cm/μs and are higher than the value for metal surfaces. This may be related to the higher E-fields that generated these breakdowns. The anodized aluminum did not show the drop in hold-off with larger gaps. This may indicate a different breakdown mechanism. The reason for constant E-field is not well understood but could be due to the high dielectric constant of aluminum oxide, which reduces the E-field at the metal-coating interface. Another possibility is the insulating properties of the coating would reduce charge build-up on loosely bound metal particles on the surface that could be accelerated across the gap.

New anodized aluminum gave a factor of two higher hold-off than bare aluminum. After severe arc marks the hold-off dropped to the value of bare aluminum. If the loose debris from arcs is cleaned off and the arc marks are coated with EVO191/DC704 diffusion pump oil the hold-off approached the value for a new anodized coating.

The current waveforms observed for machined and polished aluminum are similar to those from polished, machined and EBEST stainless steel. Late time breakdown shots have current shapes that are smooth and easily fit to our space-charge limited current model with a gap closure of ~ 3 cm/μs. Note the similarities of the current shapes for the shots represented in Figs. 37, 46, 82, and 86 and CL parameters in Figs. 49 and 83. Small gap shots have a rapid current rise because the fixed gap closure gives a large change in the CL current. There is typically a jump when the anode temperature reaches ~ 400 °C. Large gaps often have one or two spikes in the current that result in inflections in the diode voltage. It is not entirely clear what is happening to cause these pulses. Our initial thought was that the current is switching to bipolar flow. However another mechanism must also be at work to turn off the pulses. Perhaps there is plasma erosion from the anode or a pinch mechanism at work. Also large-gap shots with early turn often showed a jump in current at a temperature below the 400 °C observed [46,47] for the production of anode plasma. This could indicate bipolar flow does not cause the jumps.

The breakdown thresholds for bare aluminum were about the same for R_a from 0.08 to 3.2 μm. This was quite different from stainless steel where the best hold-offs occurred at the lowest R_a. We don't have a good explanation for this except that perhaps burrs on the stainless surfaces retained laboratory wiper lint. It was a big surprise that rough-machined aluminum gave a hold-off of 800 kV/cm at 3.5 mm gap. Both aluminum and stainless steel showed good electrical conditioning characteristics with improved hold-off after the accumulation of many arc marks. This would indicate that EBEST on aluminum would probably work well also. Aluminum surfaces showed the same drop in hold-off with increasing gap that was noted for stainless steel. This would indicate the MIV and MIM models of Latham [4], which are initiated by E-field only, may not be the dominant source of breakdowns with bare metals with gaps > 2 mm.

IX. 17 cm Stainless Steel Electrode Tests

Our last major experiment was a repeat the measurements described in section IV with clean air and larger anode-cathode gaps. These tests were done with bare-machined, HVFF, and Cr_2O_3 coated 304L and 316L rod stock stainless steel, and Z-protocol 304L rod stock electrodes. The effective diameter of the electrodes was 17 cm. The initial 0.15-μm-roughness surface on all electrodes was remachined by Gull Group [35] on our section IV electrodes. We tested with 2.5, 5 and 7.5 mm anode-cathode gaps. Although the 5-mm-gap Chang curves used give a 5% E-field enhancement at the edges for 7.5 cm gaps, examination of the arc mark locations did not show preferential arcing at the edges.

Charles A. Walker of Org 14171 applied the "green" Cr2O3 coatings to the electrodes. He used a wet HVFF process where water vapor is mixed with the hydrogen in the vacuum furnace. He applied as thick a coating as was reasonably possible. The two stainless steels are composed of:

304L 8-12% nickel, 18-20% chromium, 2% manganese
316L 10-14% nickel, 16-18% chromium, 2% manganese, and 2-3% molybdenum

The 304L alloy has about 10% more chromium content so one might conclude that the chromium oxide layer that occurs from the reaction of the hot water vapor during firing might produce a slightly thicker or robust layer. We assume this is not the case because the surfaces looked similar. Ronald Stone, Org 14192, indicated that similar coatings that he had evaluated were ~1 μm thick.

Walker also produced the HVFF coatings. The R_a measurement indicates that the HVFF process increases the roughness by ~ 0.2 μm whereas the oxide layer may decrease the roughness slightly. The 304L machined surfaces were a factor of two smoother than the 316L surfaces as is indicated in Fig. 87.

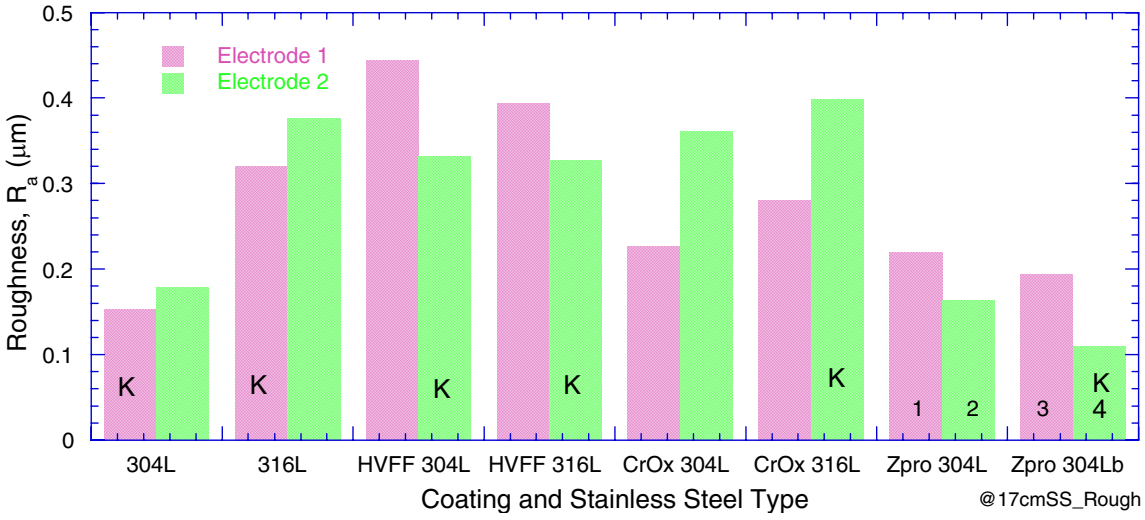

Figure 87. The roughness of the various coatings on the 17-cm-diameter stainless steel electrodes tested for high voltage hold-off.

The Z-protocol electrodes A#1 and K#2 had sustained 10 breakdowns shots when tested in laboratory air prior to the tests reported here. The cathode had only mild deposits of vaporized gold in four areas. The anode arc marks were melted regions of gold with no exposed stainless steel. Electrodes 3 and 4 had new coatings that were stored in lint free wrappers for about 18 months. The gold was poorly bonded to electrode #3 so when it was first used as an anode the gold flaked off. The result was abnormally poor hold-off.

The pulse width was about 170, 180 and 205 ns FHWM for 7.5, 5, and 2.5 mm gaps because of the $(L/C)^{1/2}$ time constant of the 35 μH inductance ringing coil circuit. Mesyats and Proskurovsky [2] indicate that the hold-off E-field scales with pulse width as $\tau^{-1/4}$ to $\tau^{-1/2}$. This gives an ~ 6% drop in hold-off for a 2.5 mm compared to 7.5 mm gap. Also the ~ 500 kV voltages used on the Cr_2O_3 coated electrode shots with 6.5 to 7.5 mm gap shots resulted in hardware support rod or crowbar switch insulator flashovers that shortened the pulse on the highest voltage shots to ~ 125 ns. Flashovers also gave ~150 ns FWHM pulses for the ~ 400 kV voltages required to achieve breakdowns with 7.5 mm gaps on bare and HVFF electrode shots. These reductions in FWHM with large gaps result in a ~ 10% expected higher hold-off for all electrodes tested at large gaps and make the drop off with higher voltage shots less apparent than would have been noted if the FWHM had been the same for all gaps. We made a concerted effort throughout the 3-year duration of this experiment to eliminate support rod flashover but as we increased the flashover threshold we also increased the available voltage. A light baffle prevented switch light from entering the electrode gap.

Figure 88 shows an overview of the breakdown results for the various 17 cm electrodes. The individual data for machined, HVFF, and Cr_2O_3 surfaces are shown in Figs. 89 to 91 and 93. A photograph of two chromium oxide electrodes is shown in Fig. 92. Much of the data for all electrodes were taken with 20 or more arc marks on the electrode surfaces. The data for machined and HVFF stainless steel also show the "total voltage effect", that manifests itself as decreased E-field hold-off for larger gaps. Although the statistics are low it appears that the HVFF treated electrodes have an ~ 10% improvement in hold-off compared to the bare surfaces. The 2.5-mm-gap data for the Cr_2O_3 coatings show about the same hold-off as the HVFF coated electrodes. Interestingly, the Cr_2O_3 coatings show ~ 10% higher hold-off for 5 mm compared to 2.5 mm gaps. Some of this is due to the 5% higher values expected because of the shorter pulse. We were not able to achieve breakdown with Cr_2O_3 coatings with 7.2 mm gaps at 500 kV. This could be caused by the expected ~ 18% increase in hold-off due to the factor of two shorter pulse available at 500 kV. As indicated by the lower plot in Fig. 91, many breakdowns occurred with the Cr_2O_3 coated 316L electrodes when the gap was 6.5 mm and the pulse only 125-ns-FWHM wide. This seems to indicate a decrease in hold-off with gap.

The individual Z-protocol hold-off data are shown in Fig. 93. The 4th test series with 4.85 mm gap gave similar hold-off to the best results of our initial tests (see Fig. 13) obtained with 3.8 mm gap. However, this series was superior in that no conditioning breakdown shots were observed. The 3rd and 7th test series with 7.31 mm gap gave hold-offs of about 400 kV. One might conclude from this that the hold-off E-field decreased with gap for gold coatings also. However this is contradicted by the 5th and 6th test series with 2.48

and 2.99 mm gaps that gave hold-offs of < 500 and ~ 600 kV/cm. Therefore we can only conclude that the Z-protocol treated electrode hold-off is similar to that observed previously with unfiltered laboratory air and about 20% lower than the value for untreated 304L rod stock stainless steel.

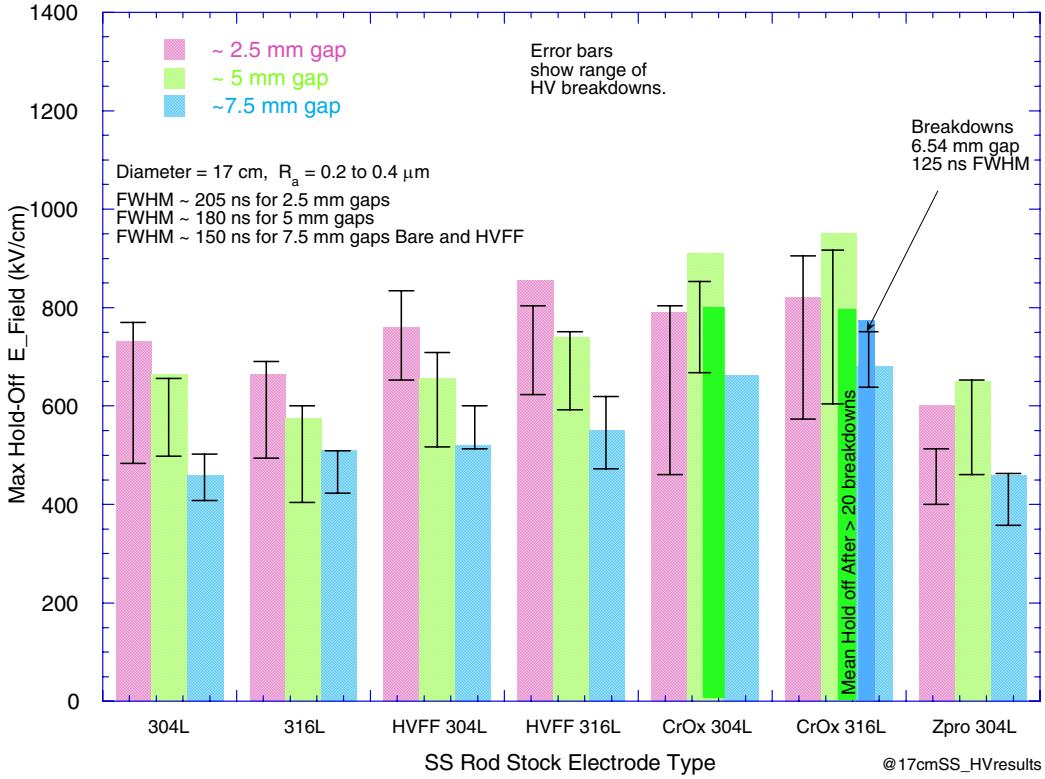

Figure 88. A summary of the breakdown results for various treatments to 17 cm stainless steel electrodes that were cleaned and installed in the filtered clean air environment.

Unfortunately our test hardware gave a shorter pulse for the 7.5 mm gap shots so it is not possible to make good comparisons to the smaller gaps for Cr_2O_3 coating. The fact that breakdowns occurred at 125 rather than 180 ns with a 6.5-mm-gap Cr_2O_3 coated 316L electrode pair, suggests that the "total voltage effect" is beginning to take effect with gaps larger than 5 mm for the Cr_2O_3 coatings. Improved test stand hardware that avoids flashovers at very high voltages would be necessary to verify this however. Our 107-ns-FWHM test data for 7.5-mm-gap shots using Cr_2O_3 coated electrodes were acquired prior to the installation of a field shaper that improved the crowbar switch hold-off time by about 20 ns. We should have repeated the 7.5-mm-gaps shots with the longer pulse. However, we chose not to do so because of time constraints and our judgment that it was unlikely we would have achieved breakdowns with the slightly longer pulse either. These results are similar to anodized aluminum that did not show a drop in E-field hold-off when the gaps were increased from 2 to 3.8 mm gaps. As with anodized aluminum, if there is a difference in hold-off scaling with gap for chromium oxide coatings, it could be related to the dielectric constant of the coating reducing the E-field at the metal coating interface or charge build-up on particles located on the surface.

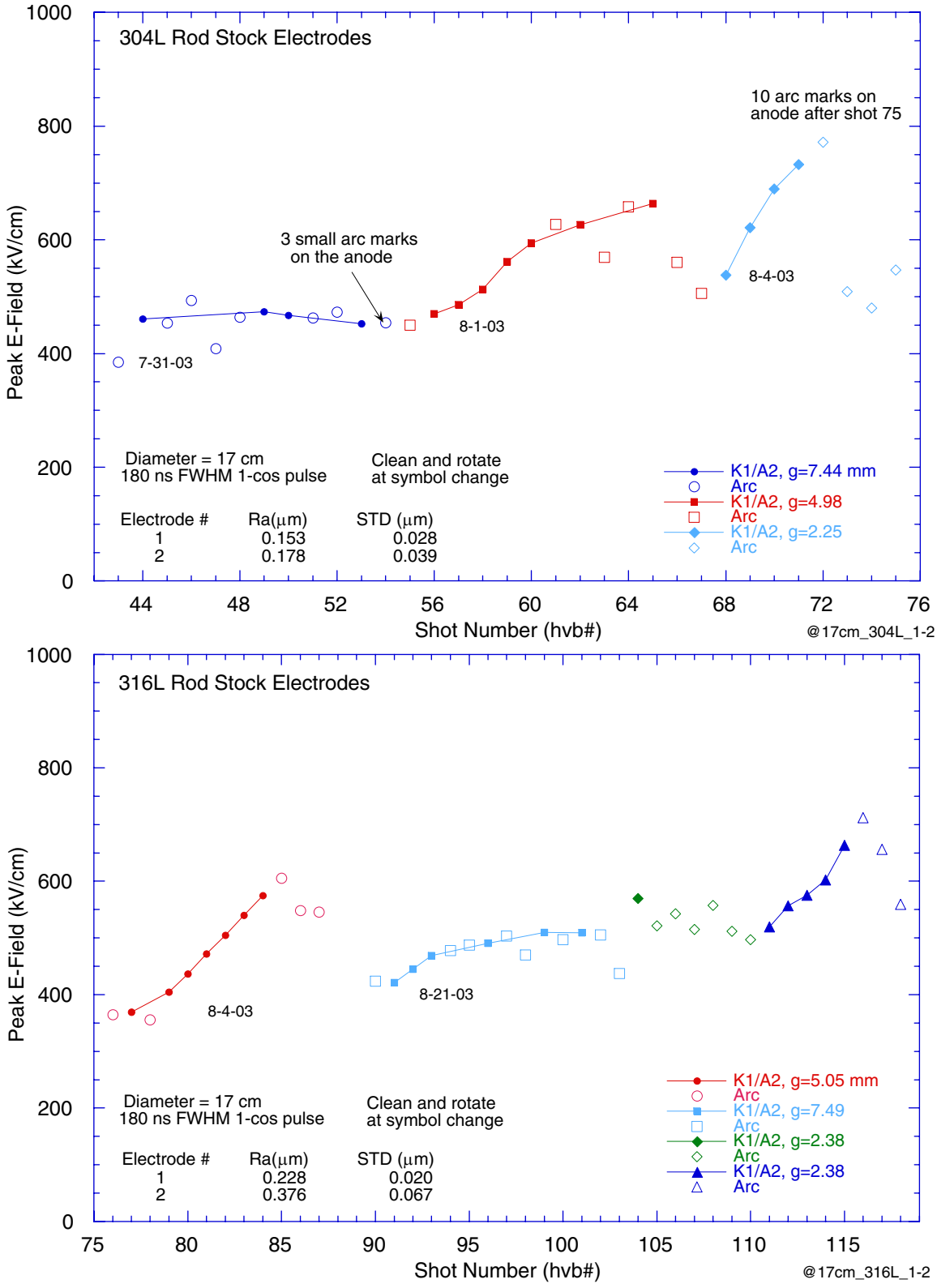

Figure 89. The breakdown data for 17-cm-diameter 304L and 316L rod stock stainless steel acquired after cleaning with acetone in the filtered air environment.

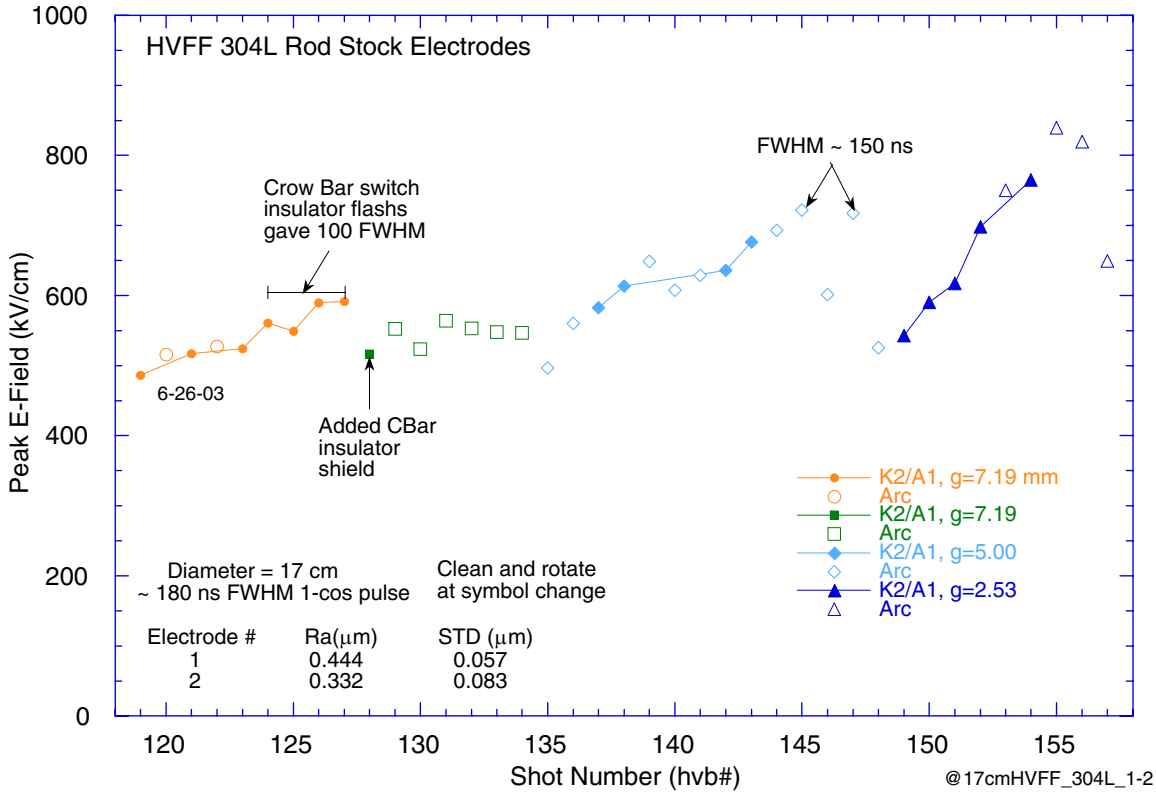

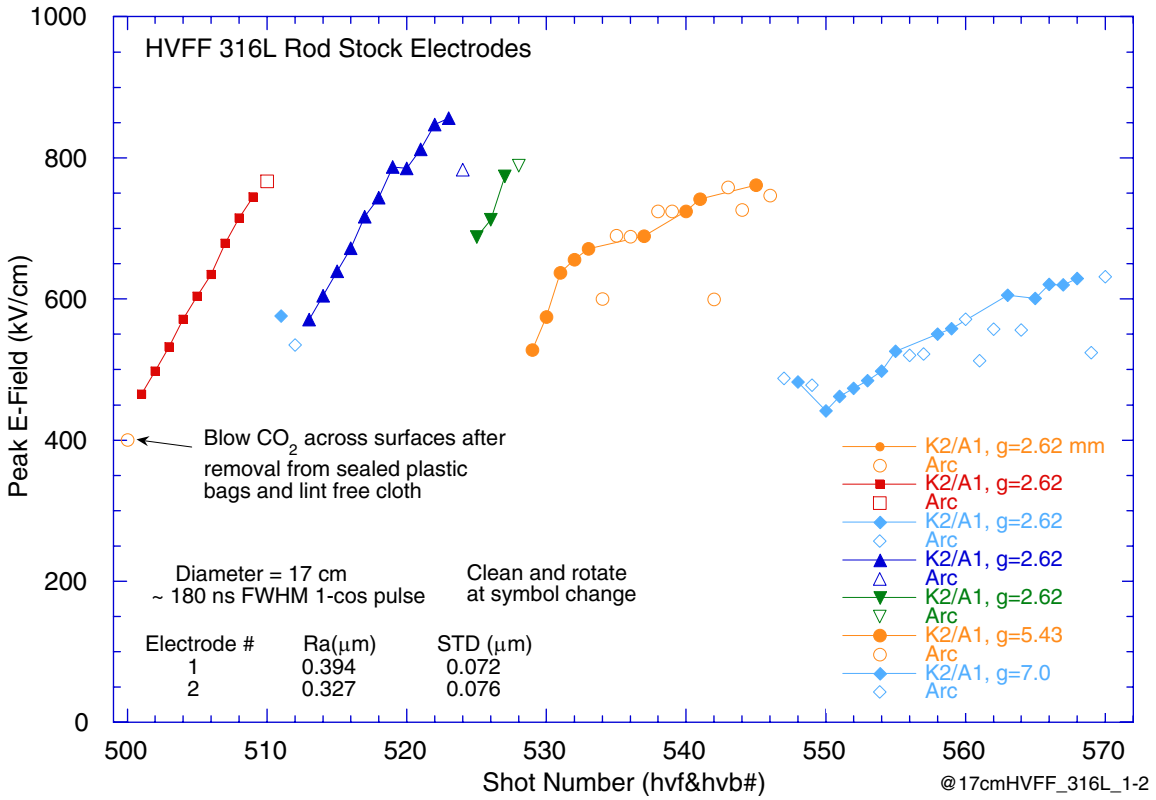

Figure 90. The breakdown data for 17-cm-diameter HVFF treated 304L and 316L rod stock stainless steel acquired after cleaning with acetone in the filtered air environment.

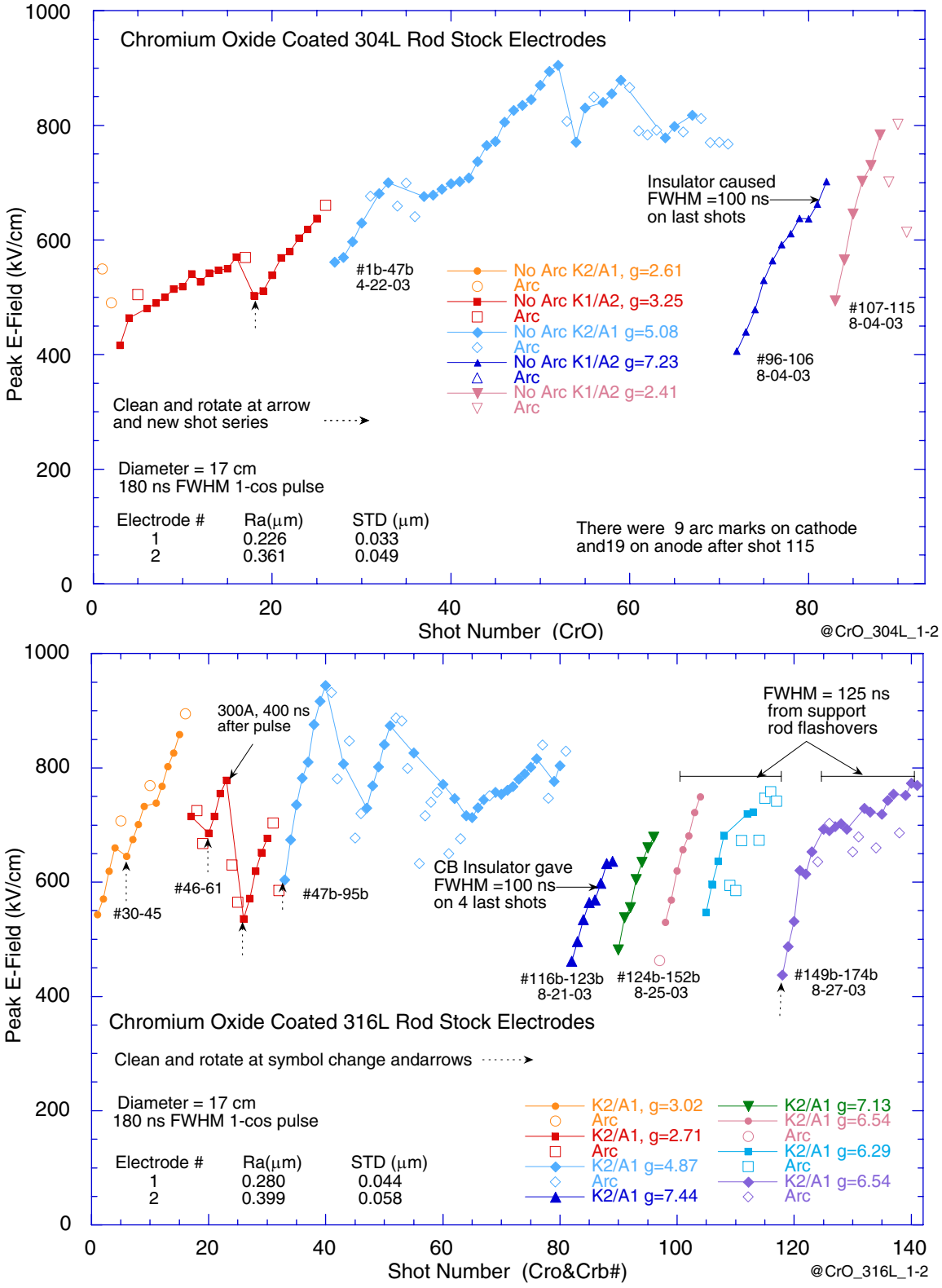

Figure 91. The breakdown data for 17-cm-diameter chromium oxide treated 304L and 316L rod stock stainless steel acquired after cleaning with acetone in the filtered air environment.

Timothy J. Renk , Org 15335, vapor deposited a 0.5-μm-thick chrome coating onto 12-cm-diameter 316L SS electrodes with the RHEPP1 accelerator pulsed ion beam. Tests with 3.5 and 5 mm gaps gave hold-offs of 350 and 250 kV/cm and a factor of two below uncoated 316L surfaces. The electrodes were etched with sulfuric acid to allow bonding.

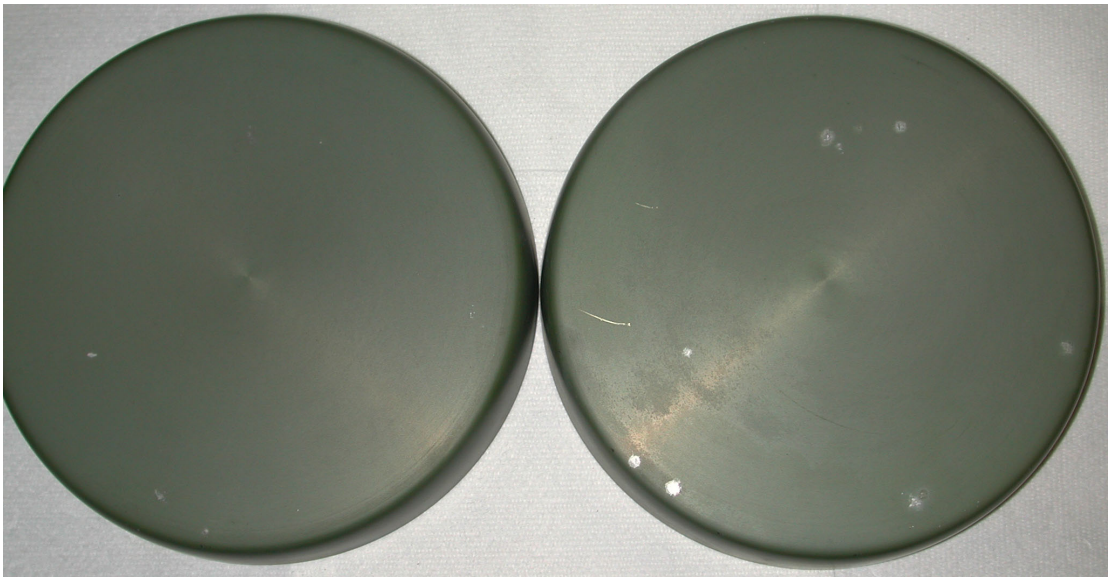

Figure 92. Photographs of chromium oxide coated 316L electrodes 1 and 2 after shot 96b of the 3rd shots series labeled with blue diamonds in Fig. 85.

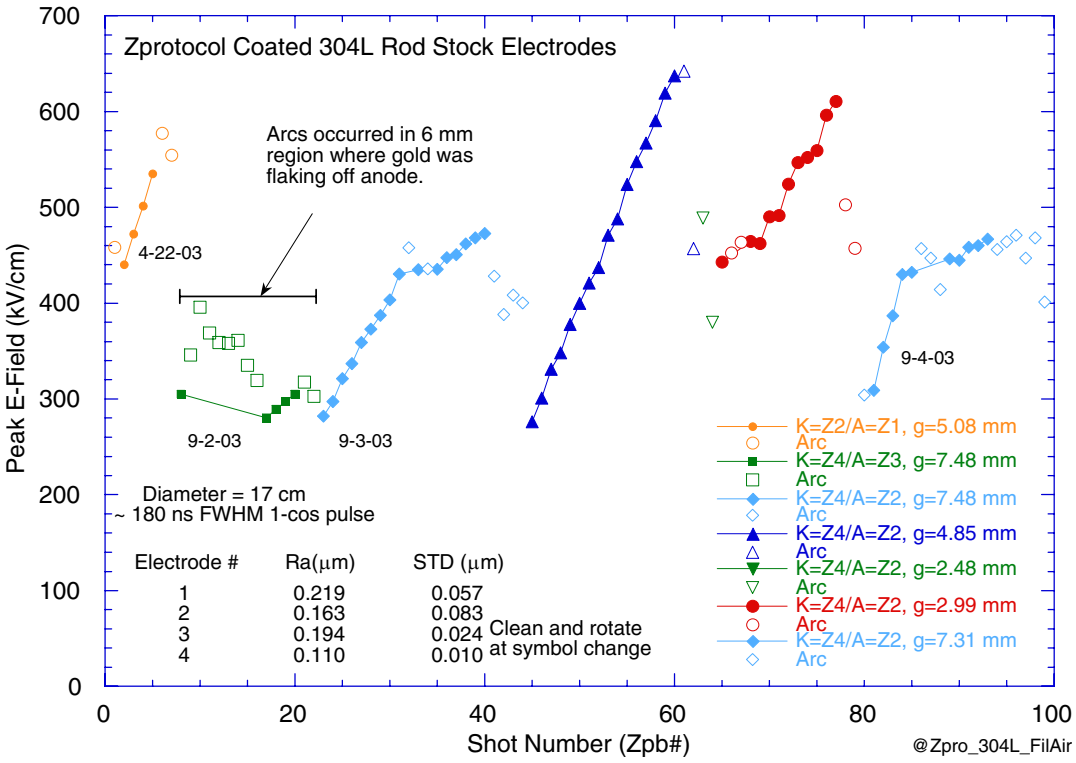

Figure 93. The breakdown data for 17-cm-diameter Z-protocol treated 304L rod stock stainless steel acquired after cleaning with acetone in the filtered air environment.

X. Conclusions

It was difficult to get precise values for the breakdown thresholds of the metals and coatings tested because the thresholds are sensitive to cleaning and voltage application protocols during a test sequence. This was especially the case with bare metal surfaces. As others have observed, firing many electrical-condition shots increased the breakdown E-field by at least 30%. Electrical conditioning shots use small discharges late in the voltage pulse to remove potential breakdown sites. To achieve good conditioning we started firing shots at ~ 60% of the expected breakdown E-field and increased the field in discrete steps of 20 to 40 kV/cm. The more steps used the higher the ultimate hold-off field. Full power shots without electrical conditioning broke down at about 60% of conditioned electrodes. This can be expected for pulsed power applications where electrical conditioning is not possible. The same effect occurred to a lesser degree with electrode cleaning in a filtered air environment. Such cleaning can achieve a 30% improvement also, but there is overlap in that cleaning eliminates many of the potential emission sites that would be removed by electrical conditioning.

With these caveats we observed the best quality stainless steel exposed to pulsed electron beam surface melting, to remove potential dielectric emission sites, gave similar hold-off to polished surfaces with R_a = 0.05 μm. The hold-off for the EBEST electrodes is insensitive to the accumulation of arc marks if the metal droplets that occur from severe arcs are removed. The hold-off measured for EBEST surfaces was also insensitive to surface roughness and density of craters from evaporated inclusions for R_a values and crater densities ranging from 1.2 to 0.3 μm, and 10 to 0.1 mm^{-2}, for 304L rod stock and HVFF 304L plate stock stainless steel, respectively. The peak hold-offs were about 1.05 MV/cm for our 170 ns FWHM 1-cos(ωt) when the gap was ~ 2.2 mm. The hold-off voltage dropped roughly as the square root of the gap with increasing gap and was about 0.6 MV/cm for a 7.5 mm gap. When the gap was 2.2 mm the hold-off for machined stainless steel with R_a = 0.5 μm was about 40% lower than the value for EBEST or polished stainless steel. This could indicate that exploding "cathode whiskers" are important for poorly machined stainless steel. We conclude that the hold-off is nearly independent of electrode surface area for areas > 50 cm^2 because the probability is already high for a least one potential emission site to occur within this area.

Dielectric surfaces such as new anodized coatings on aluminum gave a factor of two improvement in hold-off for aluminum. We observed hold-offs of ~ 1.4 MV/cm for 2 to 3.5-mm-gaps with 50-μm-thick anodized aluminum coatings. These tests used 155-cm^2-area electrodes. The hold-off appeared to be independent of gap but we could not achieve breakdowns with gaps > 4 mm where the drop in hold-off was clear with stainless steel. Minor 100-μm-wide pit marks in the cathode coating caused about a 10% reduction in hold-off. Large 1-mm-size arc marks on the anode, that removed the anodized coating and a significant amount of aluminum, reduced the hold-off field to ~ 0.5 MV/cm. Melted aluminum deposited on the cathode from anode craters gave similar reductions. Tests with polished and a 0.7 to 3-μm-roughness bare machined aluminum gave hold-offs of 0.7 and 0.5 MV/cm for 3.6 and 7.4 mm gaps, respectively.

The EVO cleaning solution mixed 50/50 with Dow Corning 704 diffusion pump oil gave a 30% increase for machined aluminum that was not electrically conditioned. The hold-off was about 0.8 MV/cm for R_a = 0.7 μm aluminum with 2.2 mm gaps. When the formula was applied locally to severe arc marks on anodized aluminum it greatly reduced the probability of arcs initiating from these marks. The hold-off under these conditions was ~ 1 MV/cm. We did not test EVO for variation in hold-off with gap.

The hold-off for 17-cm-diameter (230 cm^2 area) machined 304L and 316L rod stock electrodes was about 0.6 and 0.45 MV/cm for 2.5 and 7.5 mm gaps. Hydrogen vacuum furnace, HVFF, increased the hold-off by 10%. Chromium oxide coatings on these stainless steel alloys gave 30% improvement in hold-off with peak fields of ~ 0.8 MV/cm. This coating was quite robust so the electrodes retained these values after about 50 breakdown. The chromium oxide hold-offs were independent of gap between 2.5 and 5 mm. We could not test with a full width voltage pulse with 7.5 mm gaps because of electrode support rod flashovers, so there is uncertainty whether the hold-off is the same at these larger gaps. The hold-off for the Z-protocol applied to 304L stainless steel was about 0.5 kV/cm for 2.5 and 5 mm gaps and dropped to 0.4 MV/cm for 7.5 mm gaps.

We observed that the current waveforms for the majority of the shots could be fit well with a simple Child Langmuir space-charge limited current model with linearly closing gap and expanding source area. For large gaps the model often fit the current traces for 200 ns until the gap was 90% closed. This demonstrates that the plasmas formed at the onset of current expand ballistically during the pulse. For early turn-on shots there were often one or more pulses in the current that caused inflections in the voltage. However, these pulses terminated in about 20 ns and the current returned to the CL fit value. The plasma-closure velocities were nearly the same for all the treatments tested. This includes such diverse coatings as the polymer based EVO/pump oil mixture to the gold-coated Z-protocol electrodes.

The breakdowns for gaps < 2 mm are probably initiated by the standard MIV or MIM emission site breakdown model of Latham or possibly the metal micro-protrusion breakdown model of Mesyats. For bare metals and gaps > 2 the hold-off voltage scaled as the square root of gap. This dependence has been attributed in the past to micro-particles accelerated across the gap to create cathode or anode plasma. For this to happen with our ~100 ns pulses and similar delay times the particles must be of molecular size, with a few hundred molecular weight, and have one or two electron units of charge. It seems improbably that such molecules could impart sufficient energy on an electrode to initiate breakdown however. Therefore the breakdown mechanism for large gaps is not well understood. There is a possibility that the voltage dependence has a pathological reason such as uv-radiation or stray electrons emitted from our support rods when they were operated closer flashover at the higher voltages. We are reasonably confident this is not the cause because we saw the effect clearly with 5 mm gaps using stainless steel electrodes where there was little chance of rod flashovers. However, this possibility needs to be eliminated by additional HV tests with better hardware design. Also the measurements should be made with longer and shorter pulses and with the gap extended beyond 7.5 mm to give better guidance in to the breakdown mechanisms at work.

References

1. D. Alpert, D.A. Lee, E. M. Lyman, and J. Tomaschke, J. Vac. Sci. Technol., 1, 35-50, (1964).
2. G. A. Mesyats and D. I. Proskurovsky, "Pulsed Electrical Discharge in Vacuum", Springer-Verlag, 1988.
3. R. V. Latham, Vacuum 32, 137 (1982).
4. R. V. Latham, "High Voltage Vacuum Insulation", Academic Press 1995.
5. R. A. Millikan and R, A. Sawyer, Phys, Rev., 12, 167-170, (1918).
6. R. A. Millikan and C. C. Lauritsen, Proc. Nat. Acad. Sci. (US), 14, 45-49 (1928).
7. R. H. Folwer and L. Nordheim, Proc. Phys. Soc. (London), A119, 173 (1928).
8. R. V. Latham and E. Braun, J. Phys. D: Appl. Phys., 1, 1731-5 (1968).
9. R. V. Latham, J. Phys. D: Appl. Phys., 5, 2044-54 (1972).
10. C. S. Walters, M. W. Fox, and R. V. Latham, , J. Phys. D: Appl. Phys., 7, 911-9 (1974).
11. B. M. Cox, J. Phys. D: Appl. Phys., 8, 2065-73 (1975).
12. B. M. Cox and W. T. Williams, J. Phys. D: Appl. Phys., 10, L5-L9 (1977).
13. N. K. Allen, M. W. Cox, and R. V. Latham, J. Phys. D: Appl. Phys., 12, 969-77 (1979).
14. R. F. Hurley, J. Phys. D: Appl. Phys., 13, 1121-28 (1980).
15. N. S. Xu and Latham, J. Phys. D: Appl. Phys., 19, 447-82 (1986).
16. L. Cranberg, J. App. Phys, 23, 518-22 (1952).
17. I. N. Slivkov, Sov. Phys-Tech. Phys. 2, 1928-34 (1957).
18. P. A. Chatterton, M. M. Menon, and K. D. Srivastava, J. App. Phys, 43, 4536-43 (1972).
19. D. A. Eastham and P. A. Chatterton, IEEE Trans. on Elect. Insulation, E1-18 (3), 209-13 (1983).
20. E. W. Gray, J. Appl Phys. 59 (11), 3709-15 (1986).
21. E. W. Gray and E. W. Stinnett, J. Appl Phys. 61 (12), 5222-36 (1987).
22. N. S. Xu and R. V. Latham, IEEE Trans. on Elect. Insulation 24 (6) 901-3 (1989).
23. R. V. Latham, IEEE Trans. on Elect. Insulation, E1-18 (3), 194-203 (1983).
24. L. Jadynak, J. Appl. Phys. 35 1727-33 (1964).
25. G. B. Frazier, Proceedings of 2nd IEEE Pulsed Power Conf., New York, p 127-31 (1979).
26. D. E. Voss, "Novel High Power Microwave Source Development", Air Force Weapons Laboratory Report WL-TR-89-95, (1990).
27. R. V. Latham, K. H. Bayliss, and S. Bajic, IEEE Trans. on Diel. and Elect. Insulation, 24 (6) 897-900 (1989).
28. C. S. Mayberry, B. Wroblewski, E. Schamiloglu, and C. B. Fleddermann,, J. Appl. Phys, 76 (7), 4448-50 (1994).
29. A. V. .Batrakov, A. B. Markov, G. E. Ozur, E. I. Proskurovsky, and V. P. Rotshtein, IEEE Trans. on Diel. and Elect. Insulat. 2 (2), 237-241, (1995).
30. A. V. .Batrakov, D. S. Nazarov, G. E. Ozur, S. A. Popov, E. I. Proskurovsky, and V. P. Rotshtein, IEEE Trans. on Diel. and Elect. Insulat. 4 (6), 857-62, (1997).
31. Ph. Niedermann, N. Sankarraman, R. J. Noer, and Φ. Fischer, J. Appl. Phys. 59 (3), 892-900 (1986).
32. E. Mahner, G. Muller, H. Piel, and N. Pupeter, Vac. Sci. Tehnol. B 13 (2), 607-610 (1995).

33. N. Pupeter, A. Gohl, T. Habermann, A. Kirschner, E. Mahner,, G. Muller, H. Piel, Proc. of the 7th Workshop on RF Superconductivity,Gif-sur-Yvette, France, p67-77 (1995)
34. N. Jimenez, R. J. Noer, G. Jourve, C. Antoinet, J. Jodet, and B. Bonin, J. Phys.D: Appl. Phys, 26 1503-09 (1993).
35. M. E. Cuneo, IEEE Trans. on Diel. and Elect. Insulation, 6 (4), 469-485 (1999).
36. M. Okawa, T. Shioiri, H. Okubo, and S. Yanabu, IEEE Trans. on Diel. and Elect. Insulat. 23 (1), 77-81, (1988).
37. U. Schumann and M. Kurrat, Proc. of 20th IEEE Int. Sym. on Disc. and El. Insul. in Vac., Tours France, p459-62, July 2002.
38. S. S. Glaros, Gull Group, 777 Bay Street #7, San Francisco, CA 94109.
39. D. I. Proskurovsky, V. P. Rotshtein, G. E. Ozur, A. B. Markov, D. S. Nazarov, V. A. Shulov, Yu. F. Ivanov, R. G. Buchheit, J. Vac. Sci. Technol. A16 (4), 2480-8(1998).
40. ELECTRO, Integrated Engineering Software, 220-1821 Wellington Ave., Winnipeg, Manitoba, Canada.
41. D. I. Proskurovsky and A. Batrakov, Proc. of 19th IEEE Int. Sym. on Disc. and El. Insul. in Vac. Xi'an, China, p9-16 (2000).
42. D. J. Johnson, W. E. Fowler, M. E. Savage, and W. A. Stygar, Proc. of 20th IEEE Int. Sym. on Disc. and El. Insul. in Vac., Tours France, p131-4, July 2002.
43. M. L. Kiefer, L. F. Kelley, K. W. Struve, and M. Widner, "SCREAMER, A Pulsed Power Design Tool", Sandia National Laboratories, 1995.
44. D. I. Proskurovsky, A. V. Batrakov, V. P. Rotshtein, K. V. Karlik, and D. J. Johnson, to be published in Proc.14th IEEE Int. Pulsed Power Conf., Dallas, Texas, June 2003.
45. O. B. Ladyzhenskii, R. M. Rasputin, and A. V. Yanchuk, Instrument and Experiment Techniques, 43 (6), 836-8, 2000.
46. L. V. Spencer, "Energy Dissipation by Fast Electrons", NBS Monograph 1, US Dept. of Comm. NBS.Sept, 10, 1959.
47. A. E. Blaugrund, G. Cooperstein, and Shyke A. Goldstein, Phys. Fluids, 20 (7) 1185-94, 1977.
48. T. W. L. Sanford, J. A. Halbleib, J. W. Poukey, A. L. Pregenzer, R. C. Pate, C. E. Heath, R. Mock, G. A. Mastin, and D. C. Ghiglia, T. J. Roemer, P. W. Spence, and G. A. Proulx,, J. Appl. Phys.., 66 (1), 10-22, 1989.
49. D. Smithand N. G. Adams, J. Phys. D. 6, 700 (1973).
50. O. Lloyd and R. Hackam, Proc. Inst. Electr. Eng., 122, 1275-8, 1975.
51. O. Lloyd and J. H. Fairfield, CEG.B Res. Report, R/M/N937, 1977.
52. T. Otsuka, Y. Yamano, S. Kobayashi, T. Higo, N. Toge, K. Takada, Y. Higashi, Y. Saito, and N. Hitomi, Proc. of 20th IEEE Int. Sym. on Disc. and El. Insul. in Vac., Tours France, p556-60, July 2002.
53. D. J. Johnson, H. C. Ives, M. E. Savage, and W. A. Stygar, to be published in Proc. 14th IEEE Int. Pulsed Power Conf., Dallas, Texas, June 2003.
54. Anadite Inc, South Gate, California
55. J. C. Martin, AWE, England

Distribution

1	MS9018	Central Technical Files, 8945-1
2	MS0899	Technical Library, 9616
1	MS0323	LDRD Office, 01011
8	MS1182	B. N. Turman, 15335
10	MS1182	D. J. Johnson, 15335
1	MS1165	W. Guyton, 15300
1	MS1153	M. T. Buttram, 15330
1	MS1182	T. J. Renk, 15335
1	MS1153	P. D. Coleman, 15331
1	MS1190	J. P. Quintenz, 01600
1	MS1194	D. H. McDaniel, 01640
1	MS1194	K W. Struve, 01644
1	MS1194	M. E. Savage, 01644
1	MS1194	J. M. Elizondo-Decanini, 01644
1	MS1194	W. A. Stygar, 01644
1	MS1193	M. G. Mazarakis, 01644
1	MS1194	W. E. Fowler, 01644
1	MS1193	J. E. Maenchen, 01645
1	MS1193	D. L. Johnson, 01645
1	MS1193	J. R. Woodworth, 01645
1	MS1193	D. C. Rovang, 01645
1	MS1178	H. C. Ives, 01639
1	MS1193	M. E. Cuneo, 01673